Aus dem Institut für Toxikologie
der Heinrich-Heine-Universität Düsseldorf
Direktor: Prof. Dr. rer. nat. Gerhard Fritz

Influence of Nephrotoxins on the Differentiation Process of Human Induced Pluripotent Stem Cells (hiPSC) to Proximal Tubular Epithelial-Like Cells (PTELC)

Dissertation zur Erlangung des Grades eines Doktors
der Medizin der Medizinischen Fakultät
der Heinrich-Heine-Universität Düsseldorf

Vorgelegt von
Nazih Mohamed Zakari KOUIDRAT
Düsseldorf, 2025

Als Inauguraldissertation mit Genehmigung der Medizinischen Fakultät der Heinrich-Heine-Universität Düsseldorf gedruckt.

Dekan: Prof. Dr. med. Nikolaj Klöcher

Erstgutachterin: Prof. Dr. Nicole Schupp, Institut für Toxikologie

Zweitgutachter: Prof. Dr. James Adjaye, Institute for Stem Cell Research & Regenerative Medicine

Table of content

Published Data

Parts of this work have been published:

Mboni-Johnston I. M., **Kouidrat N. M. Z.**, Hirsch C., Weber A. G., Meißner A., Adjaye J., et al. (2024). *Sensitivity of Human Induced Pluripotent Stem Cells and Thereof Differentiated Kidney Proximal Tubular Cells towards Selected Nephrotoxins*. International Journal of Molecular Sciences, 25(1), 81. https://doi.org/10.3390/ijms25010081.

List of abbreviations

ABC	ATP-binding cassette
AKI	Acute kidney injury
ANOVA	Analysis of variance
AQP-1	Aquaporin-1
ARE	Antioxidative response element
BMP-2/7	Bone marrow protein-2/7
BSA	Bovine serum albumin
CAD-16	Cadherin-16
CAT	Catalase
CD-13	Alanyl aminopeptidase N
cDNA	Complementary deoxyribonucleic acid
CKD	Chronic kidney disease
CsA	Cyclosporin A
CTR-1/2	Copper transporter-1/2
CUBN	Cubilin
DAPI	4′,6-diamidino-2-phenylindole
dH2O	Distilled water
DiffD3/9	Differentiation day 3/9
DMEM	Dulbecco’s modified eagle medium
DMSO	Dimethyl sulfoxide
DPBS -/-	Dulbecco's phosphate buffered saline without calcium & magnesium
DTNB	5,5'-dithio-bis(2-nitrobenzoic acid)
E-CAD	Epithelial cadherin
EdU	5-Ethynyl-2′-deoxyuridine
EMT	Epithelial-mesenchymal transition
ER	Endoplasmic reticulum

ESC	Embryonic stem cells
FITC	Fluorescein isothiocyanate
GAPDH	Glyceraldehyde-3-phosphate dehydrogenase
GCL	Glutamine-cysteine ligase
GCLC	Glutamine-cysteine ligase catalytic subunit
GCLM	Glutamine-cysteine ligase regulatory subunit
GGT	Gamma-glutamyl transferase
GPX-1	Glutathione peroxidase-1
GSH	Glutathione
GSK-3β	Glycogen synthase Kinase-3β
GSR	Glutathione reductase
H_2O_2	hydrogen peroxide
HCl	Hydrochloric acid
HiPSC	Human-induced pluripotent stem cells
HK-2	Human kidney cells
HO-1	Heme oxygenase-1
HPTEC	Human proximal tubule epithelial cells
HRP	Horseradish peroxidase
hTERT	Human telomerase reverse transcriptase
IC	Inhibitory concentrations
IL-2	Interleukin-2
ISRM	Institute of Stem Cell Research and Regenerative Medicine
KEAP-1	Kelch-like ECH-associated protein-1
KIM-1	Kidney injury molecule-1
KLF-4	Kruppel-like factor-4
MCT-1	Monocarboxylate transporter-1
MDR-1	Multidrug resistance protein-1

MEG	Megalin
MET	Mesenchymal-epithelial transition
mRNA	Messenger ribonucleic acid
MRP	Multidrug resistance-associated proteins
N-CAD	Neural cadherin
NFAT	Nuclear factor of activated T cells
NGAL	Neutrophil gelatinase-associated lipocalin
NQO-1	NADPH dehydrogenase (quinone 1)
NRF-2	Nuclear factor erythroid 2-related factor-2
OAT-1/3	Organic anion transporter-1/3
OATP	Organic anion transporting polypeptides
OCT-1/2	Organic cation transporter-1/3
OCT-3/4	Octamer-binding transcription factor 3/4
OCTN-2	Organic cation/carnitine transporter-2
OD	Optical density
P-GP	Permeability glycoprotein
PAX-2	Paired box gene-2
PEPT-1/2	Peptide transporter-1/2
pNRF-2	Phosphorylated NRF-2 at Serine 40
PTEC	Proximal tubule epithelial cells
PTELC	Proximal tubule epithelial-like cells
qRT-PCR	Quantitative reverse transcription polymerase chain reaction
REGM	Renal epithelial growth medium
RIPA	Radioimmunoprecipitation assay
ROCK	Rho-associated coiled-coil containing kinases
ROS	Reactive oxygen species
RPL-32	Ribosomal Protein

RPTEC	Renal proximal tubule epithelial cells
RT	Room temperature
SDS-PAGE	Sodium dodecyl sulfate-polyacrylamide gel electrophoresis
SGLT-1/2	Sodium-glucose cotransporter-1/2
SOD	Superoxide dismutase
SOX-2	Sex determining region Y-box-2
TBST	Tris-buffered saline with Tween 20
TEMED	Tetramethylethylenediamine
TGF-β	Transforming growth factor-β
TJP-1	Tight junction protein-1
TNB	Thionitrobenzoic acid
TRX	Thioredoxin
TRXR	Thioredoxin reductase
ZO-1	Zonula occludens-1

Abstract

Proximal tubule epithelial cells (PTEC) are the most metabolically active renal segment in solute reabsorption and drug metabolism and therefore the most vulnerable to nephrotoxic insult. Many of drug-induced nephrotoxic effects observed in clinical trials remain undetected in preclinical testing models. Furthermore, although the kidney can regenerate after acute kidney injury, subclinical renal impairment sometimes persists, which increases the risk of chronic kidney disease. In this context, differentiation models based on stem cells offer a promising alternative to traditional *in vitro* systems, as they could provide more physiologically relevant, human-specific models for drug testing and disease modelling that align with the 3Rs (replace, reduce and refine) principles.

In this study, a one-step differentiation protocol adapted from Kandasamy *et al.* (2015) was used to differentiate two human-induced pluripotent stem cell (hiPSC) lines, b4 and UM51, into proximal tubule epithelial-like cells (PTELC). The differentiation efficiency was confirmed by qRT-PCR, western blot, immunocytochemistry, and also by albumin uptake assay. Dose-response experiments with well-established nephrotoxic substances like cisplatin, cyclosporin A (CsA) and hydrogen peroxide (H_2O_2), were performed on hiPSC, differentiating hiPSC and differentiated hiPSC. Further toxicity studies included cisplatin-induced oxidative stress response, analyzed by qRT-PCR, immunocytochemistry and glutathione (GSH) assay.

Differentiated b4 and UM51 cells displayed typical morphological characteristics of PTEC, confirmed by the downregulation of stem cell markers and upregulation of PTEC-specific markers at both mRNA and protein levels. Functionally, PTELC showed enhanced albumin uptake capacity. Toxicity studies revealed consisting inhibitory concentration (IC) values with existing literature, with PTELC exhibiting reduced sensitivity to cisplatin, while CsA was similarly toxic across all cell stages of cell differentiation. Interestingly, differentiating cells were more sensitive to H_2O_2 than stem cells. Cisplatin had overall a more pronounced effect on cell proliferation than CsA. In oxidative stress response to cisplatin, PTELC exhibited a dose-dependent increase in glutathione peroxidase (*GPX-1*) and NADPH (quinone) dehydrogenase-1 (*NQO-1*) at low doses, while the antioxidant defence was overwhelmed at higher doses.

In conclusion, our results suggest that the present hiPSC-derived PTELC model represents a promising 3R-compatible tool for regenerative medicine and drug toxicity studies. It could offer concrete advantages in predicting nephrotoxicity and improving preclinical drug screening.

Zusammenfassung

Die Epithelzellen des proximalen Tubulus (PTEC) tragen zum größten Teil zur Rückresorption gelöster Substanzen und zum Fremdstoffmetabolismus bei, was sie besonders anfällig für nephrotoxische Substanzen macht. Die meisten arzneimittelinduzierten nephrotoxischen Effekte, die in klinischen Studien beobachtet werden, bleiben in präklinischen Tests unentdeckt. Darüber hinaus kann trotz der Fähigkeit der Niere, sich nach einer akuten Nierenschädigung zu regenerieren, eine subklinische Nierenfunktionsstörung bestehen bleiben, die das Risiko einer chronischen Nierenerkrankung erhöht. In diesem Zusammenhang bieten stammzellbasierte Differenzierungsmodelle eine vielversprechende Alternative zu herkömmlichen *in vitro*-Systemen, da sie physiologisch relevantere, humanspezifische Modelle für Arzneimitteln-Tests und die Modellierung von Krankheiten bieten, die den 3R-Prinzipien (replace (ersetzen), reduce (reduzieren) und refine (verbessern)) entsprechen.

In dieser Studie wurde ein Differenzierungsprotokoll nach Kandasamy *et al.* (2015) verwendet, um zwei humane-induziert-pluripotente Stammzellen (hiPSC), b4 und UM51, in proximale tubuläre Epithel-ähnliche Zellen (PTELC) zu differenzieren. Die Effizienz der Differenzierung wurde durch qRT-PCR, Western Blot, Immunzytochemie und einen Albumin-Aufnahmetest untersucht. Dosis-Wirkungs-Experimente mit bekannten Nephrotoxinen wie Cisplatin, Cyclosporin A (CsA) und Wasserstoffperoxid (H_2O_2) wurden mit hiPSC, differenzierenden hiPSC und differenzierten hiPSC durchgeführt. Weitere Toxizitätsstudien umfassten die Cisplatin-induzierte oxidative Stressreaktion, die mittels qRT-PCR, Immunzytochemie und Glutathion (GSH)-Test analysiert wurde.

Differenzierte b4- und UM51-Zellen wiesen typische morphologische Merkmale von PTEC auf, was durch das Herunterregulieren von Stammzellmarkern und das Hochregulieren von PTEC-spezifischen Markern sowohl auf mRNA- als auch auf Proteinebene bestätigt wurde. Funktionell zeigten PTELC eine erhöhte Albumin-Transportkapazität. Toxizitätsuntersuchungen zeigten, dass die inhibitorischen Konzentrationen (IC) mit der Literatur übereinstimmten, wobei PTELC weniger empfindlich auf Cisplatin reagierten, während CsA in allen Differenzierungsstadien gleich toxisch war. Interessanterweise reagierten differenzierende Zellen empfindlicher auf Wasserstoffperoxid als Stammzellen. Cisplatin hatte insgesamt einen stärkeren Effekt auf die Zellproliferation als CsA. Bei der Reaktion auf oxidativen Stress durch Cisplatin zeigte PTELC einen dosisabhängigen Anstieg von Glutathion-Peroxidase (GPX-1) und NADPH-(Chinon-Dehydrogenase-1 (NQO-1) bei niedrigen Dosen, während die antioxidative Abwehr mit höheren Dosen überfordert wurde.

Unsere Ergebnisse deuten darauf hin, dass das vorliegende hiPSC-abgeleitete PTELC-Modell ein vielversprechendes 3R-kompatibles Werkzeug für die regenerative Medizin und Arzneimitteltoxizitätsstudien darstellt, das potenziell Vorteile bei der Vorhersage von Nephrotoxizität und der Verbesserung des präklinischen Wirkstoffscreenings bietet.

1 Introduction

1.1 Anatomy and physiology of the kidneys

The kidneys are paired, bean-shaped organs located in the retroperitoneal cavity on each side of the spine. In sagittal section, each kidney is divided into cortex (outer region) and medulla (inner region). The innermost portion of the medulla (papilla) drains into the ureter through the minor and major calyces. The functional unit of the kidney is the nephron, with approximately 1 million nephrons present in each kidney. Each nephron consists of a glomerulus and a tubular system. The glomerulus is a specialized capillary network situated between the afferent and efferent arterioles. It is enclosed by Bowman's capsule, which is continuous with the renal tubule. The tubular system is composed of functionally distinct segments: the proximal tubule, the loop of Henle, the distal tubule, and the collecting ducts as illustrated in **Figure 1.1** [1].

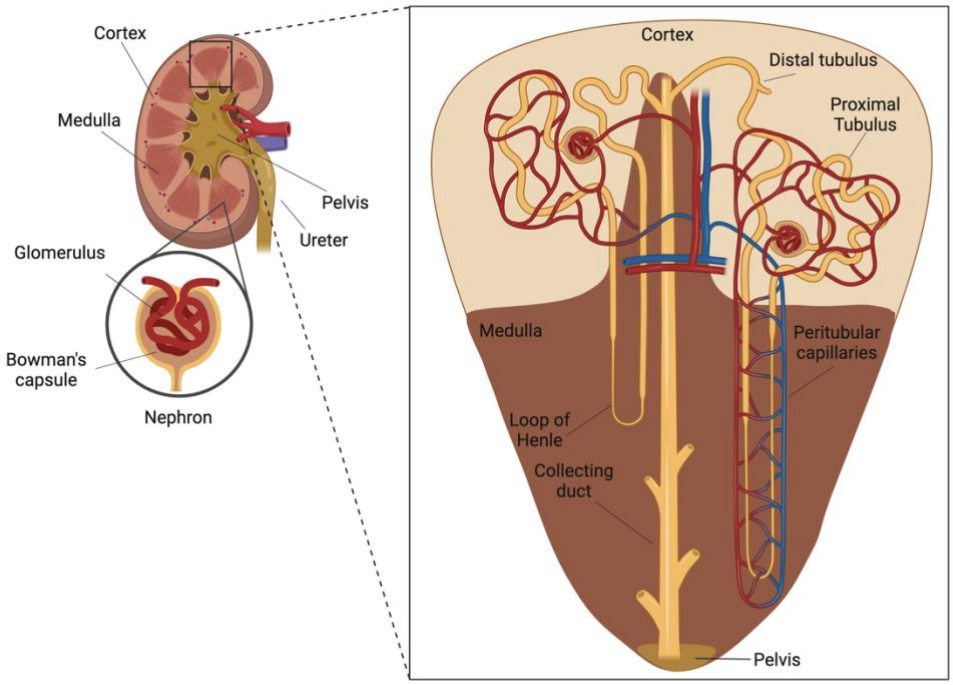

Figure 1.1: Kidney structure. In sagittal view, the kidney consists of the cortex and the medulla, which drains into the ureter. Each nephron comprises a glomerulus and a tubular system. The glomerulus is a capillary network located between the afferent and efferent arterioles and surrounded by Bowman's capsule, which is directly connected to the tubular system. The tubular system consists of several specialized segments: the proximal tubule, the loop of Henle, the distal tubule and the collecting ducts. Adapted from Costanzo Physiology 7th Edition and Human Anatomy & Physiology 12th Edition [1,2]. Figure made with BioRender.

The kidneys are essential for preserving several bodily functions. As excretory organs, they eliminate harmful substances from the body via the urine. As regulatory organs, they play a key role in maintaining homeostasis by adjusting the body's fluid balance,

including its composition, volume and pressure. As endocrine organs, the kidneys release three important hormones: erythropoietin, renin and the active form of vitamin D (calcitriol or 1,25-dihydroxycholecalciferol) [1].

The kidneys receive approximately 25 % of cardiac output, amounting to 1.25 L/min or about 1800 L/day, in an average individual with a cardiac output of 5 L/min. Blood entering the kidneys undergoes glomerular filtration in Bowman's capsule to produce approximately 170 L primary urine or ultrafiltrate per day, which contains only small solutes without larger molecules like proteins and blood cells. Fortunately, the large volume of filtrate generated is not lost as urine, epithelial cells along the renal tubules rescue the majority of the water and solutes and reabsorb them to the circulation via the peritubular capillaries. Simultaneously, renal tubular cells are involved in tubular secretion by removing waste products from the circulation and actively transporting them into the tubular lumen for excretion in the urine [1,2]. The transport in proximal tubules is further discussed in the next chapter.

1.2 Proximal tubule transport

The proximal tubule epithelial cells (PTEC) are essential for solutes reabsorption. They are responsible for the uptake of all filtered glucose and amino acids together with approximately 65 % of sodium and water from the ultrafiltrate [1,2]. To achieve this high level of activity, PTEC express specialized transporters like aquaporin-1 (AQP-1) for water transport [3] and GLUT-5 (glucose transporter-5) for facilitated fructose uptake [4]. In order to optimize the transport of peptides and glucose from the ultrafiltrate to the blood, they are reabsorbed in a sequential manner along the proximal tubule. In the early proximal tubule, low-affinity, high-capacity transporters like peptide transporter-1 (PEPT-1) and sodium-glucose cotransporter-2 (SGLT-2) are predominant, while the late proximal tubule is characterized by high-affinity, low-capacity transporters like PEPT-2 and SGLT-1 [5,6]. The clinical relevance of SGLT-2 is increasing in recent years, as SGLT-2 inhibitors display renoprotective and cardioprotective effects in diabetic patients with chronic kidney disease (CKD) [7,8].

Albumin is the most abundant protein in the bloodstream. It is essential for preserving colloid osmotic pressure, buffering pH and transporting both endogenous and exogenous substances. During glomerular filtration, potentially toxic albumin altered by oxidation or glycation or ligands in the serum, is eliminated, whereas physiologically functional albumin is reabsorbed through the megalin-cubilin (MEG-CUBN) endocytosis complex [9,10]. This complex is crucial in vitamin, drug and protein uptake and forms a

multiligand endocytic receptor complex located at the apical brush border [9,11]. Albumin reabsorption through these receptors is essential to prevent albuminuria and its related complications like malnutrition, vitamin B12 and folic acid deficiencies and cardiovascular disorders [9,10].

Many transporters in PTEC also play essential roles in drug metabolism. For example, the organic cation transporters (OCTs) are in charge of the uptake of a significant number of prescribed drugs, as approximately 40 % of them are organic cations. OCT-2 in particular is the most important transporter for the reabsorption of the chemotherapeutic drug cisplatin [12,13]. Therefore, OCT-2 could be an interesting therapeutic target to reduce the nephrotoxic side effects of cisplatin [13]. In addition, alternative cisplatin transport mechanisms have been identified via organic anion transporters (OAT-1 and OAT-3) [14], which are the most abundant anion transporters in the human kidney, involved in the secretion of antibiotics and antineoplastic agents [15]. The OATs represent also a potential therapeutic target to mitigate cisplatin nephrotoxicity, specifically through a tyrosine kinase inhibitor (nilotinib), that reduces OATs-induced nephrotoxicity without altering cisplatin anticancer activity [14].

The involvement of ion transporters in drug uptake from the circulation to the lumen can lead to high intracellular drug accumulation, potentially causing tubular toxicity. To regulate intracellular drug concentrations and prevent toxic effects, efflux transporters, like multidrug resistance protein also known as permeability glycoprotein (MDR-1/P-GP) and multidrug resistance-associated proteins (MRP), actively extrude drugs into the urine. This complex balance between drug uptake and efflux is crucial for maintaining appropriate urinary drug excretion [16,17]. Both MDR and MRP belong to the ATP-binding cassette (ABC) multidrug transporter superfamily. MDR-1 in particular is one of the most studied and demanded exporters in iPSC-derived toxicity testing models due to its polyspecific activity in extruding chemotherapeutic agents, immunosuppressants, and ß-lactam antibiotics [18,19]. However, efflux proteins play a central role in drug resistance, particularly in cancer treatment, as multidrug resistance proteins are the most common cause of treatment failure in cancer patients [16,17]. **Figure 1.2** provides an overview of all the mentioned transporters.

In summary, the fine-tuning of reabsorption and secretion in PTEC and other parts of the renal tubule, enables the kidneys to efficiently concentrate or dilute the urine, in order to preserve fluid-balance homeostasis. However, this high metabolic activity of PTEC increases their vulnerability to oxidative stress, with the underlying mechanisms and cellular defense strategies discussed in the following chapter.

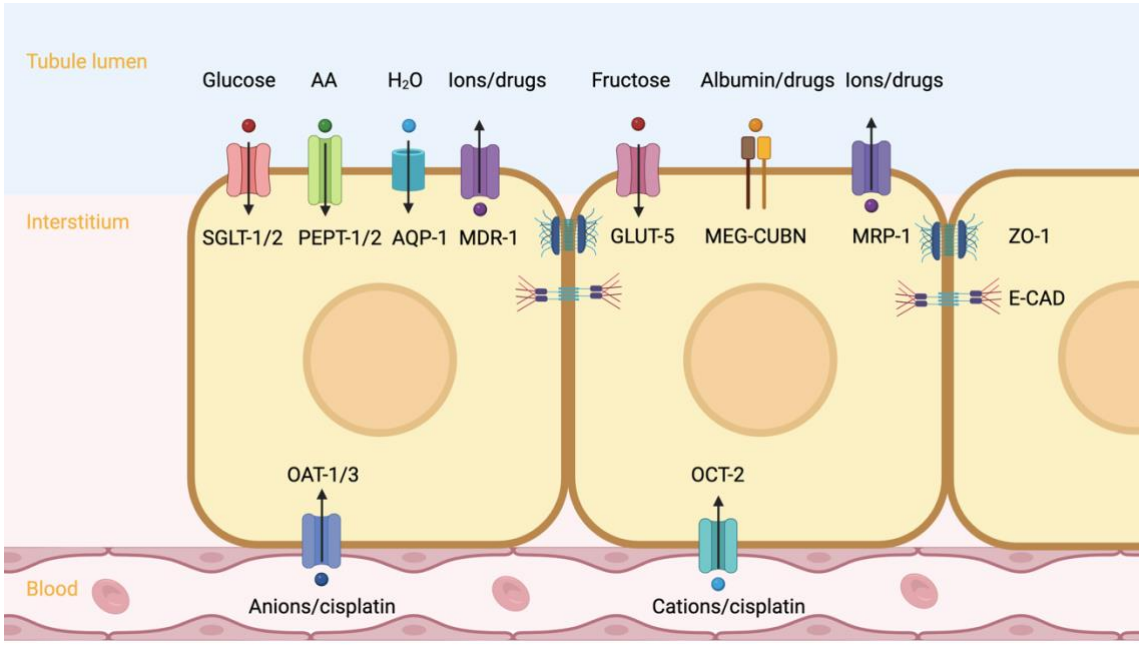

Figure 1.2: Reabsorption and secretion in PTEC. PTEC cells exhibit cellular polarity, with ZO-1 and E-CAD delimiting the lumen from interstitial space. Glucose and fructose are reabsorbed from the tubular lumen through SGLT-1/2 and GLUT-5 respectively. Amino acids and water are transported across the membrane through PEPT-1/2 and AQP-1 channels respectively. The endocytosis complex MEG-CUBN mediates the uptake of albumin and various pharmaceutical compounds. Numerous ions and drugs are absorbed from the circulation via OAT-1/3 and OCT-2, before being secreted into the lumen via MDR-1 and MRP-1 [3–6,9,13,14,16,17]. AA = amino acids, AQP-1 = aquaporin 1, CUBN = cubilin, E-CAD = epithelial cadherin, GLUT-5 = fructose transporter, MDR-1 = multidrug resistance protein 1, MEG = megalin, MRP-1 = multidrug resistance-associated protein 1, OAT-1/3 = organic anion transporter 1/3, OCT-2 = organic cation transporter 2, PEPT-1/2 = peptide transporter 1/2, PTEC = proximal tubule epithelial cells, SGLT-1/2 = sodium/glucose cotransporter 1/2, ZO-1 = zonula occludens 1. Adapted from Costanzo Physiology 7th Edition and Human Anatomy & Physiology 12th Edition [1,2]. Figure made with BioRender.

1.3 Oxidative stress and antioxidant defense mechanisms

Oxidative stress or distress describes an imbalance between the production of reactive oxygen species (ROS) and the cell's capacity to neutralize their potentially harmful effects [20]. ROS include free radicals (containing a free electron) like hydroxyl radical (OH^-) and superoxide anion (O_2^-), as well as non-radical species like hydrogen peroxide (H_2O_2) [21]. In physiological state or oxidative eustress, ROS are natural byproducts of cellular metabolism. They act as second messengers and signal transducers that control intracellular redox signaling through post-translational modifications of thiol-containing proteins, which regulate cell proliferation and immune response. However, in oxidative distress, excessive ROS formation can cause protein, lipid and DNA denaturation, and ultimately cell death [20,22].

ROS are formed following the reduction of oxygen molecules after binding with free electrons. They originate from both exogenous and endogenous sources. Exogenous sources include environmental factors like ionizing radiations, ultraviolet light and chemical agents. Endogenous sources involve cellular processes, including reactions in cytoplasm, mitochondria, endoplasmic reticulum (ER) and peroxisomes [21]. To illustrate, electrons bind to O_2 forming O_2^- in the respiratory chain of the mitochondria. Due to its short half-life, O_2^- mainly exerts local effects, before being converted by superoxide dismutase (SOD) to a more stable and freely diffusible H_2O_2. H_2O_2 can produce highly reactive hydroxyl radicals through Fenton reaction [21,23,24]. The damaging effects of oxidative stress are linked with a large spectrum of diseases like renal, neurodegenerative (Alzheimer's and Parkinson's) and cardiovascular diseases [25–28].

In order to maintain the redox balance, cells rely on a robust antioxidant defense system composed of enzymatic and non-enzymatic antioxidants. Non-enzymatic antioxidants include glutathione (GSH), thioredoxin (TRX), ascorbic acid (vitamin C) and α-tocopherol (Vitamin E). The enzymatic oxidants include catalase (CAT), SOD, NADPH dehydrogenase (quinone)-1 (NQO-1), heme oxygenase (HO-1), glutathione peroxidase (GPX), glutathione reductase (GSR), glutamate-cysteine ligase (GCL) and thioredoxin reductase (TRXR) [21].

The GSH-dependent system represents a key antioxidant pathway. Glutamate, cysteine and glycine are three amino acids that form together the tripeptide GSH, which plays a critical role in detoxifying ROS. After SOD converts O_2^- to H_2O_2, the latter is reduced to water by either CAT or GPX along with the oxidation of a GSH molecule in the case of GPX. Alternatively, GSH can be non-enzymatically oxidized after a direct interaction with ROS, which makes GSH a sensitive indicator of oxidative stress. Two oxidized GSH molecules can form glutathione-disulfide (GSSG). GSSG can then be reduced back to GSH by GSR, ensuring antioxidant regeneration [23,29].

The nuclear factor erythroid 2-related factor 2 (NRF-2) is the master regulator of antioxidant response. It is a ubiquitous transcription factor that controls redox homeostasis under both eustress and distress conditions. Under physiological conditions, NRF-2 is bound to Kelch-like ECH-associated protein 1 (KEAP-1) in the cytoplasm, which facilitates its degradation via the proteasome. Under oxidative stress, KEAP-1 undergoes conformational changes due to thiol modifications, releasing NRF-2 which translocates into the nucleus to induce expression of its target genes [20,30]. Additionally, oxidative stress activates phosphokinase C, which phosphorylates NRF-2

at Serine 40 (forming pNRF-2), stabilizing and promoting its nuclear translocation. In contrast, phosphorylation by glycogen synthase kinase-3β (GSK-3β) or Fyn kinase leads to NRF-2 transport outside the nucleus for degradation, as illustrated in **Figure 1.3** [30,31]. Recent studies suggest that the export of phosphorylated NRF-2 from the nucleus to the cytoplasm may also play a reactivation function, emphasizing the importance of continuous translocational oscillations of NRF-2 between the cytoplasm and nucleus in maintaining oxidative stress surveillance [32].

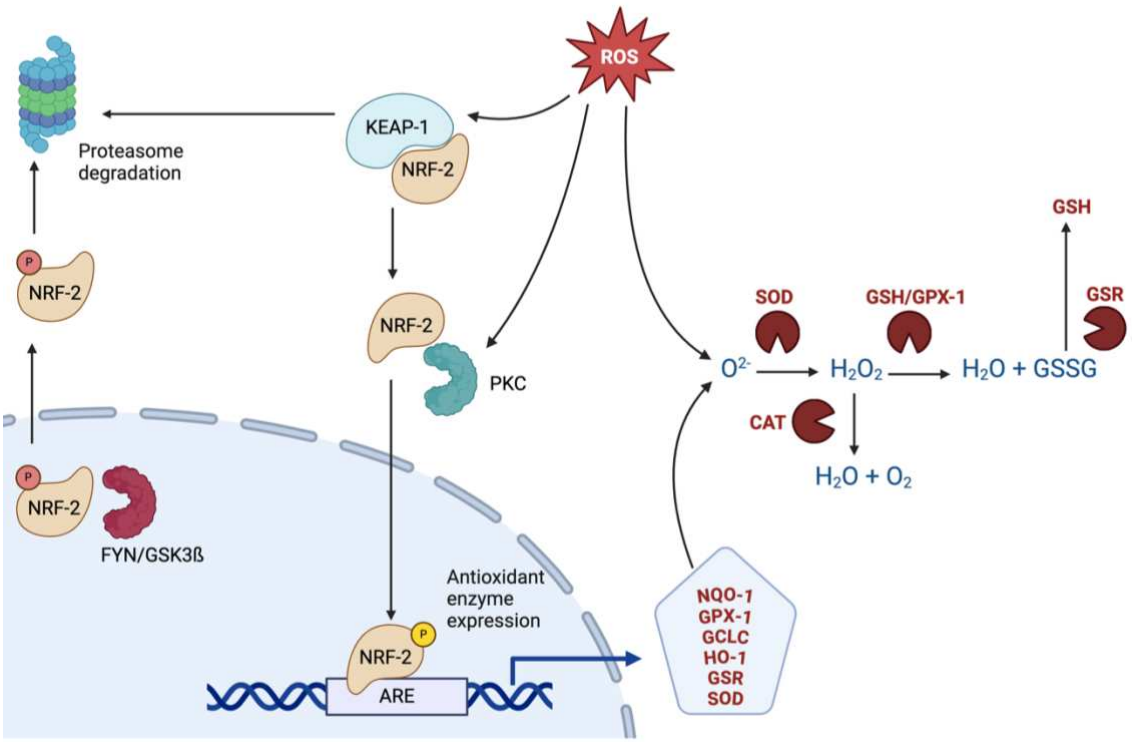

Figure 1.3: Antioxidative stress defense mechanisms. Under eustress conditions, NRF-2 is bound to KEAP-1 in the cytoplasm, which promotes its degradation via the proteasome. Under oxidative stress conditions, KEAP-1 releases NRF-2 which is phosphorylated by PKC at Serine 40, stabilizing and promoting its nuclear translocation. In the nucleus, pNRF-2 binds to the ARE and activates the transcription of several antioxidant genes. Among them SOD converts O_2^- to H_2O_2, which is then either degraded to water by CAT or reduced to water by GPX, together with the oxidation of 2 GSH molecules to form GSSG. The GSSG can ultimately be reduced back to GSH by GSR. Following its nuclear activation, NRF-2 is phosphorylated by GSK-3β or Fyn kinase to enable its transport outside the nucleus for degradation in the proteasome [23,31,33]. ARE = antioxidative response element, CAT = catalase, GCLC = glutamate-cysteine ligase catalytic subunit, GPX-1 = glutathione peroxidase 1, GSH = glutathione, GSK-3β = glycogen synthase kinase 3β, GSR = glutathione reductase, HO-1 = heme oxygenase 1, KEAP-1 = Kelch-like ECH-associated protein 1, NQO-1 = NADPH dehydrogenase (quinone)-1, NRF-2 = nuclear factor erythroid 2-related factor 2, PKC = phosphokinase C, ROS = reactive oxygen species, SOD = superoxide dismutase. Adapted from Brieger *et al.* and Kaspar *et al.,* [23,31]. Figure made with BioRender.

Once inside the nucleus, activated NRF-2 binds to the antioxidative response element (ARE) to activate the transcription of several antioxidant genes, including those involved

in the TRX pathway and GSH system (GSR, GSH-synthesizing GCL subunits GCLC (catalytic subunit) and GCLM (regulatory subunit)) [34]. NRF-2 also upregulates key ROS-detoxifying enzymes, such as SOD, NQO-1 and HO-1 [33,35].

To investigate the antioxidative defense mechanisms mentioned above, a hiPSC-based model was used in this work, as detailed in the following section.

1.4 Generation of human-induced pluripotent stem cells

Stem cells are defined by two important features: self-renewal and differentiation. They have the ability to multiply without undergoing senescence and to preserve the potential to differentiate into several specialized cell types [36]. Stem cell potency depends mainly on the stage of embryonic development. Following the fertilization of the egg, cells emerging from the first few divisions are totipotent and therefore able to produce all cell types of a developing organism, including both embryonic and extraembryonic (placenta) tissues. In contrast, pluripotent stem cells which originate either from the inner cell mass of the blastocyst or from primordial germ cells, can only produce cells of the embryo itself and cannot form extraembryonic tissues. Nevertheless, they retain the potential to differentiate into any cell type within the body. Stem cells cultured from these structures are called embryonic stem cells (ESC) and embryonic germ cells, respectively [37].

Due to the ethical considerations regarding the use of ESC in research, S. Yamanaka's groundbreaking discovery marked a turning point in the field. He was awarded a Nobel Prize for his studies on reprograming adult cells into embryonic-like cells, called human-induced pluripotent stem cells (hiPSC). This process relies on the ectopic expression of four key transcription factors *OCT-3/4, SOX-2, KLF-4* and *c-MYC*, introduced into human fibroblasts by viral transduction. The expression of these transcription factors, also known as Yamanaka factors, reverts differentiated cells back into highly immature cells similar to ESC [38]. The classical markers of pluripotency now include *OCT-3/4, NANOG* and *SOX-2*, which are important regulators of stem cell identity and are suppressed upon cell differentiation [39]. The hiPSC-based models hold a great potential in the research field as outlined in the following section.

1.5 hiPSC-based modeling

Drug-induced nephrotoxicity is responsible for about 20 % of acute kidney injury (AKI) cases. The latter are usually diagnosed by elevated blood levels of urea and creatinine. The most frequent form of intrarenal AKI is acute tubular necrosis, since the proximal tubule is the most vulnerable segment given its high metabolic activity. This highlights

the need for more efficient drug screening models, as the majority of the nephrotoxic effects observed during clinical trials remain undetected in preclinical testing [40].

Traditional *in vitro* drug screening methods rely on either animal models, human proximal tubule epithelial cells (hPTEC), or immortalized cell lines. Despite being very informative, animal models raise ethical concerns and often lack translational capacity due to interspecies differences. Indeed, human and animal physiologies can differ significantly. For instance, the anticoagulant warfarin and the anti-inflammatory drug ibuprofen are both widely used in humans but were shown to be toxic to rats [41]. Freshly isolated hPTEC could be more predictive of human responses as they retain *in vivo* phenotypes; however, they often undergo dedifferentiation and phenotype loss after few passages and lose their physiological relevance. For example, hPTEC failed to detect the nephrotoxic effects of the antiviral drug tenofovir, likely due to the lack of expression of OAT-1 [42].

In order to overcome the limitations of primary cell cultures, immortalized cells like human kidney cells (HK-2), renal proximal tubule epithelial cells immortalized by human telomerase reverse transcriptase (RPTEC/TERT1), and conditionally immortalized human cells (ciPTEC-hTERT) have been developed. However, immortalized cells frequently undergo alterations in function and morphology and often suffer from chromosomal instability in comparison to hPTEC. They tend to dedifferentiate and acquire non-tubule characteristics. Additionally, compared to hPTEC, they express elevated basal levels of injury markers, which further limits their suitability for predictive nephrotoxicity testing [40,42–44].

In contrast, hiPSC can be derived from easily accessible cell types (like skin fibroblasts), and cultured for extended passages. This provides an unlimited source of cells that are capable of differentiating into any cell type. The hiPSC offer new opportunities in regenerative medicine, as patient-derived hiPSC could be differentiated into mature cells and reintroduced into the same patient. These “patient-specific” cells address both ethical concerns and the risk of immune rejection associated with ESC. Moreover, guided hiPSC differentiation protocols that mimic developmental processes generate tissue architecture and function that replicate *in vivo* organs. These hiPSC-derived tissues or organoids could help overcome interspecies differences observed in animal models and reduce costs in preclinical and clinical phases of drug development by excluding the harmful compounds and establishing more accurate toxicity end points. Importantly, hiPSC-based models align with the 3Rs (replace, reduce and refine) principles of animal testing and meet societal demands of reducing animal usage in research [42].

1.6 Nephrotoxic substances

1.6.1 Cisplatin

Cisplatin is a potent platinum-based chemotherapeutic agent, widely used in the treatment of a broad spectrum of malignancies. Its anticancer activity is due to its property to bind to DNA and to form intra and interstrand cross links, particularly in rapidly dividing cells, like tumors. The resulting DNA damage leads to cell cycle arrest and apoptosis, which makes cisplatin a cornerstone in standard antineoplastic regiments in many cancers including those of the head, neck, lung, testis, ovary and breast [45,46]. However, its clinical use is limited by its significant nephrotoxic effects, with up to 20 % of acute renal failure cases in hospitalized patients are due to cisplatin therapy [47]. Nephrotoxicity primarily occurs due to increased uptake and activation of cisplatin within the PTEC [46].

Cisplatin is predominantly cleared from the body via the kidneys through glomerular filtration and tubular secretion [46]. In the first 24 h after cisplatin administration, over 50 % of the drug is eliminated in the urine, therefore cisplatin concentrations in the renal cortex reach several times higher levels than those in the plasma [48]. The drug accumulates particularly in PTEC because of the presence of different transport proteins, like OCT-2, OAT-1 and OAT-3 [14,18]. In addition, copper transporters-1/2 (CTR-1 and CTR-2), which are involved in cellular copper homeostasis, have been shown to influence the cellular sensitivity to cisplatin [13,49,50].

Once in the bloodstream, cisplatin undergoes initial biotransformation, then it is metabolized by brush border enzymes into cysteine conjugates in the tubular lumen before the internalization into PTEC [46]. Intracellularly, platinum-cysteine conjugates are converted into reactive thiols that bind to cytosolic proteins and DNA, and cause the death of the cells [51].

Despite the non-proliferative nature of the PTEC *in vivo*, cisplatin is a potent nephrotoxin with nephrotoxic side effects observed in 25-30% of treated patients [52,53]. Factors that contribute to this toxicity include enhanced cisplatin uptake in PTEC by different transporters, cisplatin-induced reduction in sodium-dependent glucose and amino acid transporters [54] and the metabolism of cisplatin to glutathione and cysteinyl-glycine conjugates [55]. In fact, mitochondrial DNA (mtDNA) is also very sensitive to cisplatin because of the relatively limited DNA repair mechanisms in mitochondria [56]. The role of mitochondrial injury in cisplatin toxicity has been documented in several works. For example, cisplatin cytotoxic effects were observed in enucleated cells and are reduced

in cells depleted from their mtDNA (rho0 cells) [57,58]. Mitochondrial damage induces an increase in ROS production and tubular apoptosis, which represent key pathological features of AKI and CKD [51]. This evidence indicates that cisplatin's toxicity extends beyond nuclear DNA damage and includes other mechanisms, like oxidative stress triggered by ER stress and mtDNA damage, particularly due to the high mitochondrial density in PTEC [57,59,60]. **Figure 1.4** provides a summary of cisplatin uptake and toxicity in PTEC.

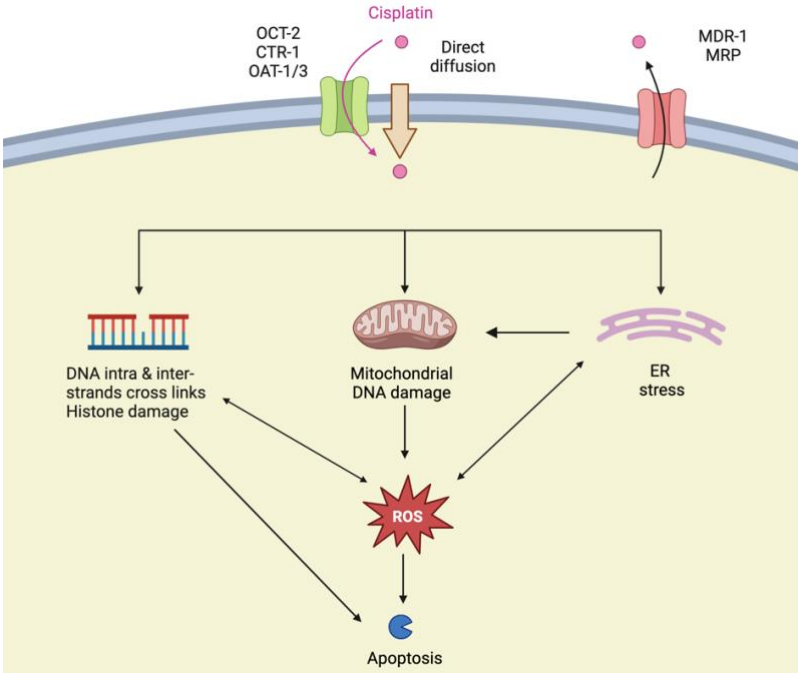

Figure 1.4: Cisplatin uptake and toxicity in PTEC. Cisplatin accumulates inside PTEC via OCT-2, OAT-1/3 and CTR-1 [14,46]. Inside the cell, cisplatin induces nuclear and mitochondrial DNA damage. It also triggers oxidative stress and ROS production via ER stress and mitochondrial dysfunction and ultimately leads to apoptosis [56,57]. To mitigate cisplatin accumulation, PTEC used efflux proteins like MRP and MDR-1 to facilitate its urinary excretion [16,18]. CTR-1 = copper transporter 1, ER = endoplasmic reticulum, MDR-1 = multidrug resistance protein 1, MRP = multidrug resistance-associated proteins, OAT-1/3 = organic anion transporter 1/3, OCT-2 = organic cation transporter 2, PTEC = proximal tubule epithelial cells, ROS = reactive oxygen species. Adapted from Miller *et al.,* [46]. Figure made with BioRender.

1.6.2 Cyclosporin A

Cyclosporin A (CsA) is an immunosuppressive agent from the calcineurin inhibitor family, commonly used to prevent immune-mediated transplant rejection and reduce relapse rates in auto-immune diseases. Its immunosuppressive action occurs after entering T-helper lymphocytes via passive diffusion, where it binds to cyclophilin to form a complex that inhibits the phosphatase activity of calcineurin. This inhibition impairs dephosphorylation and nuclear translocation of nuclear factor of activated T-cells (NFAT), so that transcription of key cytokines like interleukin-2 (IL-2) is prevented, and

therefore the activation and proliferation of T-cells is suppressed [61–63]. Although these effects are therapeutically beneficial, CsA treatment is often followed by severe acute and chronic nephrotoxic side effects [64].

CsA is a lipophilic compound, absorbed in the gastrointestinal tract through bile salts and transported in plasma by binding to lipoproteins. After entering the bloodstream, CsA undergoes broad tissue diffusion and accumulates in many organs like the liver, bone marrow, lymph nodes and kidneys. CsA is metabolized primarily in the liver and excreted via the biliary route [65]. In renal tubule cells, MDR-1 is the principal mechanism for CsA excretion. The interindividual variability in its expression and function may influence the susceptibility to CsA nephrotoxicity [61].

The nephrotoxic effects of CsA on tubule epithelial cells are primarily mediated by the induction of apoptosis, through oxidative stress following mitochondrial damage and ER stress [66,67]. ER stress plays a critical role in the development of parenchymal fibrosis by stimulating the production of transforming growth factor-beta (TGF-β) [68–70]. TGF-β overproduction and cellular immunosuppression were also associated with carcinogenic effects of CsA [71,72]. Additionally, endothelial dysregulation contributes to CsA-induced fibrogenesis. By disturbing the balance between vasoconstrictors (like endothelin, thromboxane and angiotensin II) and vasodilators (like prostaglandins and nitric oxide), CsA induces vasoconstriction of both afferent and efferent glomerular arterioles. This vasoconstriction leads to tubular hypoperfusion, ischemia and interstitial fibrosis and is often associated with systemic hypertension [61,62]. In **Figure 1.5** the mechanisms of action of CsA and its PTEC toxicity are illustrated.

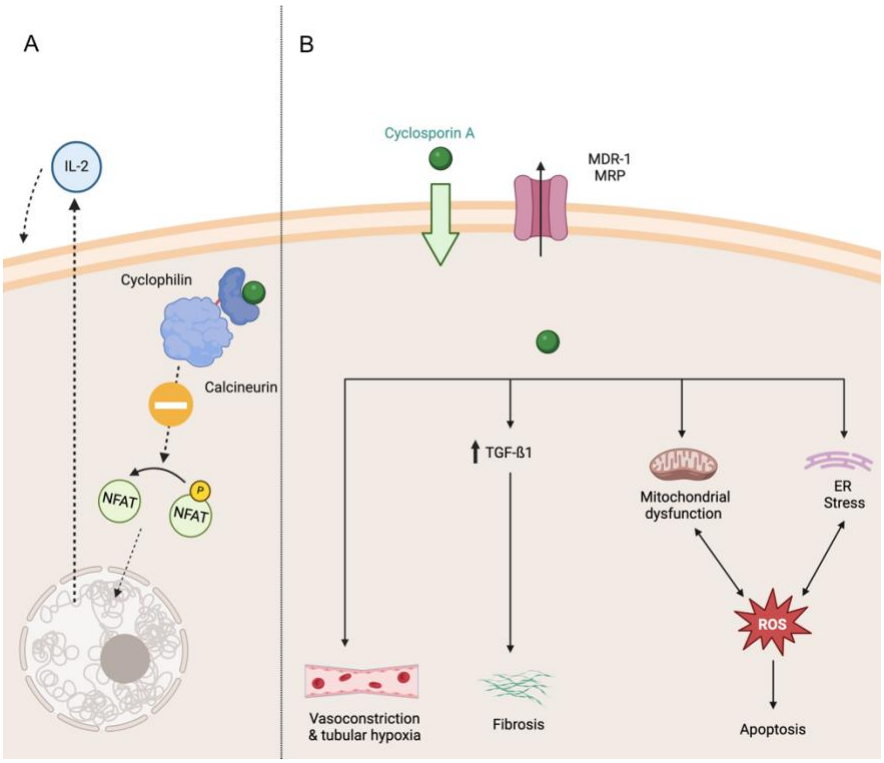

Figure 1.5: Mechanism of action and toxicity of cyclosporin A in PTEC. CsA enters cells via passive diffusion. Upon entry within T helper cells **(A)**, CsA binds to cyclophilin and inhibits the phosphatase activity of calcineurin. NFAT dephosphorylation and nuclear translocation is inhibited, preventing the transcription of IL-2 and impairing T cell activation and proliferation [61]. **(B)** In PTEC, CsA accumulation induces oxidative stress due to mitochondrial damage and ER stress and ultimately leads to apoptosis. CsA contributes to renal parenchymal fibrosis through TGF-β overproduction [66,68,69]. CsA also induces endothelial dysregulation through vasoconstriction of both afferent and efferent glomerular arterioles, resulting in tubular hypoperfusion, ischemia and interstitial fibrosis. To mitigate CsA accumulation, PTEC use efflux proteins like MDR-1 and MRP to facilitate its excretion into the urine [17,61]. CsA = cyclosporin A, ER = endoplasmic reticulum, MDR-1 = multidrug resistance protein 1, MRP = multidrug resistance-associated proteins, NFAT = nuclear factor of activated T cells, PTEC = proximal tubule epithelial cells, ROS = reactive oxygen species, TGF-β= transforming growth factor-β. Adapted from Wu *et al.* [64]. Figure made with BioRender.

1.6.3 Hydrogen peroxide (H_2O_2)

H_2O_2 is a natural byproduct of oxygen metabolism in aerobic cells and is categorized as ROS. It is a small, neutral molecule that can diffuse freely through cell membranes, although specific aquaporins, known as peroxiporins, have been shown to facilitate its translocation across membranes. The primary intracellular sources of H_2O_2 include the mitochondrial respiratory chain, the ER, the peroxisomes and the enzymatic activity of NADPH oxidase [24,73].

At physiological levels or oxidative eustress, H_2O_2 acts as a redox signaling molecule that modulates redox-sensitive phosphatases and the activity of different transcription factors. This redox signaling affects important cellular processes like morphology, proliferation and recruitment of immune cells [22,73]. To maintain the oxidative eustress

balance, H_2O_2 is rapidly reduced to water by enzymatic systems like CAT and GPX, along with the activation of the master switch NRF-2 system, as illustrated in **Figure 1.3** [24,74].

However, when the antioxidant defense mechanisms are overwhelmed, H_2O_2 induces oxidative stress or distress by generating highly reactive hydroxyl radicals. These radicals induce the oxidation of lipids, proteins and DNA and lead to growth arrest and cell death as illustrated in **Figure 1.6** [24,73,74]. Indeed, due to its potent oxidative properties, H_2O_2 is also used at higher concentrations as an antiseptic [75].

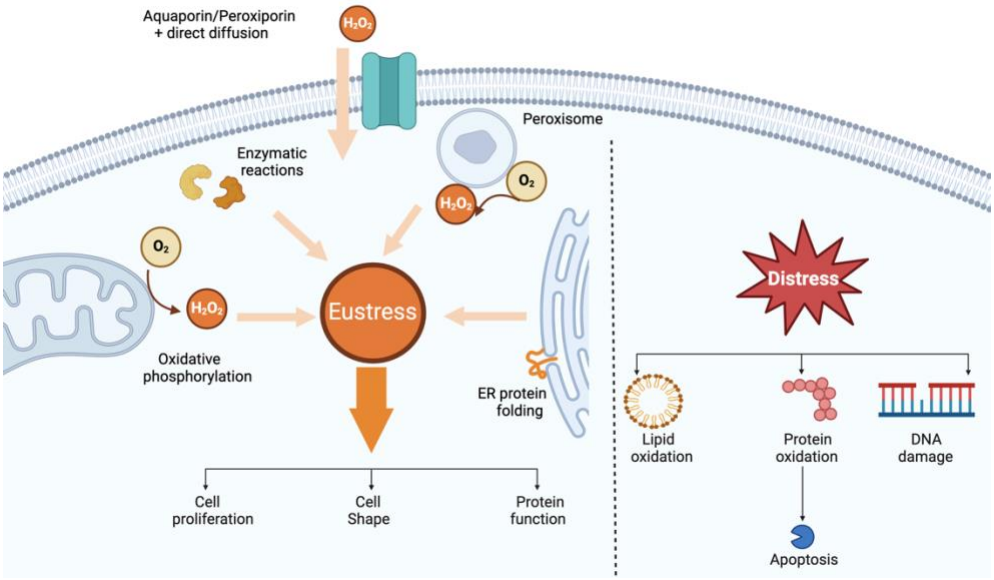

Figure 1.6: Endogenous sources of H_2O_2 and its toxicity. H_2O_2 enters cells via peroxiporins or diffuses freely through cell membranes. The primary intracellular sources of H_2O_2 include the mitochondrial respiratory chain, the ER, the peroxisomes and the enzymatic activity of NADPH oxidase. At physiological levels or oxidative eustress, H_2O_2 acts as a redox signaling molecule and modulates redox-sensitive phosphatases and the activity of various transcription factors. Under oxidative distress, H_2O_2 generates highly reactive hydroxyl radicals and induces lipid, protein and DNA oxidation which could lead to cell death [24,73]. ER = endoplasmic reticulum, H_2O_2 = hydrogen peroxide. Adapted from Sies *et al.* [24]. Figure made with BioRender.

2 Objective

Drug-induced nephrotoxicity is a major challenge for both researchers and clinicians. From a research perspective, significant efforts are dedicated to developing preclinical models capable of detecting renal adverse effects at an early stage. From a clinician perspective, physicians still face challenges with drug-induced AKI and the silent progression and chronification of acute lesions, despite normal levels of traditional injury markers. Therefore, in order to gain more knowledge about these challenges, a hiPSC-based model was used in this work, with a special focus on the proximal tubule, as it is the most frequently involved segment in intrinsic renal failure [40].

The aim of this thesis was to generate hiPSC-derived proximal tubular epithelial-like cells (PTELC) and study the effects of toxins at different stages of differentiation. To achieve this, a one-step differentiation protocol adapted from Kandasamy *et al*. (2015) was used to differentiate two hiPSC lines (b4 and UM51) into PTELC [76]. The differentiation outcomes were compared with RPTEC/TERT1 and PTELC generated from another hiPSC line (F4) of our research group, as well as data from the literature [77].

The differentiation efficiency was evaluated through the analysis of proliferation rate changes and the expression of specific PTEC markers and transporters through quantitative reverse transcription polymerase chain reaction (qRT-PCR), immunostaining and Western blot. The functionality of the PTELC was confirmed by albumin uptake assay. Dose-response experiments were conducted after treatment with known nephrotoxins at different stages of differentiation: hiPSC, differentiating hiPSC and differentiated hiPSC. The drugs used included cisplatin (a genotoxic nephrotoxin), CsA (a non-genotoxic nephrotoxin) and H_2O_2 (an oxidative stress inducer). Subsequently, the effects of these toxins on proliferation rates were assessed at different stages of differentiation, and oxidative stress responses following cisplatin treatment were investigated via qRT-PCR, immunostaining and GSH assay.

This work was designed to contribute to the global efforts of the scientific community in advancing the understanding of human pathophysiology, in order to promote safer drugs within the framework of the 3Rs principles.

3 Materials and methods

3.1 Materials

3.1.1 Cell lines and cell culture media

In this study, two different hiPSC lines were used. The first, referred to as b4-hiPSC, was isolated from human neonatal foreskin fibroblasts through retroviral transfection, after inducing the expression of a set of four defined transcription factors: *OCT-3/4, SOX-2, KLF-4,* and *c-MYC* [78]. The second hiPSC line was obtained from reprogrammed renal progenitor cells derived from the urine of a 51-year-old African male (UM51). Reprogramming was achieved by nucleofection of a combination of two episomal-based plasmids, expressing *OCT-3/4, SOX-2, NANOG, LIN-28, c-MYC and KLF-4* transcription factors. The generated hiPSC line will further be referred to as UM51 [79].

Both hiPSC lines were generously provided by Prof. James Adjaye from the Institute of Stem Cell Research and Regenerative Medicine (ISRM) at Düsseldorf university hospital, Germany. During the experiments, both stem cell lines were handled under the same conditions. Two culture wells were coated with a soluble form of basement membrane matrix (Geltrex) and the stem cells were cultured in StemMACS TM iPS-Brew XF. The differentiation protocol was performed utilizing renal epithelial growth medium (REGM) supplemented by several growth factors and additives.

Detailed information regarding the media and supplements used in the experiments are summarized in **Table 3.1**.

Table 3.1: Cell culture media and supplements.

Name	Company	Catalogue number
BMP (Bone Morphogenetic Protein) -2	Sigma-Aldrich (St.Louis, MO, USA)	B1814
BMP-7	Thermo Fisher Scientific (Waltham, MA, USA)	PHC7204
DPBS -/- no calcium, no magnesium	Gibco™ Thermo Fisher Scientific (Waltham, MA, USA)	12559069
Dulbecco's Modified Eagle Medium (DMEM) - high glucose	Sigma-Aldrich (St. Louis, MO, USA)	D0822

Geltrex™ Reduced Growth Factor Basement Membrane Matrix	Gibco™ Thermo Fisher Scientific (Waltham, MA, USA)	A1413202
Renal Epithelial Cell Growth Medium (REGM) Bulletkit	Lonza (Basel, Switzerland)	CC-3190
StemMACS™ Cryo-Brew	Miltenyi Biotec (Bergisch Gladbach, Germany)	130-109-558
StemMACS™ iPS-Brew XF	Miltenyi Biotec (Bergisch Gladbach, Germany)	130-104-368
StemPro Accutase Cell Dissociation Reagent	Thermo Fisher Scientific (Waltham, MA, USA)	A11105-01
Y-27632 dihydrochloride ROCK - Inhibitor	Sigma-Aldrich (St. Louis, MO, USA)	Y0503

3.1.2 Kits

Table 3.2: Listing of kits and assays used.

Name	Company	Catalogue number
EdU-Click-488	Baseclick GmbH (Tutzingen, Germany)	BCK-EdU488
DC™ Protein Assay Kit II	Bio-Rad Laboratories (Hercules, CA, USA)	5000112
GSH/GSSG Ratio Detection Assay Kit II	Abcam (Cambridge, UK)	ab205811
High-Capacity cDNA Reverse Transcription Kit	Thermo Fisher Scientific (Waltham, CA, USA)	4368814
RiboLock Rnase Inhibitor 40U/µl	Thermo Fisher Scientific (Waltham, CA, USA)	EO0382
RNase free DNase Set	Qiagen (Venlo, Netherlands)	79254
RNeasy Mini Kit	Qiagen (Venlo, Netherlands)	74106
SensiMix SYBR® Hi-ROX	Bioline GmbH (Luckenwalde, Germany)	QT605-05

3.1.3 Chemicals

Table 3.3: Listing of chemicals.

Name	Company
Albumin-Fluorescein-Isothiocyanat-Conjugate	Sigma-Aldrich (St. Louis, MO, USA)
β-Mercaptoethanol	Gibco™ Thermo Fisher Scientific (Waltham, MA, USA)
Bovine Serum Albumin (BSA)	Sigma-Aldrich (St. Louis, MO, USA)
Ciclosporin A	Enzo Life Sciences (Farmingdale, NY, USA)
Cisplatin	Accord Healthcare GmbH (München, Germany)
Dimethyl sulfoxide (DMSO)	Carl Roth GmbH + Co. KG (Karlsruhe, Germany)
Hydrogen peroxide H_2O_2 30 %	Carl Roth GmbH + Co. KG (Karlsruhe, Germany)
Phenylmethylsulfonylfluoride (PMSF)	Sigma-Aldrich (St. Louis, MO, USA)
Ponceau S	Sigma-Aldrich (St. Louis, MO, USA)
Powdered milk	Carl Roth GmbH + Co. KG (Karlsruhe, Germany)
Sodium dodecyl sulfate (SDS)	Carl Roth GmbH + Co. KG (Karlsruhe, Germany)
Tetramethylethylenediamine (TEMED)	Carl Roth GmbH + Co. KG (Karlsruhe, Germany)
Tris base	Sigma-Aldrich (St. Louis, MO, USA)
TWEEN® 20	Sigma-Aldrich (St. Louis, MO, USA)
Vectashield with DAPI	Vector Laboratories (Burlingame, CA, USA)

3.1.4 Appliances

Table 3.4: Listing of laboratory devices.

Appliance	Name	Company
Absorbance measurement plate reader	Tecan infinite 200 pro	Tecan (Männedorf, Switzerland)
Bright field microscope	Axiovert 40 CFL	Zeiss (Oberkochen, Germany)
Chemiluminescence protein detection	ChemiDoc™ Touch Imaging System	Bio-Rad Laboratories (Hercules, CA, USA)
Fluorescence microscope	Olympus BX43F Upright Microscope; camera: Olympus XC10	Olympus (Shinjuku, Tokio, Japan)
Gel electrophoresis for western blot	Mini-PROTEAN® Tetra Cell Elektrophorese System	Bio-Rad Laboratories (Hercules, CA, USA)
Incubator	Binder CB 53	Binder (Tuttlingen, Germany)
PCR cycler	T Personal Thermal Cycler	Biometra (Jena, Germany)
qRT-PCR	CFX96 Real-Time System and C1000 Thermal Cycler	Bio-Rad Laboratories (Hercules, CA, USA)
Spectrophotometer	Tecan Sunrise™	Tecan (Männedorf, Switzerland)
Spectrophotometer (Nanodrop)	NanoVue Plus	GE Healthcare Life Sciences (Buckinghamshire, UK)
Ultrasonic homogenizer (sonifier)	Q120AM	Active Motif® (CA, USA)

3.1.5 Software

Table 3.5: Listing of Software.

Software	Developer
Bio-Rad CFX Manager 3.1	Bio-Rad Laboratories (Hercules, CA, USA)
GraphPad Prism 6	GraphPad Software, Inc. (La Jolla, CA, USA)
ImageJ 1.53t	Wayne Rasband, NIH (Bethesda, MD, USA)
Image Lab™ Touch Software 6.0.1.	Bio-Rad Laboratories (Hercules, CA, USA)

3.1.6 Oligonucleotides

Table 3.6: Listing of primers used for quantitative real-time PCR. ACTB = β-actin, AQP-1 = aquaporin 1, CAD-16 = cadherin 16, CD-13 = alanyl aminopeptidase N, CTR-1/2 = copper transporter 1/2, CUBN = cubilin, E-CAD = epithelial cadherin, GCLC = glutamine-cysteine ligase catalytic subunit, GLUT-5 = fructose transporter, GPX-1 = glutathione peroxidase 1, GSR = glutathione reductase, HO-1 = heme oxygenase 1, MCT-1 = monocarboxylate transporter 1, MDR-1 = multidrug resistance protein 1, MEG = megalin, MRP-1 = multidrug resistance-associated protein 1, NANOG = homeobox protein, N-CAD = neural cadherin, NQO-1 = NADPH dehydrogenase quinone 1, NRF-2 = nuclear factor erythroid 2-related factor 2, OAT-1/3 = organic anion transporter 1, OATP = organic anion transporting polypeptides, OCT-2 = organic cation transporter 2, OCT-3/4 = octamer-binding transcription factor 3/4, OCTN-2 = organic cation/carnitine transporter 2, PEPT-1/2 = peptide transporter 1/2, RPL-32 = Ribosomal Protein, SGLT-2 = sodium/glucose cotransporter 2, SOX-2 = sex determining region Y-box 2, VIT-D3 = vitamin D 25-hydroxylase, ZO-1 = zonula occludens 1.

Gene	Forward	Reverse
ACTB	GAGCACAGAGCCTCGCC	TCATCATCCATGGTGAGCTGG
AQP-1	CATCCTCTCAGGCATCACCTC	CACACCATCAGCCAGGTCATTG
CAD-16	AGCACGTGTGAAGTCGAAGT	ACTGAGGTTCTGGGAAGTGATG
CD-13	TGGCCACTACACAGATGCAG	CTGGGACCTTTGGGAAGCAT
CTR-1	TGATGCCTATGACCTTCTAC	GAATGCTGACTTGTGACTTAC
CTR-2	CTGTACTGTATGAAGGCATC	AAAGTGACACAAATACCACC
CUBN	TAGCTTCGTGAAGGTGTGGG	GACTGGAAGACGGCAGTGAA
E-CAD	CAGGACCAGGACTTTGACTT	AGATACCGGGGGACACTCAT
GCLC	ACGGAGGAACAATGTCCGAG	CAGGACAGCCTAATCTGGGAA
GLUT-5	GCCAAAGTGCACCCAGAATG	GTCAGCCTCCCTTCCTTCAT
GPX-1	TTGGTGATTACTGGCTGC	TGATATTCAGCACTTTATTCTTAGTAG
GSR	ATAGCTGCTGGCCGAAAACT	CTTCCGTGAGTCCCACTGTC

HO-1	CAACAAAGTGCAAGATTC	AGAAAGCTGAGTGTAAGG
MCT-1	CTCCGGGGTTGGGAGACTT	TACTGCTGATAGGACCTCCACC
MDR-1	AGTCGGAGTATCTTCTTC	TTGAATAGCGAAACATTGA
MEG	GCCAGTGGCCAAGAATGTGA	TCCGCGTCATCTGAACAGTC
MRP-1	CTCCTGTGGCTGAATCTGGG	TCGGGGATGGAGAAGGTGAT
NANOG	ACCTCAGCTACAAACAGGTGAA	AAAGGCTGGGGTAGGTAGGT
N-CAD	AGGCTTCTGGTGAAATCGCA	GCAGTTGCTAAACTTCACATTGAG
NQO-1	GGCCGATTCAGAGTGGCAT	CCAGACGGTTTCCAGACGTT
NRF-2	GCAACTCCAGAAGGAACAGG	AGGCATCTTGTTTGGCAATG
OAT-1	AGTATGGAGGTACTCCGGGC	GCATGGAGAGGCAGAGGAAG
OAT-3	CTTTGTGCCCTTGGACTTGC	GGAAGAGGCAGCTGAAGGAG
OATP	GCCGTCACGCAAGGTATTG	GGCCAGTCAGGGAACTCTTC
OCT-2	GAAGCCGAAAATATGCAAAG	TGCAGGGATTTCTACTTTTG
OCT-3/4	ACCCACACTGCAGCAGATCA	CCACACTCGGACCACATCCT
OCTN-2	CACCATTGTGACCGAGCAAG	AGCAGGCTTCTTTCCCATCC
PEPT-1	CAAGTGCATCGGTTTTGCCA	CTCTTTAGCCCAGTCCAGCC
PEPT-2	CTGGGAGGACAAGTGGTACA	AGTCCGTTCCTCTGCATGTT
RPL-32	GTTACGACCCATCAGCCCTTG	CATGATGCCGAGAAGGAGATGG
SGLT-2	CAGTCTCCGGCATAGCAAGG	GGCCTGGGGCTCATTCATC
SOX-2	AGGATAAGTACACGCTGCCC	TAACTGTCCATGCGCTGGTT
VIT-D3	GGCTTTGGCCCAGATCCTAA	GTCTTGGGTCTAACTGGGGC
ZO-1	GAGAGGATTTGTCCGCTCAG	AGGCCTCAGAAATCCAGCTT

3.1.7 Antibodies

Table 3.7: Listing of antibodies. AQP-1 = aquaporin 1, CTR-1 = copper transporter 1, E-CAD = epithelial cadherin, GAPDH = glyceraldehyde 3-phosphate dehydrogenase, NRF-2 = nuclear factor erythroid 2-related factor 2, OCT-2 = organic cation transporter 2, OCT-3/4 = octamer-binding transcription factor 3/4, pNRF-2 = phosphorylated NRF-2 at Ser-40, URO-10 = heat stable tubular antigen.

Protein	Order number	Company	Dilution
AQP-1	AB9566	Abcam (Cambridge, UK)	1:300
CTR-1	AB129067	Abcam (Cambridge, UK)	1:25
E-CAD	610181	BD biosciences (NJ, USA)	1:100
GAPDH	2118S	Cell Signalling	1:4000
NRF-2	SC-722	Santa Cruz biotech (Dallas, USA)	1:500
pNRF-2	AB76026	Abcam (Cambridge, UK)	1:500
OCT-2	MB59600162	Biozol	1:500
OCT-3/4	AB183900	Abcam (Cambridge, UK)	1:100
URO-10	SC-58889	Santa Cruz biotech (Dallas, USA)	1:1000

3.2 Methods

3.2.1 Cell biology methods

3.2.1.1 Culturing and passaging of hiPSC

In order to reduce the risk of drug-induced phenotypic alterations, no antibiotics were used in the stem cell culture medium of both cell lines [80]. Strict sterile conditions were maintained throughout the culture process, and prewarmed media reagents were always used. To ensure the best survival conditions, stem cells were passaged twice a week and regularly tested for mycoplasma contamination.

The first cell culture step involved coating each six-well plate with a 1 ml of mixture Geltrex (maintained on ice) dissolved in cold high-glucose DMEM without supplements. The plate was either incubated for 1 h at room temperature (RT) for immediate use or sealed with parafilm and stored at 4 °C for a maximum period of 7 days. During the incubation period, the Geltrex polymerizes on the bottom of the well. Afterwards, the medium was aspirated and 1.85 ml of StemMACS supplemented with 1 µl of 10 µM ROCK-inhibitor (rho-associated coiled-coil containing kinases) was added to enhance the cell survival during the first day after the passaging [81]. The plate was kept in the incubator at 37 °C and 5 % CO_2 (refer to **Figure 3.1**).

The passaging step *per se* was initiated when the cultured plate reached approximately 70 % confluency. The medium was then aspirated and preserved in a 15 ml tube. The cells were washed once with 1 ml sterile DPBS -/- (Dulbecco's Phosphate Buffered Saline without calcium and magnesium). After discarding the DPBS, the cells were incubated for 5 min in 1 ml DPBS at 37 °C and 5 % CO_2 to facilitate the detachment of adherent cells. Following gentle scraping with a spatula to preserve the colony organization of the cells, they were suspended in the previously aspirated medium and centrifuged at 38 g for 2 min at RT. The supernatant was discarded and the pellet resuspended in 900 µl StemMACS medium to achieve a 1:6 ratio. Finally, 150 µl of the suspension was added and equally distributed in each well of the 6-well plate prepared in the first step. The medium was changed daily without the addition of ROCK-inhibitor, with the option to skip one day on weekends by doubling the volume of medium in each well. After a few passages, some wells were frozen to maintain the stock, while the remaining wells were used for experiments up to the 10^{th} passage.

3.2.1.2 Freezing and thawing of hiPSC

The initial steps of the freezing protocol are similar to those described in the passaging procedure described in 3.2.1.1. The reason is that freezing the cells as aggregates is more favorable due to the increased cell-cell contacts with neighboring cells and results in a faster recovery compared to single cells [81]. After centrifugation and aspiration of the supernatant, the cells were resuspended in 1.8 ml of cryopreservation medium (StemMACS Cryo-Brew), transferred to a cryovial and frozen in CoolCell at -80 °C for up to 24 h. Then the cells were conserved in a liquid nitrogen tank at -196 °C for long-term storage.

Prior to thawing the cells, two wells of a 6-well plate were coated with Geltrex, as detailed in 3.2.1.1. They were; however, filled with 1.5 ml of StemMACS supplemented with 2 µl of 10 µM ROCK-inhibitor, then incubated at 37 °C and 5 % CO_2. The cryovial was removed from the liquid nitrogen tank, disinfected with 80 % ethanol and thawed in a 37 °C water bath till a fine crystal ice was remaining. The cell suspension in the tube was transferred to a 50 ml falcon then 5 ml of pre-warmed high-glucose DMEM without additives was added dropwise with gentle swirling. After sedimentation at 200 g for 5 min at RT, the supernatant was aspirated and the pellet resuspended with 1 ml StemMACS. Afterward, 0.5 ml of cell suspension was seeded into each well of a Geltrex-coated plate and cultured in an incubator at 37 °C and 5 % CO_2. Until the next passage, the cell culture medium was replaced on a daily basis.

3.2.1.3 Singularizing and differentiating of hiPSC

The differentiation of hiPSC into PTELC is based on a protocol adapted from Kandasamy *et al*. (2015) with slight modifications as illustrated in **Figure 3.1**. [76].

Initially, a Geltrex-coated 12-well plate was prepared as described in 3.2.1.1 and filled with 0.5 ml of a mixture of Geltrex and cold high glucose DMEM without supplements. After 1 h incubation at RT, the medium was discarded and 1 ml of REGM, containing 0.5 µl/well (10 µM) ROCK-inhibitor, was added. The plate was stored in the incubator until seeding.

The next step involved the singularization of a 70 % confluent well from a 6-well plate. Confluent hiPSC were washed once with DPBS and incubated in 1 ml StemPro Accutase cell dissociation reagent for 5 min at 37 °C and 5 % CO_2. StemPro Accutase, a combination of enzymes that have proteolytic, collagenolytic and DNase activities, was used, as it is gentler than Trypsin [81]. After dissociation of the cells, 2 ml of pre-warmed DMEM was added to stop the proteolytic reaction and the suspension was transferred to

a 15 ml tube. Cell counting was conducted by mixing 20 µl of the cell suspension with 20 µl of a 0.4 % trypan blue solution, enabling the discrimination between living cells and dead ones, since the compromised membrane integrity of the latter allows the dye to enter and consequently stain them blue [82]. A Neubauer counting chamber was used to determine cell viability.

Cell counting was carried out while centrifuging the cell suspension at 200 g for 4 min at RT. After discarding the supernatant, the cell aggregates were resuspended in fresh REGM. Subsequently, 750 cells/cm^2 were seeded per well into the Geltrex-coated plate and incubated overnight. After 24 h, the REGM without ROCK-inhibitor was supplemented with 10 ng/ml BMP-2 (Bone Morphogenic Protein-2) and 2.5 ng/ml BMP-7 and cultured under these conditions for 9 days with a daily change of medium for induction of differentiation towards PTELC. On day 9, differentiated cells were either exposed to nephrotoxin treatment or harvested for subsequent experiments.

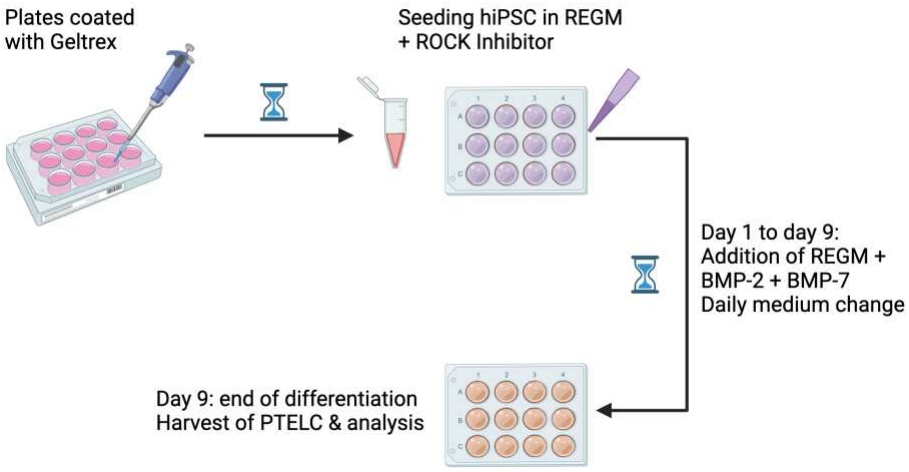

Figure 3.1: Protocol for the differentiation of hiPSC to PTELC. The seeding of singularized hiPSC on day 0 was conducted with REGM supplemented with 5 µM ROCK inhibitor. From day 1, the medium was changed daily with REGM without ROCK inhibitor but with BMP-2 and BMP-7 to drive the cells towards proximal tubular cells within 9 days of differentiation. BMP = bone morphogenetic protein, hiPSC = human induced pluripotent stem cells, PTELC = proximal tubular epithelial-like cells, REGM = renal epithelial cell growth medium, ROCK = rho-associated coiled-coil-containing protein kinase. Adapted from Kandasamy *et al.* [76]. Figure made with BioRender.

3.2.2 Molecular biology methods

3.2.2.1 RNA isolation and quantification

In order to achieve an RNA concentration of 200-2000 ng/µl sufficient for complementary DNA (cDNA) synthesis, each harvested sample (hiPSC or differentiated cells) required at least 3x10^5-1x10^6 cells. The cell number was determined after singularizing the cells with StemPro Accutase as described in 3.2.1.3. The resulting cell suspension underwent

centrifugation at 200 g, 4 °C for 5 min. The resulting pellet was washed with DPBS and transferred into a 1.5 ml Eppendorf on ice. Following another round of centrifugation under the same conditions, the supernatant was removed. The cell pellet was either frozen at -80 °C or immediately subjected to RNA isolation using RNeasy Mini Kit and RNase-free DNase Set of Qiagen, according to the manufacturer's instructions. The RNA concentration was quantified spectrophotometrically with the NanoVue Plus. Subsequently, the RNA was either stored at -80 °C or utilized immediately for cDNA synthesis.

3.2.2.2 Complementary DNA synthesis

The synthesis of cDNA was performed according to the protocol of the High-Capacity cDNA Reverse Transcription Kit in combination with the RiboLock RNase-Inhibitor according to the manufacturer's instructions. The compounds of the preparation mix are shown in **Table 3.8**.

Table 3.8: Preparation scheme for cDNA synthesis.

Reagent	Per sample [µl]
10x Puffer	2.0
25x dNTP-Mix (100 mM)	0.8
10x Random Primer	2.0
RiboLock RNase Inhibitor (40u/µL)	0.5
MultiScribe Reverse Transcriptase RT	1.0
RNase free H_2O	3.7
2000 ng RNA in RNase free H_2O	10
Total	20

The cDNA synthesis mix was transferred to the thermal cycler to allow the reverse transcriptase enzyme to synthesize the cDNA from the isolated RNA. The cDNA was then either stored at -20 °C or quantified directly using qRT-PCR.

3.2.2.3 qRT-PCR

The qRT-PCR is a potent molecular biology technique used to measure the levels of gene expression under different conditions or treatments. Following the reverse conversion of RNA into cDNA through transcriptase reverse enzyme, the resulting cDNA was enzymatically amplified via PCR. This amplification mirrors the expression levels of

the targeted genes in the sample. In this context, the objective was to relatively quantify mRNA expression of differentiation-associated markers and redox genes, with the use of the SensiMix SYBR Hi-ROX Kit. Briefly, 10.2 µl of a mixture of the synthesized cDNA and SYBR® Green (master mix 1) was pipetted into the wells of a 96-well PCR. Then, 9.8 µl of a mixture of each primer pair with highly purified PCR water (master mix 2) was added to each well (**Table 3.9**). The PCR plate was then inserted into the CFX96 Touch Real-Time PCR Detection System for amplification according to **Table 3.10**.

Table 3.9: Master Mix composition for qRT-PCR from cDNA templates.

Reagent	Concentration per well
cDNA	20 ng
SensiMix™ SYBR® Hi-ROX (2x)	1x
Forward Primers	0.25 µM
Reverse Primers	0.25 µM

Table 3.10: Real-time qRT-PCR program configuration.

Step	Temperature	Duration	
Initial denaturation	95	10 min	
Denaturation	95	15 s	x44 cycles
Primer hybridization	55	15 s	
Elongation	72	17 s	

Following the qRT-PCR analysis, the PCR plate was discarded as solid toxic waste and data were analyzed using BioRad CFX Manager software according to the manufacturer's instructions. The expression levels obtained for the genes of interest were first normalized to the mean expression of the housekeeping genes *ACT-β* and *RPL-32* and then to the control samples and expressed as a fold of this mean. Biologically relevant changes were defined as ≤ 0.5- and ≥ 2-fold changes in gene expression.

The gene-specific primer pairs utilized for amplification in this work (**Table 3.6**) were designed using NCBI (https://www.ncbi.nlm.nih.gov/nuccore/). These primer sets have been validated for specificity in qPCR using different cDNA concentrations.

3.2.3 Immunobiology methods

3.2.3.1 Immunocytochemistry

Immunofluorescence staining was performed to assess the expression of proximal tubule-related proteins and certain redox-associated response proteins in hiPSC and differentiated cells after cisplatin treatment. The proteins of interest were marked with protein-specific primary antibodies to which fluorescent secondary antibodies were then attached. The signal of the fluorescent antibodies was captured using a fluorescence microscope.

In this procedure, wells containing glass coverslips were coated with Geltrex, then hiPSC were seeded for differentiation as explained in 3.2.1.3. On differentiation day 9 (DiffD9), the coverslips were washed three times with PBS and fixed with 1 ml of 4 % cold formaldehyde/PBS for 15 min at RT. After fixation, the cells were washed three times for 5 min each with PBS and permeabilized with 0.3 % Triton in PBS for 10 min at RT. Following another three washes of 5 min each with PBS, the coverslips were incubated in a blocking buffer consisting of 5 % bovine serum albumin (BSA) in PBS for 1 h at RT to prevent unspecific binding of the primary antibody. Following the blocking step, the coverslips were incubated with primary antibodies in a humid chamber at 4 °C overnight in the dilutions indicated in **Table 3.7**. The next day, coverslips were washed three times with PBS for 5 min each to remove unbound primary antibodies. A fluorescence-conjugated secondary antibody (Alexa Fluor 488/550 goat polyclonal to mouse or rabbit) was applied at a 1:1000 dilution and incubated in the dark for 2 h. Nuclear DNA was stained with Vectashield containing 4′,6-diamidine-2-phenylindole (DAPI). Slides containing coverslips were sealed with nail polish and analyzed using an Olympus Bx43 fluorescence microscope.

3.2.3.2 EdU proliferation assay

To assess cellular proliferation during different differentiation stages and enable comparisons between hiPSC, hiPSC differentiating into PTELC on DiffD3 and hiPSC on DiffD9, the integration of fluorescent 5-ethynyl-2′-deoxyuridine (EdU) into S-phase cells was investigated using the EdU-Click-488 proliferation assay Kit, following the manufacturer's instructions.

EdU is a thymidine analogue that is integrated into DNA during DNA synthesis in proliferating cells. This integration is based on the click reaction, between the terminal

alkyne group of EdU in the major groove of DNA with an organic 6-Fluorescein azide dye in the presence of copper(I) ions [83].

In brief, hiPSC were seeded onto a Geltrex-coated culture plate with glass coverslips. The coverslips coated with hiPSC, DiffD3 and DiffD9 cells were incubated with 1 ml DMEM without phenol red supplemented with 1 µl (10 µM) EdU for 2 h at 37 °C. The cells were then washed three times with PBS and fixed in 1 ml of cold 4 % formaldehyde/PBS for 15 min at RT. After two washes with 1 ml of 3 % BSA/PBS, the cells were incubated with 1 ml of 0.5 % Triton-X/PBS for 20 min at RT. Meanwhile, the click cocktail was prepared mixing 379 µl of distilled water (dH_2O), 50 µl of 10x reaction buffer, 20 µl of catalyst solution, 1 µl of 10 mM 6-FAM azide and 50 µl of 10x buffer supplement, in this exact order. Following the incubation, the coverslips were washed and blocked three times with 3 % BSA/PBS for 5 min at RT. Subsequently, the coverslips were incubated in the click solution for 30 min at RT in the dark. Lastly, the coverslips were washed three times with 3 % BSA/PBS, then counterstained with Vectashield with DAPI and transferred to microscope slides and sealed with nail polish. For imaging, at least 200 cells were captured in dual-channel images through DAPI and fluorescein isothiocyanate (FITC) to detect fluorescent cells, using an Olympus Bx43 fluorescence microscope. The percentage of EdU-positive cells was calculated using ImageJ 1.53t.

3.2.4 Biochemistry methods - Western blot

3.2.4.1 Protein extraction

To further characterize the differentiation of hiPSC into PTELC, the expression of specific proximal tubule proteins was analyzed through western blotting.

First, after harvesting the cells, lysis was performed by adding to the cell pellet 100-150 µl of freshly prepared radioimmunoprecipitation assay (RIPA) buffer. The RIPA buffer included 1x protease inhibitor cocktail, 1x phosphatase inhibitor cocktail, and 1 mM phenylmethylsulfonyl fluoride (PMSF). Following 20 min incubation at RT, ultrasonic homogenization of cell lysates was carried out using an ultrasonic homogenizer (5 x 35 % amplitude, 2 sec pulse, 1 sec pause, 5 shocks, RT) to ensure effective degradation and solubilization of proteins. The resulting cell debris was centrifuged at 10.000 g, at 4 °C for 15 min, and the proteinaceous supernatant was transferred to a 1.5 ml Eppendorf tube. This tube could be either frozen at -80 °C or immediately subjected to protein determination.

3.2.4.2 Protein concentration determination

The protein concentration in the supernatant was determined using the DC™ protein assay based on the Bradford method, following the manufacturer's instructions. BSA standards were used for calibration, with RIPA buffer as the sample blank and dH_2O as the standard blank. In technical duplicates, 5 µl of the protein samples (1:5 dilution) and BSA standards were pipetted into the wells of a transparent 96-well flat-bottom plate. Subsequently, 25 µl of a 1:50 dilution of Reagent S in Reagent A was added to each well in addition to 200 µl of Reagent B. The reaction was incubated in the dark at RT for 15 min before measurement of light absorbance at 750 nm using a Tecan Infinite 200 pro spectrophotometer. Protein concentrations were determined by applying the linear regression formula derived from the BSA standard curve.

Next, 50 µg of the protein lysate was mixed with Roti-loading buffer in a heating block at 95 °C for 5 min. The sodium dodecyl sulfate (SDS) present in the buffer was used combined with heat to induce the denaturation of the three-dimensional structure of the proteins and coat them with negative charges. Simultaneously, the ß-mercapto-ethanol within the Roti-loading buffer further contributes to the denaturation of the protein conformation by cleaving the disulfide bridges between the peptides.

3.2.4.3 Sodium dodecyl sulfate-polyacrylamide gel electrophoresis

The previously isolated and denatured proteins were then separated by molecular weight through discontinuous sodium dodecyl sulfate-polyacrylamide gel electrophoresis (SDS-PAGE). The application of an electric field causes the migration of the negatively charged proteins and their separation according to their size and molecular weight through the pores of an acrylamide gel. The acrylamide gels used included a 5 % collection gel followed by a 10 - 12 % separation gel (**Table 3.11**). Protein separation occurred in a running buffer under a voltage of 10-30 mA. Gel electrophoresis was conducted using the MINI-Protean Tetra Cell Electrophoresis system and the PageRuler™ Plus Prestained Protein Ladder served as a reference to determine the size of the proteins.

Table 3.11: Solutions and gels prepared for western blot analysis.

Solution or gel	Components
1.5 M Tris base, pH 8.8	181.71 g Tris base in 1000 ml dH_2O pH = 8.8 Stored at 4 °C
1.5 M Tris base, pH 6.8	181.71 g Tris base in 1000 ml dH_2O pH = 6.8 Stored at 4 °C
6 % Collecting gel	5.5 ml dH_2O 1 ml 1.5 M Tris base, pH 6.8 1.3 ml acrylamide 30 % 160 µl SDS 10 % 80 µl TEMED 10 % 80 µl APS 10 % Stored at 4 °C
10 % Separation gel	7.8 ml dH_2O 5 ml 1.5 M Tris base, pH 8.8 6.7 ml acrylamide 30 % 200 µl SDS 10 % 80 µl TEMED 10 % 200 µl APS 10 % Stored at 4 °C
Blocking solution	5 % milk powder in TBST
Blotting buffer	0.025 M Tris base 0.192 M glycine 20 % (v/v) Methanol in 1000 ml dH_2O Stored at 4 °C
ECL solution	3 ml component A 30 µl component B 3 µl component C
ECL solution Component A	50 mg luminol 200 ml 0.1 M Tris HCl, pH 8.6 Stored in darkness at 4 °C
ECL solution Component B	11 mg para-coumaric acid in 10 ml DMSO Stored in darkness
ECL solution Component C	H_2O_2 30 % Stored at 4 °C
PBS (5-fold) pH 7.3 – 7.4	40.9 g NaCl 1.0 g KCl 8.9 g Na_2HPO_4 x $2H_2O$ 1.2 g KH_2PO_4
Ponceau S	0.15 % Ponceau S

	0.5 % acetic acid in dH_2O
Running buffer	25 mM Tris base 192 mM glycine 0.1 % (w/v) SDS in 1000 ml in dH_2O
Tris-buffered saline with Tween 20 (TBST)	60.1 g Tris-HCL 87.66 g NaCl 5 g Tween 20

3.2.4.4 Western blotting

After separating the proteins in SDS-PAGE, they were subsequently wet-blotted onto a nitrocellulose membrane using the Mini Trans-Blot® Cell System. The wet blotting process was conducted in a blotting buffer at 300 mA for 90 min. Afterwards, the nitrocellulose membrane was stained during a 1-minute incubation in Ponceau S solution to confirm the completion of protein transfer. Subsequently, the membrane was incubated in 5 % milk powder/Tris-buffered saline with Tween 20 (TBST) for 1 h to block nonspecific antibody binding. It was then incubated overnight with the primary antibody at 4 °C. The day after, following a series of washes with TBST, the membrane underwent incubation with a Horseradish peroxidase (HRP)-coupled secondary antibody (1 : 2000 in 5 % milk powder/TBST) for 2 h at RT. Following another round of TBST washes, the membrane was incubated with a luminol-containing chemiluminescence solution of the BM Chemiluminescence Blotting Substrate (POD) kit for 1 min at RT. The chemiluminescence intensity was captured using the ChemiDocTM Touch Imaging System and subsequently quantified using the Image Lab™ software.

3.2.5 Transport function analysis - albumin uptake assay

One of the typical transport properties of PTEC is albumin uptake. To assess the functionality of the hiPSC-derived PTELC, their ability to transport and perform endocytosis of albumin was investigated. The cells were incubated with serum-free medium of fluorescein isothiocyanate-labelled BSA (FITC-BSA of 100 µg/ml) for 2 h at 37 °C. Afterwards, the uptake of FITC-BSA was stopped by washing the cells three times with ice-cold PBS for 5 min. The cells were fixed with 0.5 % cold formaldehyde in PBS for 15 min at RT then underwent nuclear counterstaining with DAPI. Imagining was performed using the Olympus Bx43 fluorescence microscope.

3.2.6 Viability test - Alamar Blue assay

To investigate the influence of toxins on the regeneration and differentiation process, hiPSC, cells on DiffD3 and DiffD9 were subjected to treatment with varying concentrations of cisplatin, CsA, and H_2O_2.

Specifically, hiPSC were seeded into a Geltrex-coated 24-well cell+ culture plate, following the protocol outlined in 3.2.1.1. The hiPSC, DiffD3 and DiffD9 cells were treated in triplicate for 24 h with different concentrations of the specified compounds, together with the respective vehicle controls (DMSO or basal medium), except for H_2O_2, where the treatment duration was 30 min.

Nephrotoxicity induced by these drugs was assessed using the Alamar Blue assay, a colorimetric method used to assess cellular metabolic activity as an indicator of cellular viability. In fact, dehydrogenases of metabolically active cells can reduce resazurin, a non-fluorescent blue dye permeable to cell membranes, to resorufin after intracellular uptake. This conversion results in a pink dye emitting a fluorescent signal at 590 nm. The pink color is therefore an indicator of the presence of metabolically active enzymes and viable cells [84,85]. The fluorescence intensity of resorufin can be measured using a microplate reader at an emission wavelength of 590 nm and an excitation wavelength of 535 nm.

Following exposure to various agents and their corresponding vehicle controls, the culture medium was aspirated and 500 µl of newly prepared resazurin working solution (**Table 3.12**) were added to each well. The plate was then incubated in darkness for 4 h at 37 °C and 5 % CO_2. Following the incubation, 100 µl from each well were pipetted in quadruplicates into wells of a 96-well cell culture plate. Additionally, the blank control was dispensed into four wells. Lastly, the absorbance or optical density (OD) was measured at 535 nm and 590 nm using a microplate reader (Tecan infinite 200). Relative cell viability values were calculated by normalizing the samples to the respective vehicle controls and expressed as percentages.

The viability graphs were then generated with GraphPad Prism 6 and the inhibitory concentrations (IC) IC_{20} and IC_{50} were determined.

Table 3.12: Preparation of resazurin working solution.

Components	Composition
Resazurin stock solution (440 mM)	440 mM Na-resazurin in dimethylformamide
NaCl/Pi buffer	154 mM NaCl 3.77 mM Na_2HPO_4 in dH_2O 1.06 mM KH_2PO_4
Resazurin - NaCl/Pi solution (440 µM)	Resazurin stock solution diluted 1 : 1000 with NaCl/Pi buffer
Resazurin working solution (44 µM)	Resazurin - NaCl/Pi solution diluted 1 : 10 with DMEM without phenol red

3.2.7 Oxidative stress response assessment - glutathione assay

The GSH concentration post-cisplatin treatment was assessed in order to evaluate the oxidative stress defense capacity in hiPSC. The GSH Detection Assay Kit II was used following the manufacturer's instructions.

In brief, GSH is a tripeptide composed of three amino acids: glutamate, cysteine and glycine. It is a crucial defense mechanism against reactive oxygen compounds and its levels are a direct indicator of oxidative stress response [29].

The assay is based on the reaction of GSH with 5,5'-dithio-bis-(2-nitrobenzoic acid) (DTNB) which produces the chromophore 5'-thionitrobenzoic acid (TNB) and Oxidized glutathione TNB (GS-TNB). The rate of TNB formation is directly proportional to the GSH concentration in the sample. The enzyme GSR recycles GSH in two ways: by reducing either GS-TNB in the presence of NADPH or glutathione disulphide (GSSG) to 2 GSH (**Figure 1.3**). Thus, the measurement reflects the total concentration of reduced and oxidized glutathione in the sample.

Briefly, confluent hiPSC were singularized as detailed in section in 3.2.1.3; however, the pellet was resuspended in 1 ml ice-cold extraction buffer (0.1 % Triton X-100 and 0.6 % sulphosalicylic acid in 0.1 M potassium phosphate buffer) and homogenized using a sonifier in ice-cold water for 5x2 seconds at 30 % amplitude.

Following centrifugation of the cells at 3000 g, 4 °C for 4 min, the supernatant was carefully transferred to a black Eppendorf tube, leaving approximately 100 µl above the pellet. The supernatant could be either stored at -80°C or processed for further experiments.

Afterwards, a GSH standard series was prepared from the GSH standard (25 µM) diluted with 0.1 M potassium phosphate buffer to generate solutions with the following concentrations (on ice): 25 µM, 12.5 µM, 6.25 µM, 3.125 µM, 1.56 µM, 0.0 µM (only buffer). Then, 20 µl per sample, standard or blank (extraction buffer) were pipetted into a 96-well plate. Next, equal amounts of GSR (5 U/3 ml) and DTNB (2 mg/3 ml 0.1 M potassium phosphate buffer) were mixed (stable for only 15 min) and filled into a multichannel pipette reservoir. Subsequently, 120 µl of the GSR/DTNB mixture was pipetted into each well and after 30 s, 60 µl NADPH (2 mg/3 ml 0.1 M potassium phosphate buffer) was added using a multichannel pipette. The absorbance was measured with Tecan Sunrise™ at 412 nm, every 5 min.

3.2.8 Statistical analysis

Statistical analysis was performed using GraphPad Prism version 6. The data were presented as the mean ± standard deviation of three independent experiments (n = 3). For pair comparison between two groups, Student's t-test (multiple-comparison test) was applied. In cases where three or more groups were compared, one-way analysis of variance (ANOVA) was applied. Statistically significant differences between the groups were considered at a p-value < 0.05 and marked with *. A p-value of < 0.01 was considered very significant (**) and a p-value of < 0.001 highly significant (***).

4 Results

4.1 Characterization of differentiated hiPSC

4.1.1 Changes in Morphology

In this work, b4-hiPSC derived from fibroblasts and UM51 derived from renal progenitor cells, underwent the same differentiation protocol outlined in 3.2.1.3. Prior to the initiation of the differentiation, contrast microscopy observations showed that the size of pluripotent stem cells of both lines was very small and they were organized in colonies with sharp edges (**Figure 4.1**). Following cell singularization and initiation of the differentiation, the colony organization was lost, and the cells became larger by DiffD3. At DiffD9, the differentiated cells adopted a spindles-like appearance and underwent typical human proximal tubular morphological changes to tubule-like patterns and dome-like structures (hemicysts).

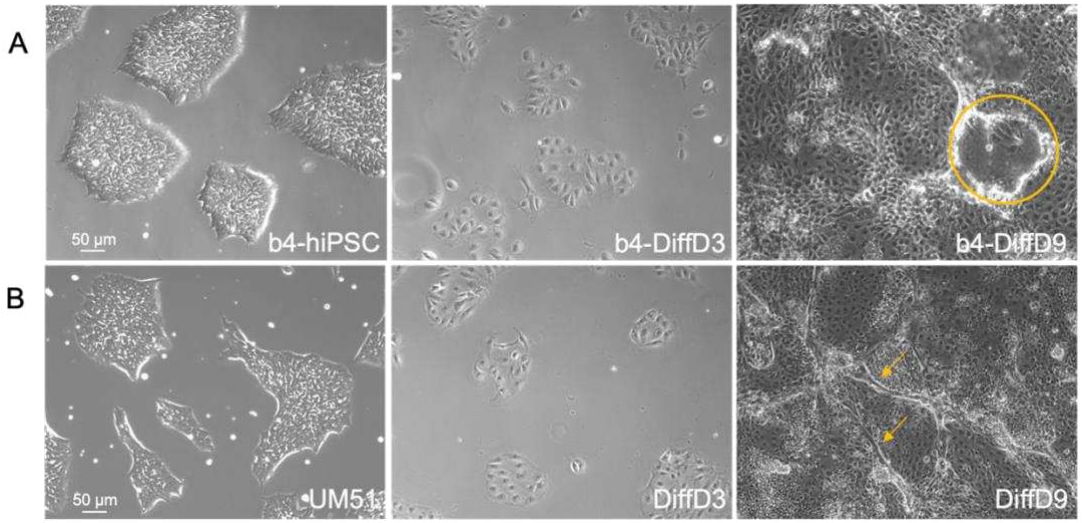

Figure 4.1: Morphological changes of b4 and UM51 during the differentiation. (A) Morphological changes of the b4-hiPSC and derived cells recorded on day 3 and day 9 as well as of **(B)** UM51 and derived cells recorded on day 3 and day 9 of the differentiation process. The scale bars represent 50 µm. The yellow circle highlights a dome-like structure and the yellow arrows show tubule-like patterns in the cell layers of the differentiated cells. DiffD = differentiation day, hiPSC = human induced pluripotent stem cells. Data are published in Mboni-Johnston, Kouidrat *et al.,* with slight modifications made in the current version [77].

4.1.2 Changes in the proliferation rate

Another way to evaluate the maturation of the differentiated cells in addition to the change in morphology is to assess the evolution of the proliferation capacity of the b4 line during the differentiation process at selected time points with the EdU assay. The fluorescence pictures in **Figure 4.2** illustrate the decline of EdU-positive cells (green) as the differentiation progresses from day 3 to day 9. The number of EdU-incorporating cells

was lower on DiffD3 compared to the hiPSC with the lowest number of proliferating cells observed on DiffD9. The quantitative analysis revealed a very high percentage of proliferating cells in hiPSC (nearly 70 %), which declined slightly but significantly on DiffD3. By DiffD9, there was a significant decrease with only around 30 % of the cells actively proliferating.

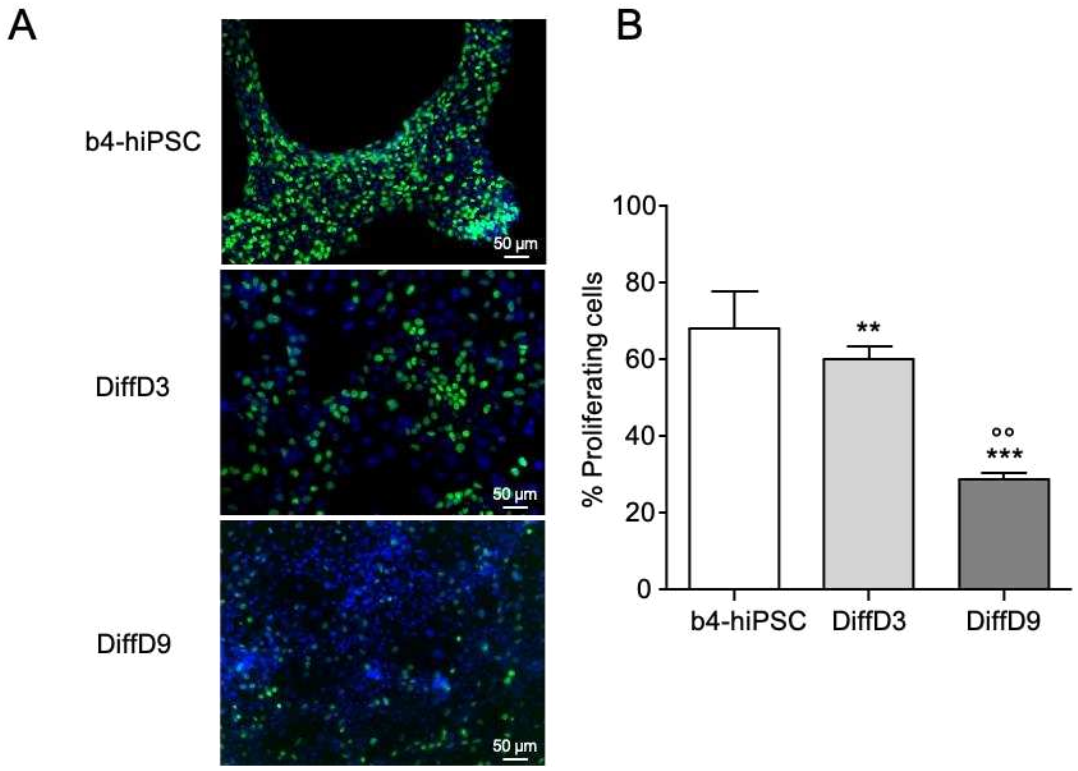

Figure 4.2: Changes in the proliferation rate of b4-hiPSC and derived cells on differentiation day 3 and day 9. (A) Representative pictures show reduced proliferation after initiation of the differentiation process in b4-hiPSC. **(B)** Quantification of the fluorescent EdU incorporated into S-phase cells. The mean % of proliferating cells of 3 independent experiments and representative pictures are shown. ** $p < 0.01$, *** $p < 0.001$ vs. hiPSC, °° $p < 0.01$ vs. DiffD3 (One-way ANOVA). The scale bars represent 50 µm. DiffD = differentiation day, EdU = 5-ethynyl-2′-deoxyuridine, hiPSC = human induced pluripotent stem cells. Data are published in Mboni-Johnston, Kouidrat *et al.* [77].

4.1.3 Changes in mRNA expression

After observing changes in the morphology and proliferation rate during the differentiation process, the mRNA expression profile of stem cells and DiffD9 cells was evaluated as described in 3.2.2. The results are shown in **Figure 4.3**, where the graph related to UM51 line only exhibited trends, based on the use of only 2 n repeats in the experiments.

The expression of stem, epithelial and proximal tubular cell markers was analyzed in DiffD9 cells from both lines in comparison to their respective stem cells. After 9 days of

differentiation, we observed a significant (in b4) and a tendential (in UM51) downregulation of the gene expression of stem cell markers *NANOG* (more than 10-fold for both lines) and *OCT-3/4* (nearly 100-fold for b4 and 1000-fold for UM51), while the pluripotency gene *SOX-2* and the renal progenitor marker *PAX-2* were only assessed in b4 line and showed no difference after differentiation (**Figure 4.3** A-B).

The expression of epithelial cadherin *(E-CAD)*, an epithelial cell marker, was similarly upregulated in both differentiated cell lines. In b4-DiffD9 cells, other epithelial markers specifically neural cadherin (*N-CAD*) and the tight junction protein (*TJP-1)* also known as *ZO-1* (zonula occludens), were assessed, with no significant difference in their expression. One explanation for the unexpected minimal difference in the expression of both epithelial markers between DiffD9 cells and hiPSC could be an already high initial expression in hiPSC. Given that the qRT-PCR software provides relative rather than absolute values, the expression levels in DiffD9 cells are relative to those in hiPSC.

To verify this hypothesis, the expression levels of epithelial markers in b4-hiPSC were compared to those in H5V cells (murine-immortalized heart endothelial cell line). The results shown in **Figure 4.3** C confirm that *E-CAD* and *ZO-1* expression was significantly increased (10-fold) in b4-hiPSC as compared to the endothelial cells. These findings indicate that the hiPSC already express high levels of epithelial markers before the differentiation and these levels may remain stable in DiffD9 cells. The downregulation of *N-CAD* in b4-hiPSC was expected, as it is a typical marker of mesenchymal cells, which our cells are demonstrably not.

A further step in characterizing DiffD9 cells involved mRNA analysis of key markers typically highly expressed in PTEC. All markers were significantly upregulated in b4-derived DiffD9 cells, including: *AQP-1*, *CAD-16* (cadherin-16), *GLUT*-5 as well as the brush border enzymes *CD-13* (alanyl aminopeptidase N) and *GGT* (gamma-glutamyl transferase) (**Figure 4.3** A). These markers were upregulated by approximately 10-fold, with the exception of *AQP-1,* which was almost 10^5-fold higher in b4-DiffD9 cells. Similarly, *AQP-1* was almost 10^4-fold higher in UM51-DiffD9 cells in comparison to their respective hiPSC (**Figure 4.3** B). However, the expression levels of *CAD-16* and *CD-13* was similar in the UM51 line before and after the differentiation. The UM51- and b4-DiffD9 cells exhibited comparable differentiation outcomes with a relative higher expression of *CAD-16*, *E-CAD* and *CD-13* in b4-DiffD9 cells.

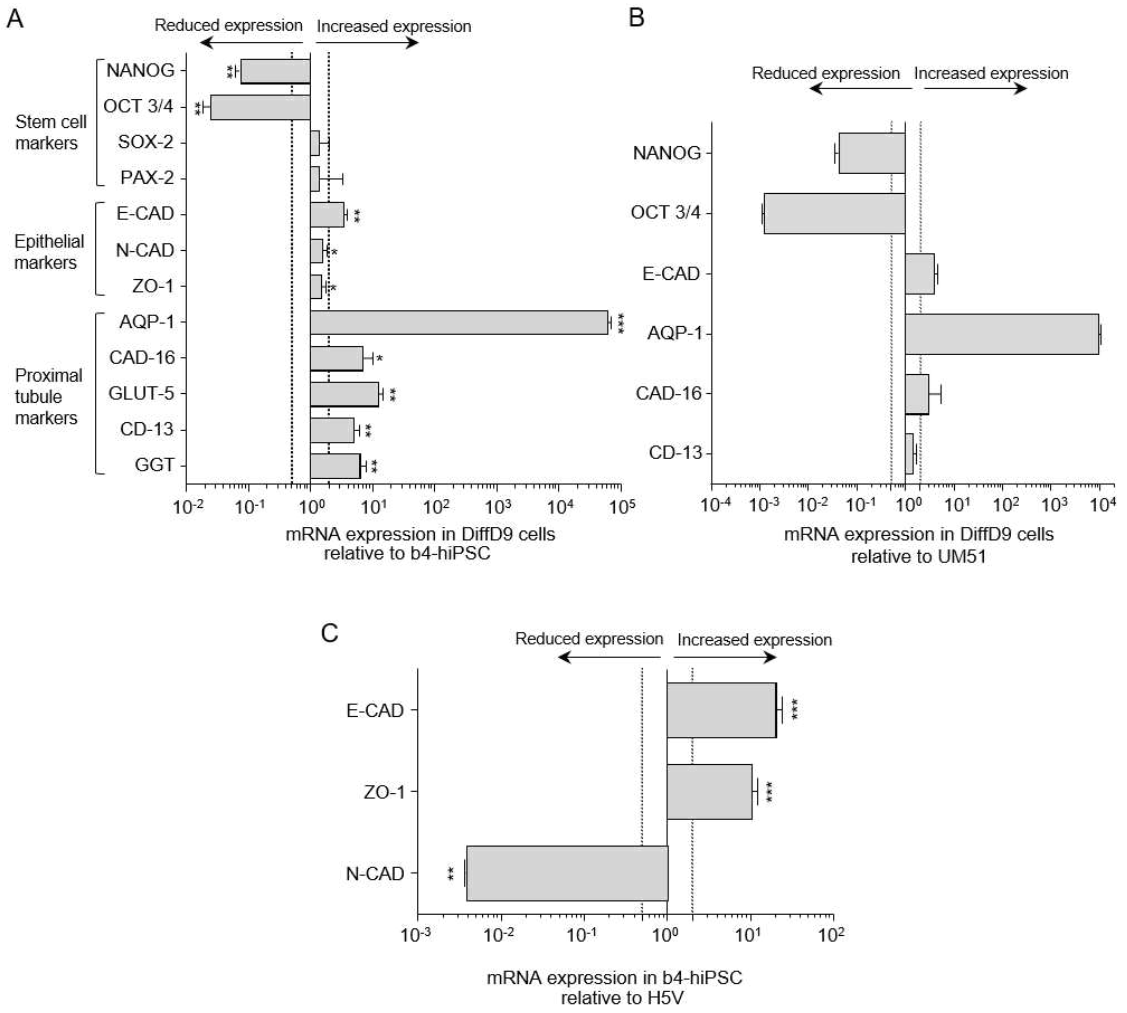

Figure 4.3: Changes in mRNA expression of differentiation markers analyzed by qRT-PCR. mRNA expression of stem cell, epithelial cell, and PTEC markers in b4-DiffD9 **(A)** and UM51-DiffD9 **(B)** cells relative to expression in their respective undifferentiated hiPSC. **(C)** mRNA expression of epithelial cell markers in b4-hiPSC relative to expression in H5V cells. Data from at least 3 independent experiments for b4 line and 2 independent experiments for UM51 line (including 3 technical qPCR replicates) are shown as mean ± SD. * $p \leq 0.05$, ** $p < 0.01$ and *** $p < 0.001$ vs. hiPSC (t-test). AQP-1 = aquaporin 1, CAD-16 = cadherin 16, CD-13 = alanyl aminopeptidase N, DiffD = differentiation day, E-CAD = epithelial cadherin, GGT = gamma-glutamyl transferase, GLUT-5 = fructose transporter, H5V = murine-immortalized heart endothelial cell line, hiPSC = human induced pluripotent stem cells, NANOG = homeobox protein, N-CAD = neural cadherin, OCT-3/4 = octamer-binding transcription factor 3/4, PAX-2 = paired box gene 2, PTEC = proximal tubular epithelial cells, SOX-2 = sex determining region Y-box 2, ZO-1 = zonula occludens 1. Data are published in Mboni-Johnston, Kouidrat *et al.,* with slight modifications made in the current version [77].

The ongoing characterization of DiffD9 cells included analyzing the mRNA expression of key transporters present in renal proximal tubules (**Figure 4.4**). After 9 days of differentiation, a significant increase in the expression of the cisplatin transporters *CTR-1* and *CTR-2* was observed in the b4 line. In the UM51 line, an increase in the expression was also noted. The expression of *OCT-2* showed an increase in UM51-DiffD9 cells, while no change was observed in b4-DiffD9 cells. Moreover, there was an approximately

100-fold higher upregulation in the expression of the carnitine transporter *OCTN-2* in both differentiated lines. Given the essential role of endocytosis as a transport mechanism in PTEC, the expression of *MEG* and *CUBN* was analyzed, both of which exhibited a significant upregulation of around 100-fold higher expression in b4-DiffD9 cells. In UM51-DiffD9 cells, an increased expression of a similar range was also observed. Nevertheless, the expression of *SGLT-2* showed a significant downregulation in differentiated b4, whereas in the UM51 line, no relevant difference in the expression was noted after differentiation. Further analysis of key PTEC transporters in the b4 line revealed a significant upregulation in the expression of *PEPT-1* and *OAT-1*, while *PEPT-2, OAT-3* and the *MDR-1* showed no biologically relevant difference in the expression post-differentiation.

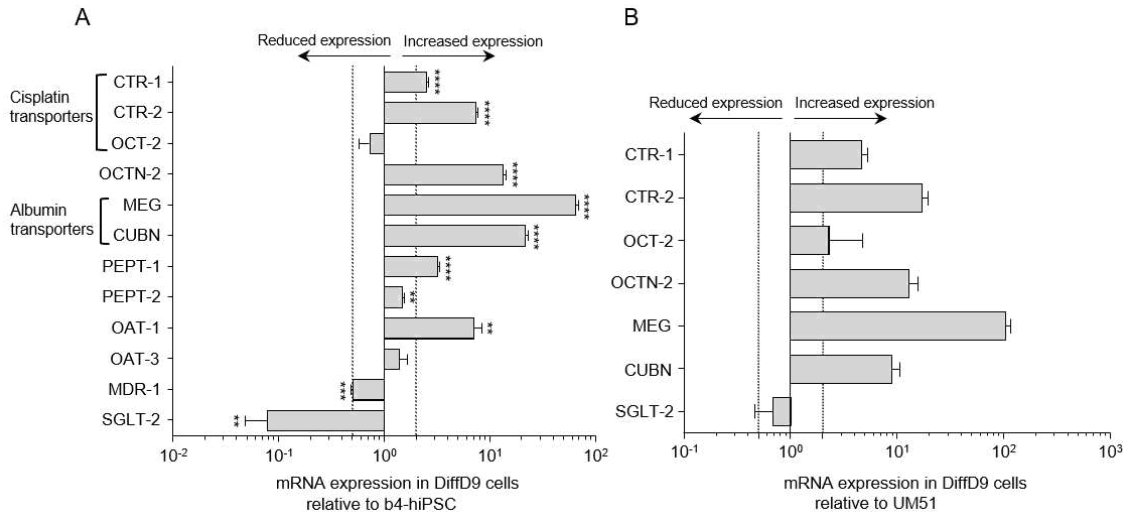

Figure 4.4: Changes in mRNA expression of key proximal tubule transporters analyzed by qRT-PCR. mRNA expression changes of PTEC transporters in b4-DiffD9 **(A)** and UM51-DiffD9 **(B)** cells relative to expression in their respective undifferentiated hiPSC. Data from at least 3 independent experiments for b4 line and 2 independent experiments for UM51 line (including 3 technical qPCR replicates) are shown as mean ± SD. * $p \leq 0.05$, ** $p < 0.01$, *** $p < 0.001$, **** $p < 0.0001$ vs. hiPSC (t-test). CTR-1/2 = copper transporter 1/2, CUBN = cubilin, DiffD = differentiation day, hiPSC = human induced pluripotent cells, MDR-1 = multidrug resistance protein 1, MEG = megalin, OAT-1/3 = organic anion transporter 1/3, OCT-2 = organic cation transporter 2, OCTN-2 = organic cation/carnitine transporter 2, PEPT-1/2 = peptide transporter 1/2, SGLT-2 = sodium/glucose cotransporter 2. Data are published in Mboni-Johnston, Kouidrat *et al.,* with slight modifications made in the current version [77].

4.1.4 Comparative gene expression analysis of b4 and F4-DiffD9 cells with RPTEC/TERT1

To place the gene expression profile of differentiated cells in a more physiologically relevant context, a comparative mRNA analysis was conducted between b4-DiffD9 cells and RPTEC/TERT1. Additionally, F4-derived DiffD9 cells subjected to the same

differentiation protocol by our working group were included in the comparison. The outcomes of this comparative analysis are shown in **Figure 4.5**.

These findings revealed similar gene expression profiles in differentiated b4 and F4. In most cases, the same genes displayed either upregulation or downregulation in both lines when compared to the reference RPTEC/TERT1. Notable variations included a significantly lower expression of *MDR-1* in differentiated b4, and a higher expression of the stem cell marker *OCT-3/4* in differentiated F4 cells, suggesting a potentially higher maturity of the differentiated b4 cells. Comparison with RPTEC/TERT1 revealed a substantial 1000-fold upregulation of the PTEC marker *AQP-1* in differentiated b4 cells; however, both *GLUT-5* and *CD-13* were significantly downregulated in both differentiated hiPSC lines. Regarding PTEC endocytic receptors, *MEG* exhibited more than a 1000-fold increase in differentiated b4 cells, while *CUBN* maintained expression levels similar to those in RPTEC/TERT1. Interestingly, the expression of the PTEC transporter *OAT-1* was significantly upregulated in differentiated b4 cells compared to both RPTEC/TERT1 and differentiated F4 cells. Other transporters like *CTR-1* and *OCT-2* together with the epithelial marker *E-CAD,* were expressed at similar levels across all three cell lines. In summary, the gene expression pattern of differentiated b4 cells was overall similar to that of differentiated F4 cells. When compared to RPTEC/TERT1, out of 12 analyzed genes, four were upregulated, four were downregulated and four showed no biologically relevant differences.

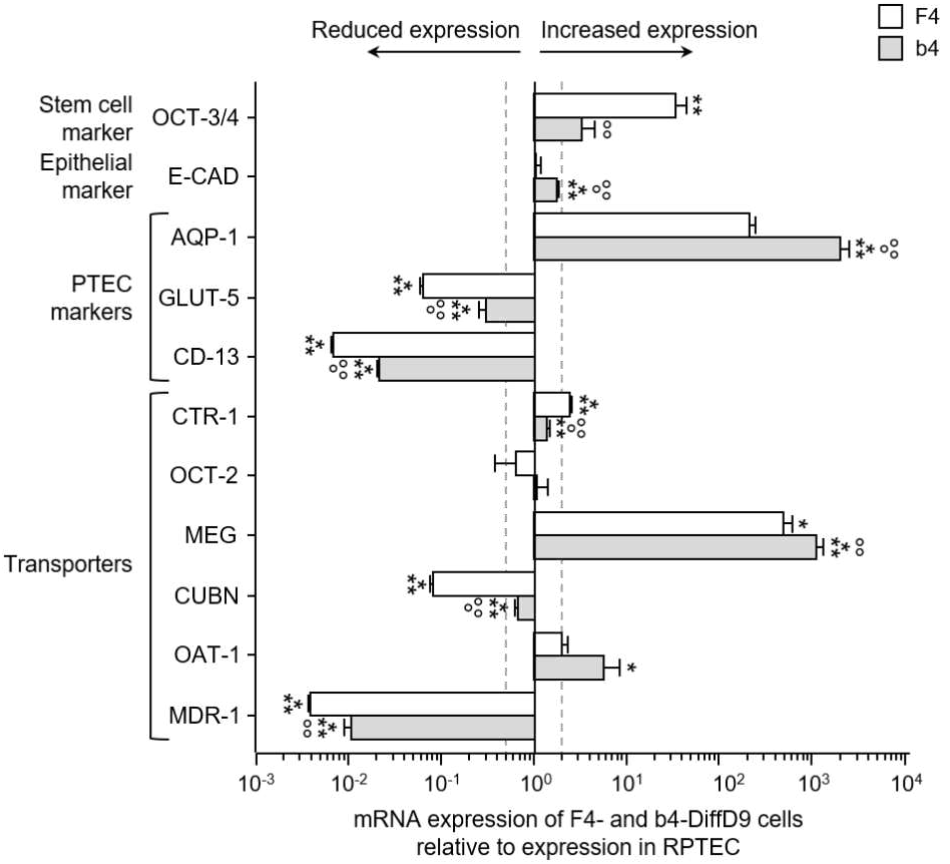

Figure 4.5: Changes in mRNA expression of selected genes in F4- and b4-derived DiffD9 cells compared to RPTEC/TERT1 analyzed by qRT-PCR. mRNA expression of a stem cell marker, an epithelial marker, several PTEC markers, and transporters relative to expression in RPTEC/TERT1. Data from at least 3 independent experiments (including 3 technical qPCR replicates) are shown as mean ± SD. * $p \leq 0.05$, ** $p < 0.01$ and *** $p < 0.001$ vs. RPTEC/TERT1, °° $p < 0.01$, °°° $p < 0.001$ vs. F4 (ANOVA). AQP-1 = aquaporin 1, CD-13 = alanyl aminopeptidase N, CTR-1 = copper transporter 1, CUBN = cubilin, DiffD = differentiation day, E-CAD = epithelial cadherin, GLUT-5 = fructose transporter, hiPSC = human induced pluripotent stem cells, MDR-1 = multidrug resistance protein 1, MEG = megalin, OAT-1 = organic anion transporter 1, OCT-2 = organic cation transporter 2, OCT-3/4 = octamer-binding transcription factor 3/4, RPTEC/TERT1 = renal proximal tubule epithelial cells/immortalized by human telomerase reverse transcriptase 1. I provided b4-DiffD9 cells' mRNA and Mboni-Johnston performed the analysis. Data are published in Mboni-Johnston, Kouidrat *et al.,* with slight modifications made in the current version [77].

4.1.5 Changes in protein expression detected with immunofluorescence and western blot

After the assessment of stem cell, epithelial and PTEC markers at the mRNA level, the expression of selected markers was analyzed at the protein level through immunofluorescence staining and western blot analysis. Antibodies against different markers were analyzed with western blot or through FITC-coupled secondary antibodies with nuclei stained in blue. Representative pictures are presented in **Figure 4.6**. Following 9 days of differentiation, immunostaining confirmed the reduction in the expression of the stem cell marker OCT-3/4 with decreased FITC-positive cells (green),

which was further confirmed in western blot. Consistent with the mRNA findings, the expression of the epithelial marker E-CAD was confirmed in stem cells but appeared to be higher in differentiated cells. Conversely, the expression of the proximal tubular markers AQP-1 and URO-10 was elevated in DiffD9 cells as compared to b4-hiPSC. The protein expression of the PTEC transporters CTR-1 and OCT-2 appeared to be higher in DiffD9 cells.

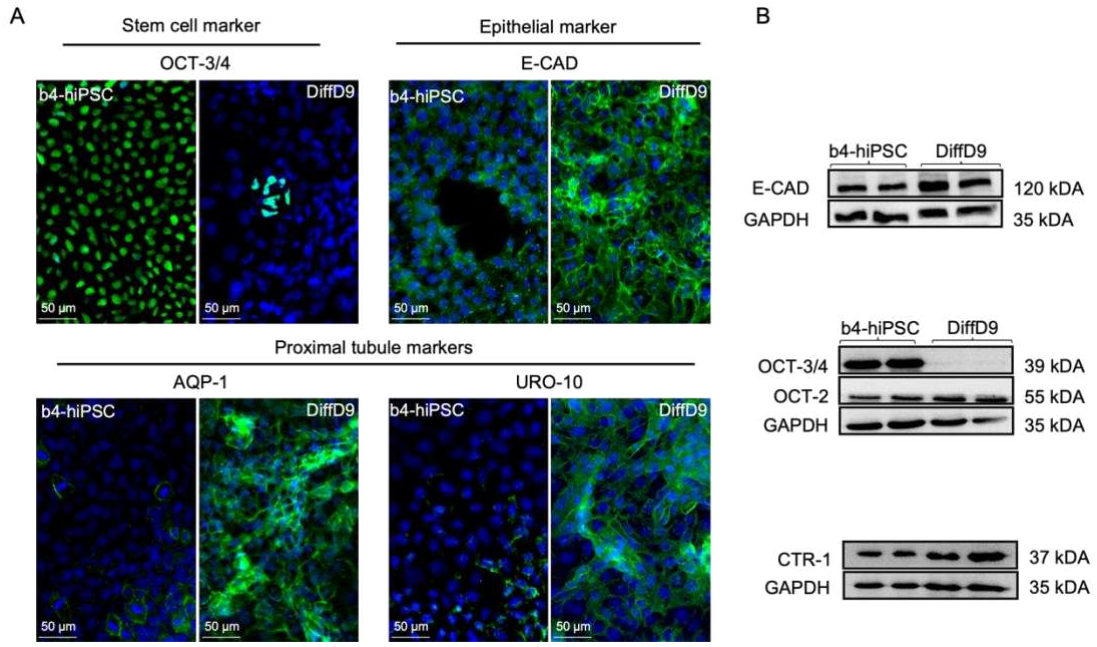

Figure 4.6: Changes in protein expression in b4-hiPSC and b4-DiffD9 cells analyzed using immunocytochemical staining and western blot. **(A)** Antibodies against the different markers are visualized with FITC-coupled secondary antibodies (green), and nuclei are stained with DAPI (blue). The scale bars represent 50 µm. **(B)** Representative blots of a selected stem cell and a selected epithelial marker and proximal tubule transporters. AQP-1 = aquaporin 1, CTR-1 = copper transporter 1, DAPI = 4′,6-diamidino-2-phenylindole, DiffD = differentiation day, E-CAD = epithelial cadherin, FITC = fluorescein isothiocyanate, GAPDH = glyceraldehyde-3-phosphate dehydrogenase, hiPSC = human induced pluripotent stem cells, OCT-2 = organic cation transporter 2, OCT-3/4 = octamer-binding transcription factor 3/4, URO-10 = heat stable tubular antigen. Data are published in Mboni-Johnston, Kouidrat *et al.,* with slight modifications made in the current version [77].

4.1.6 Changes in the functional ability of albumin transport

To gain deeper insight into the characteristics of the DiffD9 cells, a functional assay was conducted to determine their albumin uptake ability, a crucial function of human PTEC. After 2 h incubation in FITC-labelled BSA-containing medium, BSA uptake was analyzed by immunofluorescence staining and representative images are shown in **Figure 4.7**. After 9 days of differentiation of both b4 and UM51, an increase in FITC-positive cells was observed. This indicates an increased capacity of the DiffD9 cells to uptake fluorescently-labelled albumin through cubilin/megalin-mediated endocytosis when compared to the respective undifferentiated cells. In agreement with the mRNA findings,

this assay represents an additional evidence for the presence and the functional activity of both cubilin and megalin proteins in the differentiated cells.

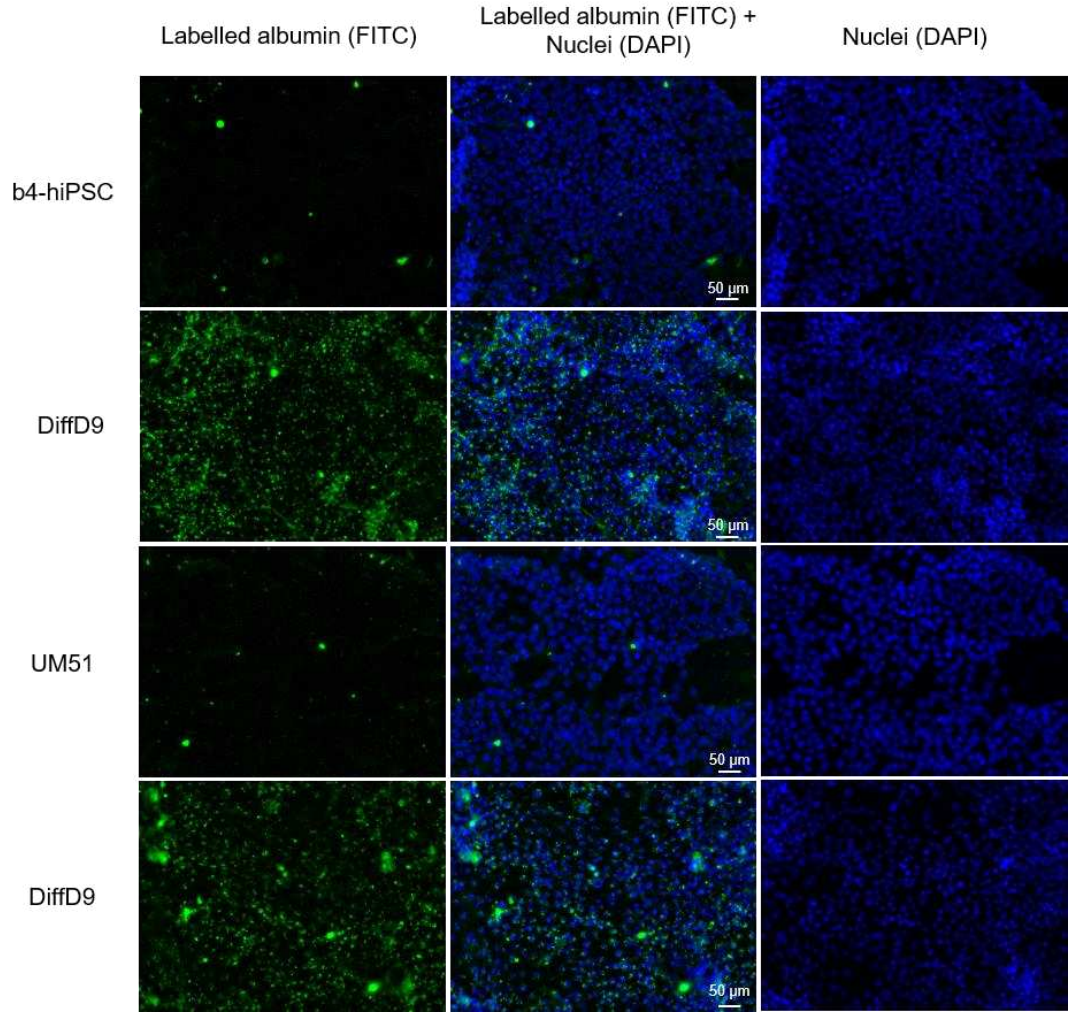

Figure 4.7: Gain of functional albumin uptake in differentiated cells. Analysis of albumin uptake into undifferentiated and differentiated b4 and UM51 cells using FITC-labelled BSA. Shown are representative immunofluorescence pictures from at least 3 independent experiments. The scale bars represent 50 µm. BSA = bovine serum albumin, DAPI = 4′,6-diamidino-2-phenylindole, DiffD = differentiation day, FITC = fluorescein isothiocyanate, hiPSC = human induced pluripotent stem cells. Data are published in Mboni-Johnston, Kouidrat *et al.,* with slight modifications made in the current version [77].

4.2 Effects of known nephrotoxic substances on the viability, proliferation and stress response in hiPSC, DiffD3 and DiffD9 cells

4.2.1 Effects on cellular viability

Three well-established toxic agents were used to study the sensitivity of b4 cells at different stages of differentiation: in the pluripotent stem cell state prior to the start of the protocol, during differentiation at DiffD3 and post-differentiation at DiffD9. Dose-response curves were generated following a 24 h exposure to cisplatin as a genotoxic nephrotoxin, CsA as a non-genotoxic nephrotoxin, and a 30 min exposure to H_2O_2 as an oxidative stress inducer. The UM51 line was exclusively treated in the pluripotent state and H_2O_2 was not tested. The cell viability post-treatment was measured using the Alamar Blue Assay and the IC_{20} (80 % viability) and IC_{50} (50 % viability) of the substances were determined and later used for further toxicological investigations.

Figure 4.8 A illustrates the cell response to cisplatin. While b4-hiPSC had an IC_{50} of approximately 3 µM cisplatin, DiffD3 cells demonstrated reduced sensitivity with a 2-fold higher IC_{50} (6 µM). Notably, DiffD9 cells displayed the least sensitivity across all differentiation stages with an IC_{50} 10 to 20 times higher than b4-hiPSC and DiffD3 b4-cells. When compared to UM51 (**Figure 4.8** A and D), b4-hiPSC were more sensitive to cisplatin, showing a lower IC_{50} by a factor of two. However, according to **Figure 4.8** B and E, UM51 cells displayed similar sensitivities to CsA as b4 line at all three differentiation stages with IC_{50} values around 10 µM. In contrast to cisplatin and CsA results, H_2O_2 treatment (**Figure 4.8** C) revealed that b4-hiPSC were more resistant than b4-DiffD3 cells, differing by a factor of 4 in their IC_{50} value.

The very high IC_{50} concentration of cisplatin in b4-DiffD9 cells was expected given the reduced proliferation shown in the EdU assay (**Figure 4.2**). Another explanation would be the possible expression of certain proteins after the differentiation that make the cells more resistant to cisplatin. To answer this question, a comparison in gene expression of transporters associated with drug resistance was performed in b4 pre- and post-differentiation. The mRNA expression analysis demonstrated an upregulation of *MCT-1* (monocarboxylate transporter-1), whereas *MDR-1* showed no biologically relevant changes as shown in **Figure 4.8** F and **Figure 4.4** A respectively [86,87]. Nevertheless, the expression of *OATP*, an organic anion transporting polypeptide, was significantly downregulated, while the expression of *MRP-1* has shown no biologically relevant change (**Figure 4.8** F) [88].

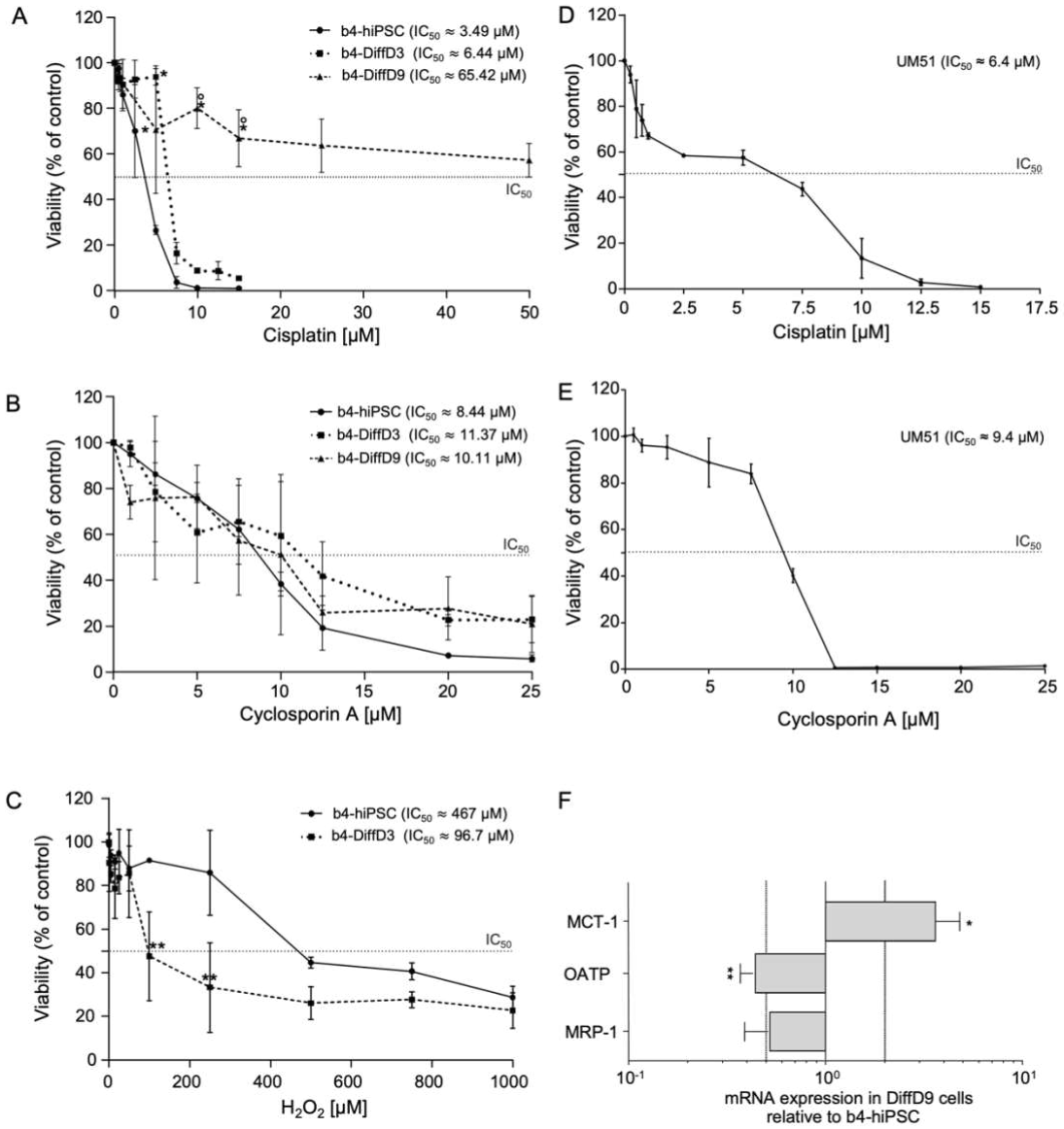

Figure 4.8: Cell viability after exposure to cisplatin, cyclosporin A and H_2O_2 in hiPSC, DiffD3 and DiffD9 cells, and mRNA expression changes of drug resistance-related genes analyzed by qRT-PCR. Sensitivity of the cells was assessed by measuring the cell viability with the Alamar Blue assay after 24 h treatment with cisplatin or cyclosporin A and after 30 min treatment with H_2O_2 in the indicated concentrations. Cells of the b4 line on differentiation days 0 (hiPSC), 3 (DiffD3), and 9 (DiffD9) were treated with cisplatin **(A)** and cyclosporin A **(B)** while H_2O_2 (**C)** was tested only on hiPSC and DiffD3 cells. UM51 were treated with cisplatin **(D)** and cyclosporin A **(E)** only in the pluripotent state. **(F)** mRNA expression changes of drug resistance-related genes in b4-DiffD9 cells relative to expression in undifferentiated hiPSC. The concentrations at which 50 % of the cells were dead are given as IC_{50} values in the graphs. Data from at least 3 independent experiments are shown as mean ± SD. * $p \leq 0.05$, ** $p < 0.01$ vs. hiPSC, ° $p \leq 0.05$ vs. DiffD3 (One-way ANOVA and t-test). DiffD = differentiation day, hiPSC = human induced pluripotent stem cells, IC = inhibitory concentration, MCT-1 = monocarboxylate transporter 1, MRP-1 = multidrug resistance-associated protein 1, OATP = organic anion transporting polypeptides. Data are published in Mboni-Johnston, Kouidrat *et al.,* with slight modifications made in the current version [77].

4.2.2 Effects on cellular proliferation

For further studies of the influence of toxins on the differentiation process, we shifted our focus to the b4 line. Cells at different stages of differentiation (b4-hiPSC, DiffD3, DiffD9), were treated for 24 h with different concentrations of two nephrotoxic substances, cisplatin and CsA. The objective was to investigate the influence of these nephrotoxins on cell proliferation by comparing EdU uptake with untreated cells throughout the differentiation process.

4.2.2.1 Effects of cisplatin

To ensure comparable outcomes, cells were exposed to a low cisplatin concentration (0.2 µM) and the IC_{20} of b4-hiPSC (1 µM) at all stages. Additionally, DiffD3 cells were treated with their IC_{20} (3 µM) and DiffD9 cells with their IC_{50} (65 µM). **Figure 4.9** A illustrates representative fluorescent pictures of the EdU-positive cells at each differentiation stage and under the concentrations applied. The immunostaining revealed a trend of increased proliferating cells (green) in all stages after treatment with 1 µM cisplatin. Notably, no proliferating cells were visible anymore after DiffD9 cells treatment with their respective IC_{50}.

Quantification of the pictures confirmed the observed trend (**Figure 4.9** B). Following treatment with the IC_{20} of b4-hiPSC (1 µM), a significant increase in EdU uptake was observed across all stages compared to untreated cells, whereas the uptake was also significantly higher in DiffD3 cells after 0.2 µM treatment (more than 10% increase). Besides, treatment of DiffD9 cells with their IC_{50} (65 µM) resulted in a complete shutdown of the proliferation; while, DiffD3 cells treated with their IC_{20} (3 µM) showed no difference compared to the untreated control.

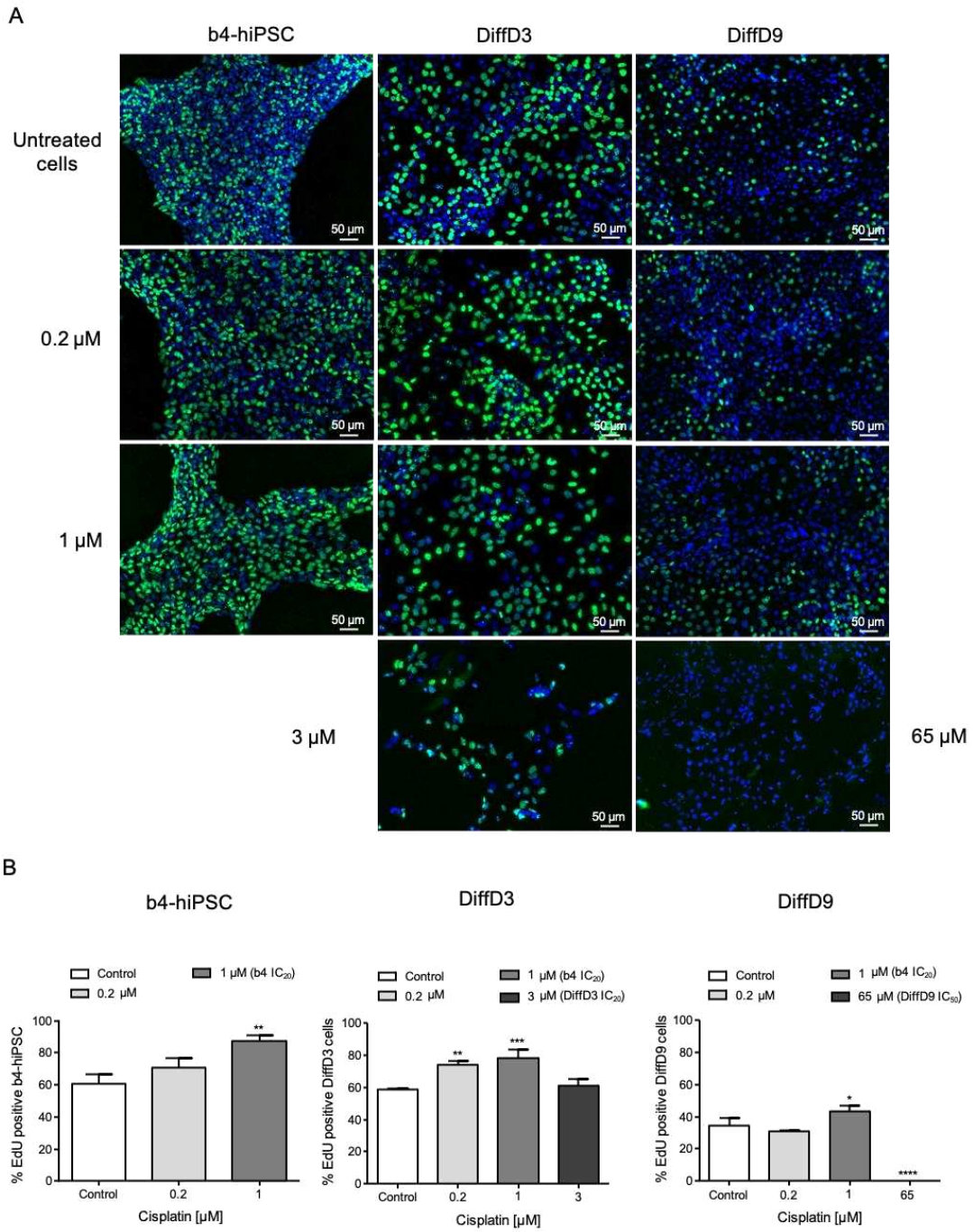

Figure 4.9: Effects of cisplatin on cellular proliferation of b4-hiPSC, DiffD3 and DiffD9 cells. **(A)** Representative immunofluorescence images of EdU-positive cells at different differentiation stages after 24 h cisplatin treatment with selected concentrations 0.2 µM, 1 µM, 3 µM and 65 µM. **(B)** Percentage of proliferating b4-hiPSC and DiffD3 and DiffD9 cells after 24 h of cisplatin treatment, quantified by the incorporation of fluorescent EdU into S-phase cells. The mean % of proliferating cells of 3 independent experiments is shown as mean ± SD. * $p \leq 0.05$, ** $p < 0.01$, *** $p < 0.001$ and **** $p < 0.0001$ vs. untreated cells. (One-way ANOVA). The scale bars represent 50 µm. DiffD = differentiation day, EdU = 5-ethynyl-2′-deoxyuridine, hiPSC = human induced pluripotent stem cells. IC = inhibitory concentration.

4.2.2.2 Effects of cyclosporin A

To ensure comparable outcomes, cells were exposed to CsA at equimolar doses, using both the IC_{20} (2 µM) and IC_{50} (8 µM) concentrations of b4-hiPSC at all stages, with additional treatment of DiffD9 cells with their respective IC_{50} (10 µM).

Figure 4.10 A illustrates representative fluorescent pictures of the EdU-positive cells at each differentiation stage and the applied concentrations. The immunostaining shows a trend where the number of proliferating cells appears to be preserved in each stage despite the treatment.

Quantitative analysis confirmed the observed trend (**Figure 4.10** B). CsA treatment had no significant effect on cellular proliferation at all stages compared to untreated cells, except for DiffD9 cells after IC_{50} treatment, displaying a 13% decrease in actively proliferating cells compared to the control.

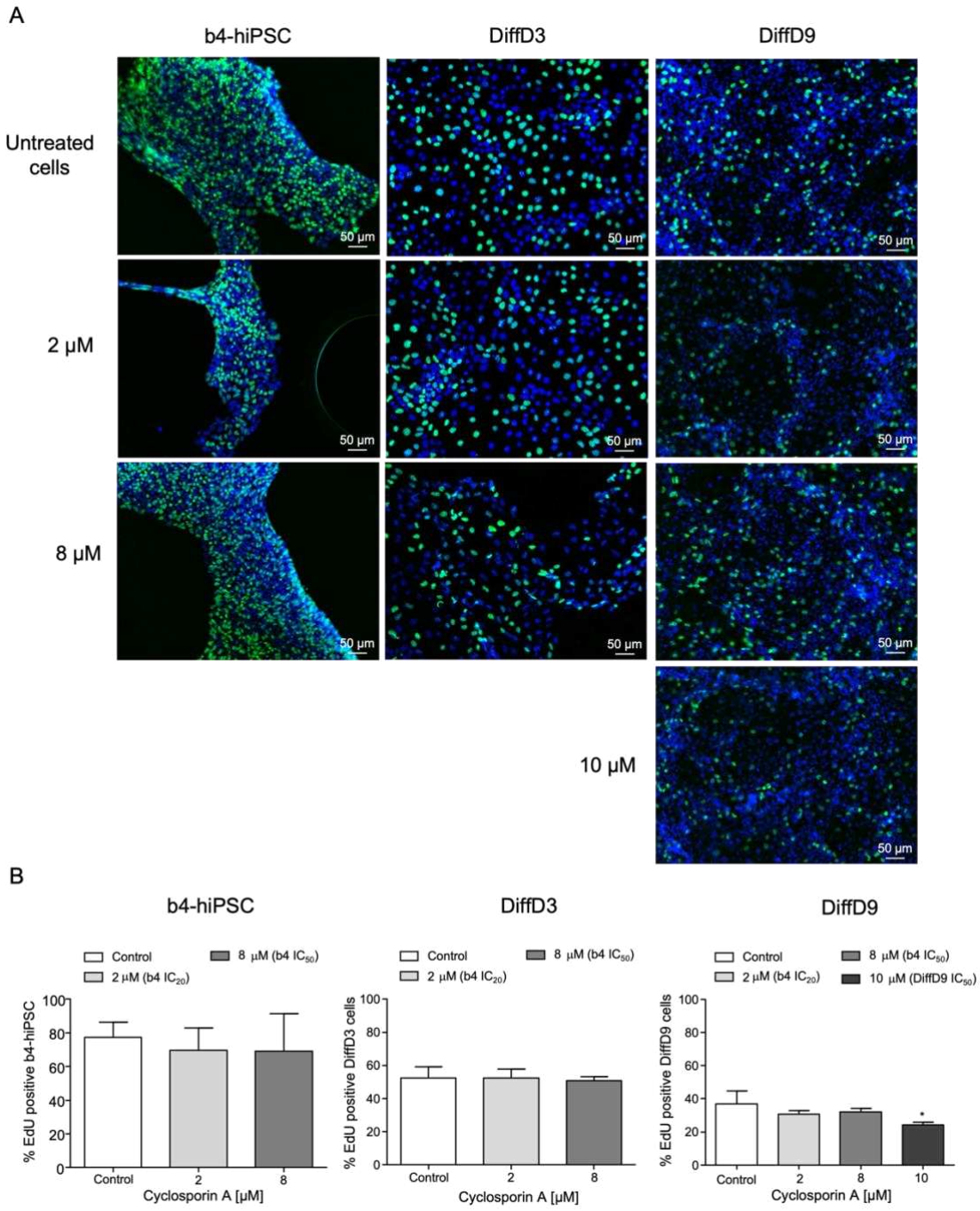

Figure 4.10: Effects of cyclosporin A on cellular proliferation of b4-hiPSC, DiffD3, DiffD9 cells. (A) Representative immunofluorescence images of EdU-positive cells at different differentiation stages after 24 h cyclosporin A treatment with selected concentrations 2 µM, 8 µM and 10 µM. **(B)** Percentage of proliferating b4-hiPSC and DiffD3 and DiffD9 cells after 24 h of cyclosporin A treatment, quantified by the incorporation of fluorescent EdU into S-phase cells. The mean % of proliferating cells of 3 independent experiments is shown as mean ± SD, except for untreated b4-hiPSC and DiffD9 IC_{20} (2 experiments). * $p \leq 0.05$ vs. untreated cells. (One-way ANOVA). The scale bars represent 50 µm. DiffD = differentiation day, EdU = 5-ethynyl-2′-deoxyuridine, hiPSC = human induced pluripotent stem cells. IC = inhibitory concentration.

4.2.3 Evaluation of oxidative stress response after cisplatin treatment

4.2.3.1 Effects of cisplatin on the expression of oxidative stress genes

To assess and compare the oxidative stress response of b4-hiPSC and DiffD9 cells, both differentiation states underwent a 24 h cisplatin treatment, given its potent prooxidative properties. Undifferentiated b4 and DiffD9 cells were exposed to their respective IC_{20} (1 µM for hiPSC and 13 µM for DiffD9 cells) and IC_{50} (3 µM for hiPSC and 65 µM DiffD9 cells) concentrations. Afterwards, treated and untreated cells were harvested, and qRT-PCR was conducted to analyze the expression of selected oxidative stress markers. The results show trends and no significance testing was conducted due to the limited sample size, with only two replicates used in the experiments.

In stem cells, exposure to the selected concentrations (IC_{20} and IC_{50}) induced no relevant changes in the expression of the selected markers when compared to untreated cells (**Figure 4.11** A).

In DiffD9 cells, a dose-dependent response was observed. IC_{20} treatment showed a tendential upregulation in the expression of *GPX-1* and *NQO-1*, while no relevant changes were noted in other genes. Conversely, IC_{50} treatment induced a tendential downregulation in the expression of *NRF-2, GSR* and *GCLC*. *GPX-1* was the only gene that showed a tendential upregulation after IC_{50} treatment, while *NQO-1* expression remained similar to the control (**Figure 4.11** B).

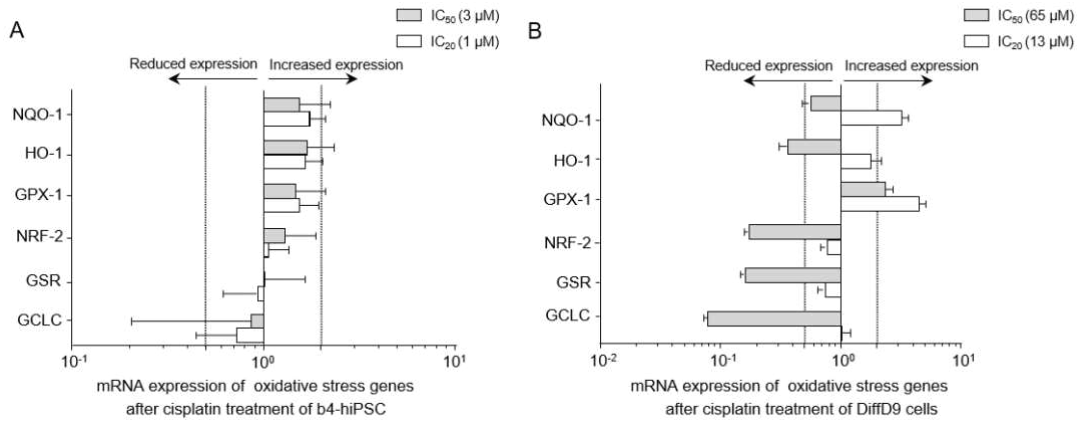

Figure 4.11: Changes in mRNA expression of selected oxidative stress-related genes after cisplatin treatment of b4-hiPSC and DiffD9 cells analyzed by qRT-PCR. Expression of oxidative stress genes after 24 h treatment with the IC_{20} and IC_{50} concentrations of cisplatin in b4-hiPSC **(A)** and DiffD9 cells **(B)** relative to their expression in untreated cells analyzed by qRT-PCR. Data from 2 independent experiments (including 3 technical replicates) are shown as mean ± SD. DiffD = differentiation day, GCLC = glutamine-cysteine ligase catalytic subunit, GPX-1 = glutathione peroxidase 1, GSR = glutathione reductase, hiPSC = human induced pluripotent stem cells, HO-1 = heme oxygenase 1, IC = inhibitory concentration, NQO-1 = NADPH dehydrogenase (quinone 1), NRF-2 = nuclear factor erythroid 2-related factor 2.

4.2.3.2 Effects of cisplatin on the phosphorylation of NRF-2

Following the analysis of the gene expression of oxidative stress response factors after prooxidative treatment, the impact of cisplatin was further evaluated at the protein level by fluorescent immunostaining. Stem cells were treated for 24 h with their IC_{20} (1 µM) and DiffD9 cells with both their IC_{20} (13 µM) and IC_{50} (65 µM) concentrations of cisplatin. Afterwards, the cells were stained for the detection of pNRF-2 (phosphorylated at Ser40), the activated form of NRF-2. The fluorescence intensity was measured and compared with untreated cells.

As illustrated in **Figure 4.12**, the nuclei of both treated and untreated stem cells were stained, which indicates the presence of pNRF-2 in the nucleoplasm at similar levels. Quantitative analysis confirmed this trend and showed no significant difference in intensity between the control and IC_{20}-treated hiPSC.

In DiffD9 cells, the microscopic observation revealed a similar expression pattern in IC_{20}-treated cells compared to the control. However, FITC-positive cells showed lower intensity after IC_{50} treatment with cisplatin. Quantitative analysis confirmed the observed trend with a significant decrease in NRF-2 activation after IC_{50} treatment.

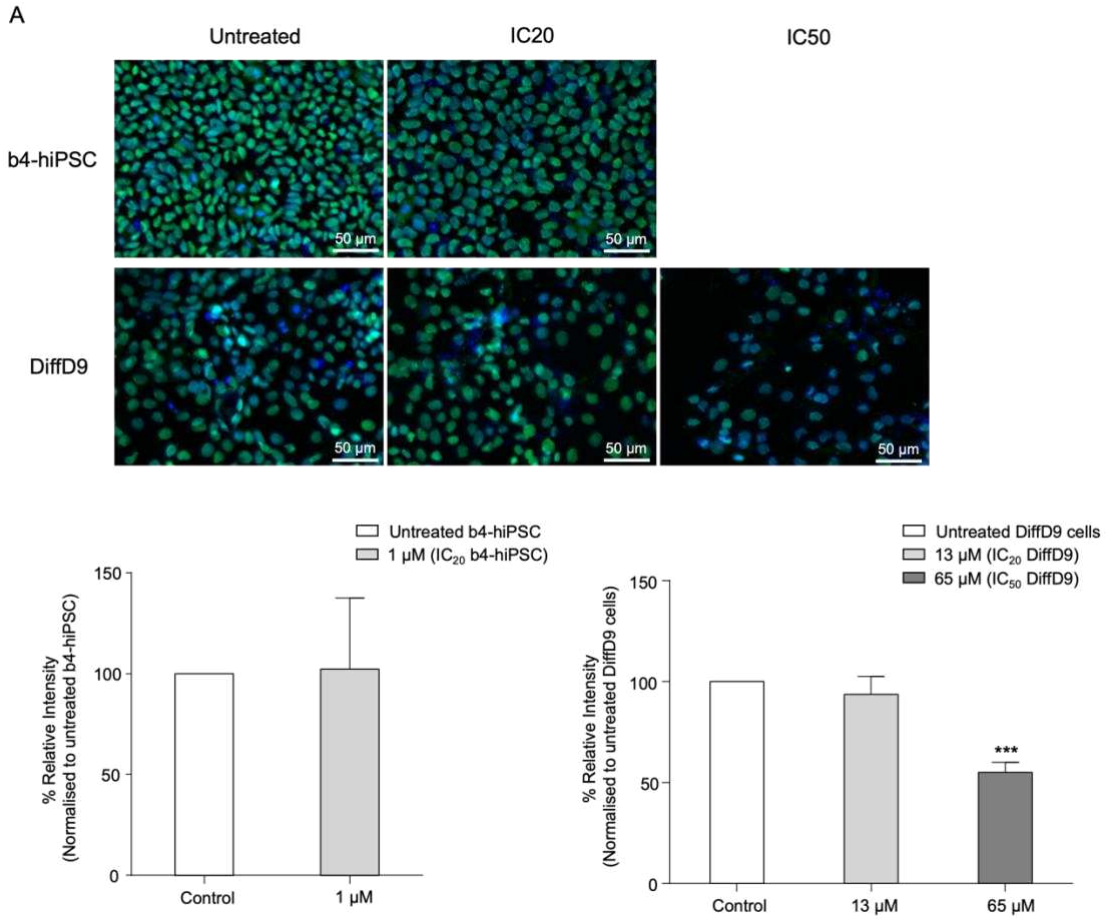

Figure 4.12: Effects of cisplatin on pNRF-2 expression in b4-hiPSC and DiffD9 cells. (A) Representative immunofluorescence images of pNRF-2 staining after 24 h cisplatin treatment at selected concentrations 1 µM, 13 µM and 65 µM. **(B)** Intensity of pNRF-2 staining expressed in percentage related to the control of b4-hiPSC and DiffD9 cells after 24 h of cisplatin treatment, quantified by integrated fluorescence density of FITC-positive cells. The mean % of the expression of 3 independent experiments is shown as mean ± SD. *** $p < 0.001$ vs. untreated cells (One-way ANOVA). The scale bars represent 50 µm. DiffD = differentiation day, hiPSC = human induced pluripotent stem cells, IC = inhibitory concentration, pNRF-2 = nuclear factor erythroid 2-related factor-2 phosphorylated at Ser40.

4.2.3.3 Effects of cisplatin on glutathione levels

To conclude our toxicological studies, an additional method was performed to assess the cisplatin-induced oxidative stress response at the protein level. Following a 24 h cisplatin treatment, GSH levels were quantified in b4-hiPSC as described in section 3.2.7.

GSH levels are a reliable indicator of oxidative stress response, given the key role of GSH in non-enzymatic cellular antioxidant defense. The graph in **Figure 4.13** shows a significant increase in GSH levels after b4-hiPSC treatment with the IC_{20} concentration of cisplatin (1 µM), exceeding twice those of untreated cells.

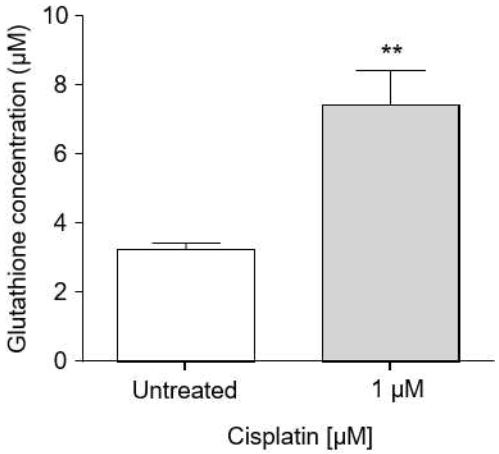

Figure 4.13: Effects of cisplatin on glutathione levels in b4-hiSPC. GSH was measured in hiPSC treated with the IC_{20} concentration of cisplatin (1 µM) for 24 hours using GSH Assay Kit II. Data from at least 3 independent experiments are shown as mean ± SD. ** $p \leq 0.01$ vs. untreated hiPSC (One-way ANOVA). hiPSC = human induced pluripotent stem cells, IC = inhibitory concentration.

5 Discussion

In the present thesis, the differentiation process in two hiPSC lines into PTELC was investigated, with a focus on the response to toxic substances and therefore the potential of PTELC for drug screening application. Relying on a differentiation protocol adapted from Kandasamy *et al.* (2015) [76], b4-hiPSC line and for the first time UM51 line were differentiated into PTELC. The expression of specific markers and transporters was determined at the mRNA and protein levels, and the functionality of differentiated cells after 9 days was confirmed. The main toxicological studies were conducted on the b4 line and focused on the influence on the differentiation process of cisplatin, a genotoxic nephrotoxin; CsA, a non-genotoxic nephrotoxin; and H_2O_2, a pro-oxidative agent.

As sensitivity analysis is essential in order to establish toxicity thresholds in drug screening assessments, the IC_{50} and IC_{20} concentrations of drugs were determined to evaluate their specific effects without a heavy impact on cell viability. Our research group is the first to investigate cells during the differentiation (DiffD3), since previous works typically involved treatment either at the stem cell stage or after the end of differentiation. The following sections provide a detailed discussion of the outcomes of the experiments in this thesis.

5.1 b4-hiPSC and UM51 differentiation generates PTELC

The contrast microscopy observations on DiffD9 revealed that differentiated cells from both hiPSC lines (b4 and UM51) showed typical morphological features of proximal tubule cells. These included tubule-like organization and the formation of hemicysts, which are indicators of the development of transporting epithelia and transepithelial fluid dynamic in differentiated cells [89]. These results are in agreement with the findings of Kandasamy *et al.* (2015) and Mboni-Johnston, Kouidrat *et al.* (2024) where the same protocol was utilized on different hiPSC lines [76,77].

Another indicator of cell differentiation is the gradual decline in proliferation frequency across the differentiation process, as demonstrated by the EdU assay performed on the b4 line. This decline aligns with the known behavior of tubule cells, which classically do not proliferate under normal physiological conditions *in vivo* [90]. Nonetheless, as seen in other works, DiffD9 cells showed a persistent but low proliferation rate which likely mimicks the *in vivo* ability of renal cells to re-enter the cell cycle after kidney damage. The differences between *in vivo* and *in vitro* culture conditions may also contribute to the residual minimal proliferation observed in DiffD9 cells [76,91–93]. To promote more physiological maturation and further reduce the retained proliferation, growth stimulation

from the medium could be diminished through dynamic adjustments of the medium composition, like modifying growth factors concentration throughout the differentiation process.

Further characterization of the differentiated cells revealed a significant downregulation of stem cell markers at gene and protein levels. However, an unchanged expression level of stemness and progenitor markers *SOX-2* and *PAX-2* was observed in b4-DiffD9 cells. This pattern was similarly observed in F4-DiffD9 cells by our research group using the same protocol on F4-hiPSC [77]. This expression aligns with the residual proliferative state of differentiated cells seen in the EdU assay and other studies [93,94]. The residual expression of these two markers suggest either a degree of immaturity in the DiffD9 cells or their potential to dedifferentiate from a mature state to a stem cell-like state for tissue repair following kidney injury, as established *in vivo* [95,96]. Furthermore, human PTEC have also been shown to re-express nephron progenitor markers like *PAX-2* under *in vitro* conditions, maybe due to partial dedifferentiation [43,97]. The expression of embryonic markers is a recurring challenge in stem cell-derived models [19,76,98]. One possible reason for the lack of full maturity in iPSC-derived models is that complete maturation of some tissues like the cerebral cortex takes years and exceeds the capabilities of current culturing methods. Innovative methods for maturation enhancement, like more complex culture conditions could be highly beneficial [99]. Taken together, these findings suggest that DiffD9 cells have successfully transitioned from a stem cell state to a more specialized cell type, though with a certain degree of immaturity.

Analysis of epithelial markers revealed an upregulation of *E-CAD* in DiffD9 cells from both lines comparable to RPTEC/TERT1 and F4-DiffD9 cells. However, a high expression of *E-CAD* and *ZO-1* in b4-hiPSC was also observed. This implies relatively stable levels of epithelial markers pre- and post-differentiation. Although this expression pattern may appear counterintuitive, elevated levels of *E-CAD* and *ZO-1* in stem cells are consistent with their established role in cell adherence and the preservation of the integrity of hiPSC colony organization [100,101]. Besides *E-CAD*‘s implication in maintaining pluripotency in murine pluripotent cells following fibroblast reprogramming [100,102], the recent discoveries of Park *et al.* (2024) highlighted a novel role for *ZO-1* in mesenchymal stem cell migration [103]. Accordingly, the protein analysis with western blot and immunostaining demonstrated high E-CAD protein expression in both b4 stem and differentiated cells.

It is noteworthy to underline that the differentiation process is often associated with epithelial-mesenchymal transition-like (EMT) and mesenchymal-epithelial transition-like (MET) events [100]. EMT refers to the transdifferentiation of epithelial cells into more motile mesenchymal cells, while the reverse process is called MET. EMT is initiated by physiological reprogramming of the gene expression, leading to the loss of epithelial organization through the dissolution of cell junctions, like the downregulation of E-CAD, which is counterbalanced by the expression of the less adhesive N-CAD, as cells reorganize their cytoskeleton to become motile for migration and dissemination [100,101]. N-CAD is thus regarded as a mesenchymal cadherin, which may explain why it was not upregulated in b4-DiffD9 cells. To sum up this hypothesis, b4 cell colonies initially expressed high levels of *E-CAD* and *ZO-1,* alongside low levels of *N-CAD*. Upon differentiation, *E-CAD* and *ZO-1* were downregulated, so one could speculate that a transient switch to *N-CAD* could have occurred and persisted until DiffD9, at which point cells could have restored higher *E-CAD* levels. This hypothesis could highlight the dynamic changes that characterize the plasticity of the epithelial phenotype, enabling several rounds of EMT and MET in several physiological and pathological contexts including tissue repair, organogenesis, fibrogenesis and carcinogenesis [101]. Additional expression analysis of cells during the differentiation process could provide deeper insight into this dynamic phenomenon. Collectively, these outcomes indicate that DiffD9 cells have shifted towards an epithelial phenotype.

Furthermore, the generated DiffD9 cells from both lines expressed *CAD-16* which is a kidney specific marker [76,104], together with *AQP-1,* which is constitutively expressed at high levels in the proximal tubule [3,97]. One might have anticipated higher *CAD-16* expression in UM51-DiffD9 cells; however, since UM51 cells are reprogrammed from cells of renal origin, they may have retained elevated baseline levels of *CAD-16,* since it is a kidney specific marker [79]. In b4-DiffD9 cells, the protein expression of AQP-1 was further confirmed through immunostaining, along with URO-10, a specific antigen of proximal convoluted tubule cells [105]. We confirmed the findings of previous PTEC differentiation studies [76,77,98], and additionally showed that b4-DiffD9 cells displayed a significantly higher mRNA expression of AQP-1 compared to RPTEC/TERT1 and F4-DiffD9 cells.

Other essential markers typically associated with PTEC like *CD-13* and *GGT* were upregulated after b4 line differentiation, consistent with the findings of other research groups [76,106]. The gene expression levels of *CD-13* and *GLUT-5* were higher in b4-DiffD9 cells compared to F4-DiffD9 cells, although still lower than in RPTEC/TERT1.

However, the detection of *GLUT-5* is an encouraging result as other works failed to detect it [77,98]. In UM51-DiffD9 cells, *CD-13* expression remained unchanged after differentiation, which was expected as UM51 cells are derived out of urinary progenitor cells known for their high *CD-13* levels [107]. The same rationale could explain the downregulation of *SGLT-2* in b4-DiffD9 cells and its unchanged expression in UM51-DiffD9 cells, as reports showed retained *SGLT-2* expression in stem cells [108,109]. Protein expression analysis or functional assays may be needed to confirm the expression of the markers that were not upregulated in differentiated cells. Overall, discrepancies in marker expression between kidney tissues and DiffD9 cells are inevitable, owing to the inherent differences between *in vivo* and *in vitro* conditions. *In vivo* tissues are part of complex organs with a 3D architecture and multiple cell types, all finely regulated by external and local stimulations. In contrast, cells grown in 2D *in vitro* cultures are typically monocellular and lack the ability to from tissues, as they develop in a uniform environment without the intricate signaling and spatial organization present in human organs.

The PTEC are the most metabolically active cells of the nephron in drug metabolism and therefore the most vulnerable to drug-induced toxicity [42]. Consequently, a fundamental feature for any meaningful iPSC-derived toxicity screening model is the expression of drug transporters. For instance, it is well established that transport systems for organic anions and cations play an essential role in drug uptake and secretion [110].

Consistent with other studies using other differentiation models, almost all selected markers of key PTEC transporters were upregulated in both differentiated lines [19,76,98]. We demonstrated the upregulation of *OCTN-2,* an important transporter for carnitine and antiseizure drugs [18,110]. Other upregulated markers included those associated with cisplatin handling, like *CTR-1, CTR-2* and *OCT-2*. Notably, *OCT-2*, the most abundant member of the OCT family in PTEC and the most important for cisplatin uptake [18,49,111], showed increased mRNA levels in differentiated UM51 cells, in contrast to b4-DiffD9 cells; however, its protein expression was confirmed by western blot analysis. The observed discrepancy between gene and protein expression is perhaps due to the often poor correlation between mRNA and protein levels, as usually experienced in cell culture and other iPSC differentiation models [19,77]. When comparing b4- and F4-DiffD9 cells with RPTEC/TERT1, similar levels of mRNA expression for *CTR-1* and *OCT-2* were observed. Interestingly, other studies have neither studied *CTR-1/2* expression [19,76,98,112] nor succeeded to confirm *OCT-2* expression, which is a common issue in organoids [112,113].

In our model, and consistent with previous literature, b4-DiffD9 cells were characterized by the upregulation of other key proximal tubule transporters like *PEPT-1* [76,98] and *OAT-1* [76,93,114]. However, no significant differences were observed in the expression levels of *PEPT-2* and *OAT-3* pre-and post-differentiation. The expression of OATs is essential for studying drug metabolism, yet it is well-documented that their expression is usually lost *in vitro* [15]. Existing proximal tubule models, relying on immortalized human PTEC lines like HK-2 cells, RPTEC-hTERT and ciPTEC-hTERT, either lack the expression of OCTs and OATs or require additional lentiviral transduction of each transporter for drug toxicity assessments [15,40,115]. Moreover, OATs are also known to be unstable in organoid systems and other differentiation models [19,112]. Since the expression in DiffD9 cells is related to the hiPSC, a Western blot analysis could provide precise quantification of the protein levels before and after differentiation. To validate our findings, further functional assays are recommended to confirm transporter activity [93].

Another hallmark of a successful differentiation into PTEC is the expression of megalin, a scavenger receptor predominantly expressed in proximal tubules in the human body [19]. In our study, *MEG* and *CUBN* were upregulated in both differentiated lines. Notably, *MEG* expression was higher in b4-DiffD9 cells compared to F4-DiffD9 cells and RPTEC/TERT1, while *CUBN* expression was elevated compared to F4-DiffD9 cells but similar to RPTEC/TERT1. This upregulation may address the *in vitro* drawback of low *MEG* expression in HK-2 cells [115]. The functional activity of both proteins was confirmed in differentiated cells of both lines as demonstrated by the increased albumin uptake capacity. While similar functionality has been observed in organoids, RPTEC/TERT1 are known to lack functional albumin uptake [77,112]. Overall, these findings suggest that following the differentiation, DiffD9 cells demonstrate a satisfactory functionality consistent with proximal tubular characteristics.

In summary, the upregulation of established proximal tubule markers and the functional activity in DiffD9 cells indicate that b4 and UM51 hiPSC lines exhibited comparable differentiation capacity and achieved after 9 days of differentiation a functional proximal tubule epithelial-like cell phenotype.

5.2 Toxicity studies

5.2.1 Consistency of dose-response curves with literature confirms the potential of the PTELC in drug toxicity screening

Following the characterization of the PTELC, nephrotoxicity studies were conducted to evaluate the suitability of this differentiation model for drug screening and repair

mechanism studies. Dose-response curves were established to determine the IC_{20} and IC_{50} concentrations of cisplatin, CsA and H_2O_2. For the first time, we extended our interest to the transitional phase of differentiating cells at DiffD3 stage.

To determine dose-response curves following treatment with a genotoxic nephrotoxin, cells were treated with cisplatin at different stages of differentiation. Both stem cell lines exhibited comparable IC_{50} concentrations for cisplatin (approximately 3 µM for b4 and 6 µM for UM51), in agreement with previous studies using hiPSC and ESC-based protocols [77,116,117]. The IC_{50} concentration in b4-DiffD3 cells was also similar, likely due to the comparable proliferation rates observed with b4-hiPSC in the EdU assay. This could also explain why b4-PTELC were more resistant to cisplatin ($IC_{50} \approx 65$ µM) than their respective stem and DiffD3 cells, as their proliferation frequency was significantly reduced. The IC_{50} concentration of cisplatin in b4-PTELC was five-fold higher than that of F4-PTELC [77]. This raised the question of intrinsic cisplatin resistance in b4-PTELC. Subsequently, further analysis of markers associated with cisplatin resistance revealed an upregulation of *MCT-1* and *CTR-2* gene expression, together with a downregulation of *OATP-1,* while *MDR-1* showed no biologically relevant changes. This expression pattern could unlikely indicate cisplatin resistance as these markers were similarly expressed in F4-PTELC (unpublished data) and, more importantly, *MDR-1* was significantly lower comparted to RPTEC/TERT1. However, the expression at the protein level as well as the activity of these transporters should still be compared in future studies. Nevertheless, these findings align with an earlier study, reporting lower *MDR-1* expression in hiPSC-derived PTEC relative to human PTEC [76]. Additionally, b4-PTELC exhibited upregulation of proteins enhancing cisplatin sensitivity, including *OCT-2*, CTR-1 and *OAT-1*. Lastly, although the IC_{50} concentration in b4-PTELC may seem high, it is in agreement with predictions and values reported in other stem cell-based models [93,109,117–119].

Interestingly, at all cell stages, cells derived from b4 displayed lower sensitivity to cisplatin compared to those from F4 [77]. Difference in sensitivity between two stem cell lines against cisplatin was already reported [117]. Polymorphism and differences in activity of OCT-2 and MDR-1 might explain the difference in IC_{50} concentrations between PTELC derived from b4 and F4 [12,47,120]. For instance, the interindividual variability in MDR-1 leads to different patient responses to opioids [121]. Therefore, functional analysis of MDR-1 activity could further help understanding the differences in response between the two cell lines. These observations highlight that different hiPSC lines subjected to the same differentiation protocol may show different behaviors and

differentiation profiles. Elucidating the extent to which this discrepancy is significant needs further investigations. These results suggest that selecting an appropriate stem cell line may be as essential as choosing the right differentiation protocol, given the possibility that iPSC might retain some characteristics of the original tissue from which they were reprogrammed.

Similarly, both b4-hiPSC and b4-DiffD3 cells showed lower sensitivity to H_2O_2 compared to the corresponding F4 cell stages [77]. However, DiffD3 cells from both lines displayed increased sensitivity to H_2O_2 (b4-DiffD3 $IC_{50} \approx 97$ µM) when compared to their respective stem cells (b4-hiPSC $IC_{50} \approx 467$ µM), in contrast to cisplatin response where stem cells were more sensitive. One hypothesis would be that the increased sensitivity of DiffD3 cells to H_2O_2 may indicate a downregulation of some oxidative stress defense mechanisms in cells undergoing differentiation process, which could be investigated in the future with antioxidant defense expression analysis. Another explanation could be the stress associated with differentiation, as cells undergo drastic changes like increased mitochondrial biogenesis, leading to elevated ROS levels. Stem cells may have a more robust oxidative stress defense before undergoing differentiation [122]. Since the physiological interstitial H_2O_2 concentration in the human body is typically around 20 µM, the observed IC_{50} values may appear elevated. In fact, most studies with H_2O_2 use concentrations exceeding 100 µM. Several factors may account for this: first, high concentrations are often required to generate an oxidative response due to the rapid turnover of antioxidant enzymes, which can neutralize hundreds of micromoles of H_2O_2 within minutes. Second, such high concentrations may mirror conditions reported during inflammatory states *in vivo* [123].

Regarding CsA, the treatment was used as a non-genotoxic control to cisplatin. UM51 and b4-hiPSC showed similar sensitivities to CsA. Interestingly, the IC_{50} values, approximately 9 ± 1 µM, were consistent across all b4-derived cell stages, indicating that CsA toxicity is independent from the differentiation state. Although comparable studies on CsA treatment in hiPSC and hiPSC-derived cells are lacking, a similar response was observed in different differentiation stages of F4 after CsA treatment [77].

In summary, the generated inhibitory concentrations values for the selected drugs were consistent with those reported in the literature, which makes this model promising for drug toxicity screening.

5.2.2 Effects of nephrotoxins on proliferation rates support the predictive value of the PTELC

Stem cell proliferation and differentiation *in vitro* might mimic the repair mechanisms of PTEC after kidney injury *in vivo*. To explore this, cells at different stages of the differentiation were exposed to genotoxic and non-genotoxic nephrotoxins, to assess their impact on proliferation. For the first time, we extended our attention to the transitional phase of differentiation at DiffD3.

A low cisplatin concentration (0.2 µM) significantly increased EdU uptake in DiffD3 cells, suggesting enhanced nuclear incorporation of fluorescent nucleotides to ensure DNA synthesis after cisplatin-induced sub-lethal damage [124]. A similar response was observed across all cell stages when treated with the IC_{20} concentration of cisplatin for stem cells (1 µM), as stem cells demonstrated the highest cisplatin sensitivity. The observed elevation in EdU-positive cells likely corresponded to active repair process. In DiffD9 cells in particular, fluorescent cells may have resulted either from cells retaining proliferative potential or differentiated cells undergoing dedifferentiation [92]. Moreover, low-dose cisplatin treatment may have triggered pro-survival pathways via ROS-mediated signaling to cope with low cisplatin damage. Previous studies have shown that pre-incubation of bone marrow stem cells with low levels of a prooxidative agent could enhance stress responses and reduce apoptosis under oxidative stress [125]. Further investigations into repair mechanisms and EMT are needed to provide more insights. Additionally, it is well-established that high cisplatin concentrations cause cell cycle arrest and hinder DNA repair, which was confirmed by the absence of fluorescent labeling in DiffD9 cells following treatment with their IC_{50} concentration of cisplatin (65 µM) [45].

Regarding CsA, consistent results were obtained across all cell stages following treatment with 8 µM CsA, which corresponds to the IC_{50} for b4-hiPSC. CsA had no significant effect on proliferation rates, except for a slight reduction in EdU uptake in PTELC when treated with their IC_{50} concentration of 10 µM. These outcomes align with previous findings, showing no cytostatic effects of CsA [126]. Such results were anticipated since CsA's toxicity mechanisms do not comprise direct DNA damage, but are instead mediated by other conserved pathways involving ROS generation, mainly through mitochondrial and ER stress [67,68,127].

In summary, genotoxic and non-genotoxic treatments induced expected effects on the proliferation rates, indicating that the PTELC model responded appropriately and demonstrated a satisfactory predictive value regarding nephrotoxicity.

5.2.3 Cisplatin-induced antioxidant response confirms the potential of the PTELC in oxidative stress studies

Given the potential of cisplatin to induce oxidative stress [46,60], the genotoxic and oxidative stress response of b4-PTELC and b4-hiPSC was assessed following treatment with their respective IC_{20} (1 µM in b4 and 13 µM in PTELC) and IC_{50} concentrations (3 µM in b4 and 65 µM in PTELC).

In hiPSC, cisplatin treatment did not result in a change in the expression of oxidative stress response genes compared to untreated cells, which indicates a relative resistance of hiPSC to cisplatin-induced oxidative stress. This finding was supported by the results of the staining for the activated regulator of the response to oxidative stress, pNRF-2, which showed no difference in pNRF-2 expression intensity after cisplatin treatment. Indeed, stem cells with their unlimited proliferation and differentiation capacity, have a highly efficient machinery to fight various stressors. In addition to their robust DNA repair systems, hiPSC rely on anaerobic metabolism with a reduced number of mitochondria, which decreases ROS production [128]. Additionally, stem cells maintain a favorable redox environment with increased levels of intracellular GSH. This feature was confirmed by the significantly elevated GSH levels after IC_{20} cisplatin treatment, which highlights GSH's key role in cisplatin detoxification [129,130]. Oxidative stress has been shown to reduce stem cell proliferation and induce differentiation in adult stem cells [130,131]. These findings suggest that spontaneous differentiation may be a possible defense mechanism against oxidative stress in stem cells. Another explanation would be the activation of alternative pathways (like autophagy and apoptosis) that could prevent the activation of *NRF-2* and its downstream targets. Other works have reported that in hematopoietic stem cells*, NRF-2*-mediated survival was independent of ROS levels [130].

In PTELC, cisplatin treatment induced a dose-dependent oxidative stress response. At IC_{20} (13 µM), the oxidative stress was sufficient to activate antioxidant genes (*NQO-1* and *GPX-1)*, without affecting *NRF-2* expression. *NQO-1* activation is however, an indicator of NRF-2 activity since *NQO-1* is the most specific target of NRF-2 [132]. At IC_{50} (65 µM), the high oxidative stress levels resulted in persistent *GPX-1* expression but a downregulation of *NRF-2* and other associated genes, indicating cellular exhaustion. The reduced pNRF-2 expression intensity at IC_{50} further confirms that NRF-2 activation diminished as oxidative stress increased, potentially due to the induction of negative regulators of NRF-2 like GSK-3ß or to intracellular depletion of pNRF-2 [132]. Moreover, Xue *et al.* (2015) demonstrated that under oxidative stress, *ARE* is activated through an

increased rate of translocational oscillations of NRF-2, without changes in the total cellular NRF-2 protein levels [32].

These results suggest that while protective antioxidant mechanisms are initiated at IC_{20}, they may be overwhelmed at IC_{50}, possibly due to epigenetic modifications caused by cisplatin, such as DNA methylation and histone modifications, which could downregulate the *NRF-2* gene or its pathways [133]. Additionally, high cisplatin doses may activate pro-apoptotic pathways that overcome the protective role of NRF-2 and its targets. For example, p53 activation after DNA damage is known to suppress *NRF-2* expression [134]. Furthermore, multiple animal studies have documented the downregulation of *NRF-2* following cisplatin exposure, with its expression restored through several antioxidant agents [135–137]. Downregulation of stress defense markers after pro-oxidative treatment has also been observed in differentiated human ESC [122,138] and primary human renal PTEC [139]. Importantly, as this analysis was conducted 24 h post-treatment, a time-course study could provide information about a potential fluctuation in gene expression over time before the observed downregulation.

These findings suggest that PTELC exhibited a more dynamic response to cisplatin treatment compared to hiPSC. The gene expression changes showed a mild oxidative stress responses at IC_{20} and a decrease of oxidative stress responses at IC_{50}. When comparing the respective absolute IC_{20} and IC_{50} values, hiPSC appear more sensitive than PTELC. However, the relative effects of each IC_{20} and IC_{50} value on the expression of antioxidant genes in hiPSC and PTELC suggest that PTELC may be more susceptible to elevated oxidative stress levels by rapidly activating cell death pathways. In other words, the threshold for activation of antioxidant defence system is lower in PTELC. The increased sensitivity in PTELC could be attributed to variations in oxidative stress defense mechanisms and different cisplatin toxicity pathways, where PTELC may be predominantly affected by oxidative stress, while hiPSC may be more vulnerable to DNA damage [45,57,59,60]. Additionally, studies suggest that cisplatin-induced nephrotoxicity and tumor toxicity occur through different pathways [50]. Further analysis of DNA damage markers and necrosis, apoptosis or senescence pathways, could help better characterizing the toxicity mechanisms of cisplatin in these cell types.

In summary, PTELC showed a dose-dependent response to cisplatin treatment and displayed an appropriate antioxidant response, which suggests that PTELC may be a reliable model for drug toxicity screening. However, additional substances should be tested to further validate and strengthen the conclusions drawn from the findings of this study.

Overall, the behaviour of the PTELC after treatment with established nephrotoxins aligns with the expected outcomes of a drug toxicity testing platform, in terms of proliferative response, as well as gene and protein expression. Injury mechanisms linked to PTEC toxicity in humans were specifically induced and accurately detected. This indicates that the PTELC-based *in vitro* model is a promising tool for drug screening.

6 Overview and Conclusion

In this study, b4- and for the first time UM51-hiPSC were successfully differentiated into PTELC. The PTELC generated form these two cell lines displayed comparable morphology changes, functionality and expression of PTEC markers and transporters after differentiation. Comparisons of b4-PTELC, F4-PTELC and RPTEC/TERT1 indicated overall similarity in expression profiles without the limitations associated with immortalized primary cells. Nevertheless, some important PTEC transporters like SGLT-2 were downregulated. This might be explained by the unknown gene expression in hiPSC and could possibly be verified by protein expression analysis or glucose uptake assays. Additional experiments on the effects of nephrotoxins on differentiation markers and cellular function may provide better characterization of PTELC.

In toxicity studies, b4-PTELC exhibited a greater resistance to cisplatin. This suggests a potential influence of the type of the hiPSC line on differentiation outcomes. Moreover, in line with the results from the F4 line, differentiating cells at DiffD3 stage were more sensitive to oxidative stress as compared to stem cells [77]. Investigating stress response mechanisms in DiffD3 cells could enhance our understanding of biological changes during differentiation *in vitro* and provide insights into *in vivo* repair mechanisms and the subclinical renal function decline post-AKI.

The genotoxic cisplatin had a more pronounced effect on the proliferation throughout the differentiation as compared to the non-genotoxic CsA. However, the increased proliferation observed in b4-hiPSC and DiffD3 cells at lower cisplatin concentrations could indicate enhanced repair following DNA damage. Moreover, treatment of PTELC with IC_{20} concentrations of cisplatin induced a dose-dependent response, characterized by the upregulation of antioxidant markers *NQO-1* and *GPX-1*, while most genes were downregulated at IC_{50} concentrations. Furthermore, the reduction in pNRF-2 expression intensity observed through immunocytochemistry indicates overwhelmed antioxidant mechanisms through alternative cell injury pathways. Additional time-course analysis including DiffD3 cells may help understanding the dynamic changes in oxidative stress responses during differentiation and repair. In contrast, hiPSC appeared more robust against oxidative stress, as shown by the increased GSH levels in b4-hiPSC after IC_{20} cisplatin treatment but this observation needs further investigation in PTELC for comparative analysis. All together, these results highlight the satisfactory performance of this stem cell-based model as a promising tool for drug toxicity tests and repair mechanisms studies.

As with many current stem cell-based differentiation models, there is room for further improvement in the PTELC model. Questions regarding the maturity and purity of the generated PTELC remain. Additionally, electron microscopy could help identify villi and brush borders and determine cellular polarity. Another improvement could involve detecting segment-specific proximal tubule markers like SGLT-2 (S1 segment) carbonic anhydrase IV (S2) and ecto-adenosine triphosphatase (S3) [140].

Besides studying cell death pathways in toxicity assays, examining other mechanistic aspects, like changes in cellular polarity, membrane integrity and mitochondrial function could offer a more comprehensive understanding of differentiating and differentiated cell responses to toxic substances and their repair mechanisms. Further research into analysis of novel AKI markers, like KIM-1 (kidney injury molecule) and NGAL (neutrophil gelatinase-associated lipocalin), may also be beneficial, especially as prior attempts using RPTEC and HPTEC were unsuccessful to detect them [40,42,43]. Protocol optimization to extend and stabilize PTELC cultures could further enhance the model's applicability, by modifying culture media and extracellular matrix components or introducing 3D structures to support long-term and complex studies of PTELC.

In summary, considering the above mentioned limitations and the proposed improvements, the constellation of gene and protein expression profiles for epithelial and proximal tubule markers, along with the functionality of the PTELC and their responses to nephrotoxicity tests, make this model ready for use in drug toxicity and regenerative medicine studies.

References

1. Costanzo L. (2021). Costanzo Physiology E-Book: Costanzo Physiology E-Book. Elsevier Health Sciences

2. Marieb Human Anatomy & Physiology. https://www.pearson.com/en-us/subject-catalog/p/marieb-human-anatomy--physiology/P200000011643/9780138244415. Accessed 3.9.2024. https://www.pearson.com/en-us/subject-catalog/p/marieb-human-anatomy--physiology/P200000011643/9780138244415. Accessed September 3, 2024

3. Maunsbach A. B., Marples D., Chin E., Ning G., Bondy C., Agre P., et al. (1997). Aquaporin-1 water channel expression in human kidney. Journal of the American Society of Nephrology, *8*(1), 1-14. https://doi.org/10.1681/ASN.V811

4. Sugawara-Yokoo M., Suzuki T., Matsuzaki T., Naruse T., & Takata K. (1999). Presence of fructose transporter GLUT5 in the S3 proximal tubules in the rat kidney. Kidney International, *56*(3), 1022-1028. https://doi.org/10.1046/j.1523-1755.1999.00635.x

5. Daniel H., & Rubio-Aliaga I. (2003). An update on renal peptide transporters. American Journal of Physiology-Renal Physiology, *284*(5), F885-F892. https://doi.org/10.1152/ajprenal.00123.2002

6. Wright E. M. (2001). Renal Na+-glucose cotransporters. American Journal of Physiology-Renal Physiology, *280*(1), F10-F18. https://doi.org/10.1152/ajprenal.2001.280.1.F10

7. Kaze A. D., Zhuo M., Kim S. C., Patorno E., & Paik J. M. (2022). Association of SGLT2 inhibitors with cardiovascular, kidney, and safety outcomes among patients with diabetic kidney disease: a meta-analysis. Cardiovascular Diabetology, *21*(1), 47. https://doi.org/10.1186/s12933-022-01476-x

8. Podestà M. A., Sabiu G., Galassi A., Ciceri P., & Cozzolino M. (2023). SGLT2 Inhibitors in Diabetic and Non-Diabetic Chronic Kidney Disease. Biomedicines, *11*(2), 279. https://doi.org/10.3390/biomedicines11020279

9. Molitoris B. A., Sandoval R. M., Yadav S. P. S., & Wagner M. C. (2022). Albumin uptake and processing by the proximal tubule: physiological, pathological, and therapeutic implications. Physiological Reviews, *102*(4), 1625-1667. https://doi.org/10.1152/physrev.00014.2021

10. Romero-González G., Rodríguez-Chitiva N., Cañameras C., Paúl-Martínez J., Urrutia-Jou M., Troya M., et al. (2024). Albuminuria, Forgotten No More: Underlining the Emerging Role in CardioRenal Crosstalk. Journal of Clinical Medicine, *13*(3), 777. https://doi.org/10.3390/jcm13030777

11. Nielsen R., Christensen E. I., & Birn H. (2016). Megalin and cubilin in proximal tubule protein reabsorption: from experimental models to human disease. Kidney International, *89*(1), 58-67. https://doi.org/10.1016/j.kint.2015.11.007

12. Ciarimboli G., Deuster D., Knief A., Sperling M., Holtkamp M., Edemir B., et al. (2010). Organic cation transporter 2 mediates cisplatin-induced oto- and

nephrotoxicity and is a target for protective interventions. The American Journal of Pathology, *176*(3), 1169-1180. https://doi.org/10.2353/ajpath.2010.090610

13. Ciarimboli G. (2014). Membrane Transporters as Mediators of Cisplatin Side-effects. Anticancer Research, *34*(1), 547-550.

14. Hu S., Leblanc A., Gibson A., Hong K., Kim J., Janke L., et al. (2017). Identification of OAT1/OAT3 as Contributors to Cisplatin Toxicity. Clinical and Translational Science, *10*(5), 412-420. https://doi.org/10.1111/cts.12480

15. Caetano-Pinto P., & Stahl S. H. (2023). Renal Organic Anion Transporters 1 and 3 In Vitro: Gone but Not Forgotten. International Journal of Molecular Sciences, *24*(20), 15419. https://doi.org/10.3390/ijms242015419

16. Fang Z., Chen W., Yuan Z., Liu X., & Jiang H. (2018). LncRNA-MALAT1 contributes to the cisplatin-resistance of lung cancer by upregulating MRP1 and MDR1 via STAT3 activation. Biomedicine & Pharmacotherapy, *101*, 536-542. https://doi.org/10.1016/j.biopha.2018.02.130

17. Interaction of immunosuppressive drugs with human organic anion transporter (OAT) 1 and OAT3, and multidrug resistance-associated protein (MRP) 2 and MRP4 - PubMed. https://pubmed.ncbi.nlm.nih.gov/24036158/. Accessed 4.9.2024. https://pubmed.ncbi.nlm.nih.gov/24036158/. Accessed September 4, 2024

18. George B., You D., Joy M. S., & Aleksunes L. M. (2017). Xenobiotic transporters and kidney injury. Advanced Drug Delivery Reviews, *116*, 73-91. https://doi.org/10.1016/j.addr.2017.01.005

19. Chandrasekaran V., Carta G., Da Costa Pereira D., Gupta R., Murphy C., Feifel E., et al. (2021). Generation and characterization of iPSC-derived renal proximal tubule-like cells with extended stability. Scientific Reports, *11*(1), 11575. https://doi.org/10.1038/s41598-021-89550-4

20. Sies H., Berndt C., & Jones D. P. (2017). Oxidative Stress. Annual Review of Biochemistry, *86*, 715-748. https://doi.org/10.1146/annurev-biochem-061516-045037

21. Birben E., Sahiner U. M., Sackesen C., Erzurum S., & Kalayci O. (2012). Oxidative Stress and Antioxidant Defense. World Allergy Organization Journal, *5*(1), 9-19. https://doi.org/10.1097/WOX.0b013e3182439613

22. Niki E. (2016). Oxidative stress and antioxidants: *Distress* or *eustress*? Archives of Biochemistry and Biophysics, *595*, 19-24. https://doi.org/10.1016/j.abb.2015.11.017

23. Brieger K., Schiavone S., Miller F. J., & Krause K.-H. (2012). Reactive oxygen species: from health to disease. Swiss Medical Weekly, *142*, w13659. https://doi.org/10.4414/smw.2012.13659

24. Sies H. (2017). Hydrogen peroxide as a central redox signaling molecule in physiological oxidative stress: Oxidative eustress. Redox Biology, *11*, 613-619. https://doi.org/10.1016/j.redox.2016.12.035

25. Rudolph V., Andrié R. P., Rudolph T. K., Friedrichs K., Klinke A., Hirsch-Hoffmann B., et al. (2010). Myeloperoxidase acts as a profibrotic mediator of atrial fibrillation. Nature Medicine, *16*(4), 470-474. https://doi.org/10.1038/nm.2124

26. Müller M., Donhauser E., Maske T., Bischof C., Dumitrescu D., Rudolph V., et al. (2023). Mitochondrial Integrity Is Critical in Right Heart Failure Development. International Journal of Molecular Sciences, *24*(13), 11108. https://doi.org/10.3390/ijms241311108

27. Dinkova-Kostova A. T., Kostov R. V., & Kazantsev A. G. (2018). The role of Nrf2 signaling in counteracting neurodegenerative diseases. The Febs Journal, *285*(19), 3576-3590. https://doi.org/10.1111/febs.14379

28. Gyurászová M., Gurecká R., Bábíčková J., & Tóthová Ľ. (2020). Oxidative Stress in the Pathophysiology of Kidney Disease: Implications for Noninvasive Monitoring and Identification of Biomarkers. Oxidative Medicine and Cellular Longevity, *2020*, 5478708. https://doi.org/10.1155/2020/5478708

29. Nuhu F., Gordon A., Sturmey R., Seymour A.-M., & Bhandari S. (2020). Measurement of Glutathione as a Tool for Oxidative Stress Studies by High Performance Liquid Chromatography. Molecules, *25*(18), 4196. https://doi.org/10.3390/molecules25184196

30. Sihvola V., & Levonen A.-L. (2017). Keap1 as the redox sensor of the antioxidant response. Archives of Biochemistry and Biophysics, *617*, 94-100. https://doi.org/10.1016/j.abb.2016.10.010

31. Kaspar J. W., Niture S. K., & Jaiswal A. K. (2009). Nrf2:INrf2 (Keap1) signaling in oxidative stress. Free Radical Biology and Medicine, *47*(9), 1304-1309. https://doi.org/10.1016/j.freeradbiomed.2009.07.035

32. Xue M., Momiji H., Rabbani N., Barker G., Bretschneider T., Shmygol A., et al. (2015). Frequency Modulated Translocational Oscillations of Nrf2 Mediate the Antioxidant Response Element Cytoprotective Transcriptional Response. Antioxidants & Redox Signaling, *23*(7), 613-629. https://doi.org/10.1089/ars.2014.5962

33. Hayes J. D., & Dinkova-Kostova A. T. (2014). The Nrf2 regulatory network provides an interface between redox and intermediary metabolism. Trends in Biochemical Sciences, *39*(4), 199-218. https://doi.org/10.1016/j.tibs.2014.02.002

34. Moinova H. R., & Mulcahy R. T. (1999). Up-regulation of the human gamma-glutamylcysteine synthetase regulatory subunit gene involves binding of Nrf-2 to an electrophile responsive element. Biochemical and Biophysical Research Communications, *261*(3), 661-668. https://doi.org/10.1006/bbrc.1999.1109

35. Alam J., Stewart D., Touchard C., Boinapally S., Choi A. M. K., & Cook J. L. (1999). Nrf2, a Cap'n'Collar Transcription Factor, Regulates Induction of the Heme Oxygenase-1 Gene *. Journal of Biological Chemistry, *274*(37), 26071-26078. https://doi.org/10.1074/jbc.274.37.26071

36. Morrison S. J., & Kimble J. (2006). Asymmetric and symmetric stem-cell divisions in development and cancer. Nature, *441*(7097), 1068-1074. https://doi.org/10.1038/nature04956

37. Yamzon J. L., Kokorowski P., & Koh C. J. (2008). Stem Cells and Tissue Engineering Applications of the Genitourinary Tract. Pediatric Research, *63*(5), 472-477. https://doi.org/10.1203/PDR.0b013e31816a704a

38. Takahashi K., Tanabe K., Ohnuki M., Narita M., Ichisaka T., Tomoda K., et al. (2007). Induction of pluripotent stem cells from adult human fibroblasts by defined factors. Cell, *131*(5), 861-872. https://doi.org/10.1016/j.cell.2007.11.019

39. Boyer L. A., Lee T. I., Cole M. F., Johnstone S. E., Levine S. S., Zucker J. P., et al. (2005). Core Transcriptional Regulatory Circuitry in Human Embryonic Stem Cells. Cell, *122*(6), 947-956. https://doi.org/10.1016/j.cell.2005.08.020

40. Faria J., Ahmed S., Gerritsen K. G. F., Mihaila S. M., & Masereeuw R. (2019). Kidney-based in vitro models for drug-induced toxicity testing. Archives of Toxicology, *93*(12), 3397-3418. https://doi.org/10.1007/s00204-019-02598-0

41. Kim J., Koo B.-K., & Knoblich J. A. (2020). Human organoids: model systems for human biology and medicine. Nature Reviews Molecular Cell Biology, *21*(10), 571-584. https://doi.org/10.1038/s41580-020-0259-3

42. Nieskens T. T. G., & Sjögren A.-K. (2019). Emerging *In Vitro* Systems to Screen and Predict Drug-Induced Kidney Toxicity. Seminars in Nephrology, *39*(2), 215-226. https://doi.org/10.1016/j.semnephrol.2018.12.009

43. Tiong H. Y., Huang P., Xiong S., Li Y., Vathsala A., & Zink D. (2014). Drug-Induced Nephrotoxicity: Clinical Impact and Preclinical in Vitro Models. Molecular Pharmaceutics, *11*(7), 1933-1948. https://doi.org/10.1021/mp400720w

44. Van Der Hauwaert C., Savary G., Gnemmi V., Glowacki F., Pottier N., Bouillez A., et al. (2013). Isolation and Characterization of a Primary Proximal Tubular Epithelial Cell Model from Human Kidney by CD10/CD13 Double Labeling. PLoS ONE, *8*(6), e66750. https://doi.org/10.1371/journal.pone.0066750

45. Wang D., & Lippard S. J. (2005). Cellular processing of platinum anticancer drugs. Nature Reviews. Drug Discovery, *4*(4), 307-320. https://doi.org/10.1038/nrd1691

46. Miller R. P., Tadagavadi R. K., Ramesh G., & Reeves W. B. (2010). Mechanisms of Cisplatin Nephrotoxicity. Toxins, *2*(11), 2490-2518. https://doi.org/10.3390/toxins2112490

47. Filipski K. K., Mathijssen R. H., Mikkelsen T. S., Schinkel A. H., & Sparreboom A. (2009). Contribution of organic cation transporter 2 (OCT2) to cisplatin-induced nephrotoxicity. Clinical pharmacology and therapeutics, *86*(4), 396-402. https://doi.org/10.1038/clpt.2009.139

48. Cisplatin nephrotoxicity - UpToDate. https://sso.uptodate.com/contents/cisplatin-nephrotoxicity?search=nephrotoxicity%20cisplatin&source=search_result&selectedTitle=1%7E150&usage_type=default&display_rank=1. Accessed 5.8.2024. https://sso.uptodate.com/contents/cisplatin-nephrotoxicity?search=nephrotoxicity%20cisplatin&source=search_result&selectedTitle=1%7E150&usage_type=default&display_rank=1. Accessed August 5, 2024

49. Blair B. G., Larson C. A., Safaei R., & Howell S. B. (2009). Copper Transporter 2 Regulates the Cellular Accumulation and Cytotoxicity of Cisplatin and Carboplatin.

Clinical Cancer Research, *15*(13), 4312-4321. https://doi.org/10.1158/1078-0432.CCR-09-0311

50. Cristofori P., Zanetti E., Fregona D., Piaia A., & Trevisan A. (2007). Renal Proximal Tubule Segment-Specific Nephrotoxicity: An Overview on Biomarkers and Histopathology. Toxicologic Pathology, *35*(2), 270-275. https://doi.org/10.1080/01926230601187430

51. Mapuskar K. A., Steinbach E. J., Zaher A., Riley D. P., Beardsley R. A., Keene J. L., et al. (2021). Mitochondrial Superoxide Dismutase in Cisplatin-Induced Kidney Injury. Antioxidants, *10*(9), 1329. https://doi.org/10.3390/antiox10091329

52. Beyer J., Rick O., Weinknecht S., Kingreen D., Lenz K., & Siegert W. (1997). Nephrotoxicity after high-dose carboplatin, etoposide and ifosfamide in germ-cell tumors: incidence and implications for hematologic recovery and clinical outcome. Bone Marrow Transplantation, *20*(10), 813-819. https://doi.org/10.1038/sj.bmt.1700980

53. Arany I., & Safirstein R. L. (2003). Cisplatin nephrotoxicity. Seminars in Nephrology, *23*(5), 460-464. https://doi.org/10.1016/s0270-9295(03)00089-5

54. Xu E. Y., Perlina A., Vu H., Troth S. P., Brennan R. J., Aslamkhan A. G., et al. (2008). Integrated Pathway Analysis of Rat Urine Metabolic Profiles and Kidney Transcriptomic Profiles To Elucidate the Systems Toxicology of Model Nephrotoxicants. Chemical Research in Toxicology, *21*(8), 1548-1561. https://doi.org/10.1021/tx800061w

55. Townsend D. M., Deng M., Zhang L., Lapus M. G., & Hanigan M. H. (2003). Metabolism of Cisplatin to a nephrotoxin in proximal tubule cells. Journal of the American Society of Nephrology: JASN, *14*(1), 1-10. https://doi.org/10.1097/01.asn.0000042803.28024.92

56. Olivero O. A., Chang P. K., Lopez-Larraza D. M., Semino-Mora M. C., & Poirier M. C. (1997). Preferential formation and decreased removal of cisplatin-DNA adducts in Chinese hamster ovary cell mitochondrial DNA as compared to nuclear DNA. Mutation Research, *391*(1-2), 79-86. https://doi.org/10.1016/s0165-1218(97)00037-2

57. Mandic A., Hansson J., Linder S., & Shoshan M. C. (2003). Cisplatin induces endoplasmic reticulum stress and nucleus-independent apoptotic signaling. The Journal of Biological Chemistry, *278*(11), 9100-9106. https://doi.org/10.1074/jbc.M210284200

58. Montopoli M., Bellanda M., Lonardoni F., Ragazzi E., Dorigo P., Froldi G., et al. (2011). “Metabolic reprogramming” in ovarian cancer cells resistant to cisplatin. Current Cancer Drug Targets, *11*(2), 226-235. https://doi.org/10.2174/156800911794328501

59. Qian W., Nishikawa M., Haque A. M., Hirose M., Mashimo M., Sato E., et al. (2005). Mitochondrial density determines the cellular sensitivity to cisplatin-induced cell death. American Journal of Physiology. Cell Physiology, *289*(6), C1466-1475. https://doi.org/10.1152/ajpcell.00265.2005

60. Yang Y., Liu H., Liu F., & Dong Z. (2014). Mitochondrial dysregulation and protection in cisplatin nephrotoxicity. Archives of Toxicology, *88*(6), 1249-1256. https://doi.org/10.1007/s00204-014-1239-1

61. Naesens M., Kuypers D. R. J., & Sarwal M. (2009). Calcineurin Inhibitor Nephrotoxicity. Clinical Journal of the American Society of Nephrology, *4*(2), 481. https://doi.org/10.2215/CJN.04800908

62. Bobadilla N. A., & Gamba G. (2007). New insights into the pathophysiology of cyclosporine nephrotoxicity: a role of aldosterone. American Journal of Physiology-Renal Physiology, *293*(1), F2-F9. https://doi.org/10.1152/ajprenal.00072.2007

63. Olyaei A. J., de Mattos A. M., & Bennett W. M. (2001). Nephrotoxicity of immunosuppressive drugs: new insight and preventive strategies. Current Opinion in Critical Care, *7*(6), 384.

64. Wu Q., Wang X., Nepovimova E., Wang Y., Yang H., & Kuca K. (2018). Mechanism of cyclosporine A nephrotoxicity: Oxidative stress, autophagy, and signalings. Food and Chemical Toxicology: An International Journal Published for the British Industrial Biological Research Association, *118*, 889-907. https://doi.org/10.1016/j.fct.2018.06.054

65. Pharmacology of calcineurin inhibitors - UpToDate. https://www.uptodate.com/contents/pharmacology-of-calcineurin-inhibitors?search=cyclosporin%20a&source=search_result&selectedTitle=3%7E150&usage_type=default&display_rank=2. Accessed 8.8.2024. https://www.uptodate.com/contents/pharmacology-of-calcineurin-inhibitors?search=cyclosporin%20a&source=search_result&selectedTitle=3%7E150&usage_type=default&display_rank=2. Accessed August 8, 2024

66. de Arriba G., Calvino M., Benito S., & Parra T. (2013). Cyclosporine A-induced apoptosis in renal tubular cells is related to oxidative damage and mitochondrial fission. Toxicology Letters, *218*(1), 30-38. https://doi.org/10.1016/j.toxlet.2013.01.007

67. Pallet N., Rabant M., Xu-Dubois Y.-C., LeCorre D., Mucchielli M.-H., Imbeaud S., et al. (2008). Response of human renal tubular cells to cyclosporine and sirolimus: A toxicogenomic study. Toxicology and Applied Pharmacology, *229*(2), 184-196. https://doi.org/10.1016/j.taap.2008.01.019

68. Pallet N., Bouvier N., Bendjallabah A., Rabant M., Flinois J. P., Hertig A., et al. (2008). Cyclosporine-Induced Endoplasmic Reticulum Stress Triggers Tubular Phenotypic Changes and Death. American Journal of Transplantation, *8*(11), 2283-2296. https://doi.org/10.1111/j.1600-6143.2008.02396.x

69. Liu Q., Ye J., Yu L., Dong X., Feng J., Xiong Y., et al. (2017). Klotho mitigates cyclosporine A (CsA)-induced epithelial–mesenchymal transition (EMT) and renal fibrosis in rats. International Urology and Nephrology, *49*(2), 345-352. https://doi.org/10.1007/s11255-016-1439-0

70. McMorrow T., Gaffney M. M., Slattery C., Campbell E., & Ryan M. P. (2005). Cyclosporine A induced epithelial–mesenchymal transition in human renal proximal tubular epithelial cells. Nephrology Dialysis Transplantation, *20*(10), 2215-2225. https://doi.org/10.1093/ndt/gfh967

71. Olshan (Chair) A. F., Mattison D. R., & Zwanenburg T. S. B. (1994). Cyclosporine A: Review of genotoxicity and potential for adverse human reproductive and developmental effects: Report of a working group on the genotoxicity of cyclosporine A, August 18, 1993. Mutation Research/Reviews in Genetic Toxicology, *317*(2), 163-173. https://doi.org/10.1016/0165-1110(94)90023-X

72. Walsh S. B., Xu J., Xu H., Kurundkar A. R., Maheshwari A., Grizzle W. E., et al. (2011). Cyclosporine a mediates pathogenesis of aggressive cutaneous squamous cell carcinoma by augmenting epithelial-mesenchymal transition: Role of TGFβ signaling pathway. Molecular Carcinogenesis, *50*(7), 516-527. https://doi.org/10.1002/mc.20744

73. Veal E. A., Day A. M., & Morgan B. A. (2007). Hydrogen Peroxide Sensing and Signaling. Molecular Cell, *26*(1), 1-14. https://doi.org/10.1016/j.molcel.2007.03.016

74. Finkel T., & Holbrook N. J. (2000). Oxidants, oxidative stress and the biology of ageing. Nature, *408*(6809), 239-247. https://doi.org/10.1038/35041687

75. Juven B. J., & Pierson M. D. (1996). Antibacterial Effects of Hydrogen Peroxide and Methods for Its Detection and Quantitation†. Journal of Food Protection, *59*(11), 1233-1241. https://doi.org/10.4315/0362-028X-59.11.1233

76. Kandasamy K., Chuah J. K. C., Su R., Huang P., Eng K. G., Xiong S., et al. (2015). Prediction of drug-induced nephrotoxicity and injury mechanisms with human induced pluripotent stem cell-derived cells and machine learning methods. Scientific Reports, *5*(1), 12337. https://doi.org/10.1038/srep12337

77. Mboni-Johnston I. M., Kouidrat N. M. Z., Hirsch C., Weber A. G., Meißner A., Adjaye J., et al. (2024). Sensitivity of Human Induced Pluripotent Stem Cells and Thereof Differentiated Kidney Proximal Tubular Cells towards Selected Nephrotoxins. International Journal of Molecular Sciences, *25*(1), 81. https://doi.org/10.3390/ijms25010081

78. Wang Y., & Adjaye J. (2011). A Cyclic AMP Analog, 8-Br-cAMP, Enhances the Induction of Pluripotency in Human Fibroblast Cells. Stem Cell Reviews and Reports, *7*(2), 331-341. https://doi.org/10.1007/s12015-010-9209-3

79. Bohndorf M., Ncube A., Spitzhorn L.-S., Enczmann J., Wruck W., & Adjaye J. (2017). Derivation and characterization of integration-free iPSC line ISRM-UM51 derived from SIX2-positive renal cells isolated from urine of an African male expressing the CYP2D6 *4/*17 variant which confers intermediate drug metabolizing activity. Stem Cell Research, *25*, 18-21. https://doi.org/10.1016/j.scr.2017.10.004

80. Baer P. C., Tunn U. W., Nunez G., Scherberich J. E., & Geiger H. (1999). Transdifferentiation of Distal but Not Proximal Tubular Epithelial Cells from Human Kidney in Culture. Experimental Nephrology, *7*(4), 306-313. https://doi.org/10.1159/000020618

81. Uhrig M., Ezquer F., & Ezquer M. (2022). Improving Cell Recovery: Freezing and Thawing Optimization of Induced Pluripotent Stem Cells. Cells, *11*(5), 799. https://doi.org/10.3390/cells11050799

82. Kuijpers L., Veen E. van, Pol L. A. van der, & Dekker N. H. (2023). Automated cell counting for Trypan blue-stained cell cultures using machine learning. PLOS ONE, *18*(11), e0291625. https://doi.org/10.1371/journal.pone.0291625

83. Ligasová A., & Koberna K. (2018). DNA Replication: From Radioisotopes to Click Chemistry. Molecules, *23*(11), 3007. https://doi.org/10.3390/molecules23113007

84. Glass R. H., Ericsson S. A., Ericsson R. J., Drouin M. T., Marcoux L. J., & Sullivan H. (1991). The resazurin reduction test provides an assessment of sperm activity. Fertility and Sterility, *56*(4), 743-746. https://doi.org/10.1016/S0015-0282(16)54609-3

85. O'Brien J., Wilson I., Orton T., & Pognan F. (2000). Investigation of the Alamar Blue (resazurin) fluorescent dye for the assessment of mammalian cell cytotoxicity. European Journal of Biochemistry, *267*(17), 5421-5426. https://doi.org/10.1046/j.1432-1327.2000.01606.x

86. MCT1 promotes the cisplatin-resistance by antagonizing Fas in epithelial ovarian cancer - PMC. https://www.ncbi.nlm.nih.gov/pmc/articles/PMC4440085/. Accessed 24.9.2024. https://www.ncbi.nlm.nih.gov/pmc/articles/PMC4440085/. Accessed September 24, 2024

87. Felmlee M. A., Jones R. S., Rodriguez-Cruz V., Follman K. E., & Morris M. E. (2020). Monocarboxylate Transporters (SLC16): Function, Regulation, and Role in Health and Disease. Pharmacological Reviews, *72*(2), 466-485. https://doi.org/10.1124/pr.119.018762

88. Silvy F., Lissitzky J.-C., Bruneau N., Zucchini N., Landrier J.-F., Lombardo D., et al. (2013). Resistance to cisplatin-induced cell death conferred by the activity of organic anion transporting polypeptides (OATP) in human melanoma cells. Pigment Cell & Melanoma Research, *26*(4), 592-596. https://doi.org/10.1111/pcmr.12108

89. Lever J. E. (1979). Inducers of mammalian cell differentiation stimulate dome formation in a differentiated kidney epithelial cell line (MDCK). Proceedings of the National Academy of Sciences, *76*(3), 1323-1327. https://doi.org/10.1073/pnas.76.3.1323

90. Vogetseder A., Karadeniz A., Kaissling B., & Le Hir M. (2005). Tubular cell proliferation in the healthy rat kidney. Histochemistry and Cell Biology, *124*(2), 97-104. https://doi.org/10.1007/s00418-005-0023-y

91. Vogetseder A., Palan T., Bacic D., Kaissling B., & Le Hir M. (2007). Proximal tubular epithelial cells are generated by division of differentiated cells in the healthy kidney. American Journal of Physiology-Cell Physiology, *292*(2), C807-C813. https://doi.org/10.1152/ajpcell.00301.2006

92. Castrop H. (2019). The Role of Renal Interstitial Cells in Proximal Tubular Regeneration. Nephron, *141*(4), 265-272. https://doi.org/10.1159/000496278

93. Ngo T. T. T., Rossbach B., Sébastien I., Neubauer J. C., Kurtz A., & Hariharan K. (2022). Functional differentiation and scalable production of renal proximal tubular epithelial cells from human pluripotent stem cells in a dynamic culture system. Cell Proliferation, *55*(3), e13190. https://doi.org/10.1111/cpr.13190

94. Fuente Mora C., Ranghini E., Bruno S., Bussolati B., Camussi G., Wilm B., et al. (2012). Differentiation of Podocyte and Proximal Tubule-Like Cells from a Mouse Kidney-Derived Stem Cell Line. Stem Cells and Development, *21*(2), 296-307. https://doi.org/10.1089/scd.2010.0470

95. Humphreys B. D., Czerniak S., DiRocco D. P., Hasnain W., Cheema R., & Bonventre J. V. (2011). Repair of injured proximal tubule does not involve specialized progenitors. Proceedings of the National Academy of Sciences, *108*(22), 9226-9231. https://doi.org/10.1073/pnas.1100629108

96. Kusaba T., Lalli M., Kramann R., Kobayashi A., & Humphreys B. D. (2014). Differentiated kidney epithelial cells repair injured proximal tubule. Proceedings of the National Academy of Sciences of the United States of America, *111*(4), 1527-1532. https://doi.org/10.1073/pnas.1310653110

97. Baer P. C., Bereiter-Hahn J., Schubert R., & Geiger H. (2006). Differentiation Status of Human Renal Proximal and Distal Tubular Epithelial Cells in vitro*:* Differential Expression of Characteristic Markers. Cells Tissues Organs, *184*(1), 16-22. https://doi.org/10.1159/000096947

98. Narayanan K., Schumacher K. M., Tasnim F., Kandasamy K., Schumacher A., Ni M., et al. (2013). Human embryonic stem cells differentiate into functional renal proximal tubular–like cells. Kidney International, *83*(4), 593-603. https://doi.org/10.1038/ki.2012.442

99. Rossi G., Manfrin A., & Lutolf M. P. (2018). Progress and potential in organoid research. Nature Reviews Genetics, *19*(11), 671-687. https://doi.org/10.1038/s41576-018-0051-9

100. Soncin F., & Ward C. M. (2011). The Function of E-Cadherin in Stem Cell Pluripotency and Self-Renewal. Genes, *2*(1), 229-259. https://doi.org/10.3390/genes2010229

101. Lamouille S., Xu J., & Derynck R. (2014). Molecular mechanisms of epithelial–mesenchymal transition. Nature Reviews Molecular Cell Biology, *15*(3), 178-196. https://doi.org/10.1038/nrm3758

102. Redmer T., Diecke S., Grigoryan T., Quiroga-Negreira A., Birchmeier W., & Besser D. (2011). E-cadherin is crucial for embryonic stem cell pluripotency and can replace OCT4 during somatic cell reprogramming. EMBO reports, *12*(7), 720-726. https://doi.org/10.1038/embor.2011.88

103. Park A., Choi S., Do J., Kim Y., Kim K.-S., Koh E., et al. (2024). ZO-1 regulates the migration of mesenchymal stem cells in cooperation with α-catenin in response to breast tumor cells. Cell Death Discovery, *10*(1), 19. https://doi.org/10.1038/s41420-023-01793-4

104. Shen S. S., Krishna B., Chirala R., Amato R. J., & Truong L. D. (2005). Kidney-specific cadherin, a specific marker for the distal portion of the nephron and related renal neoplasms. Modern Pathology, *18*(7), 933-940. https://doi.org/10.1038/modpathol.3800373

105. Bander N. H., Finstad C. L., Cordon-Cardo C., Ramsawak R. D., Vaughan E. D. Jr., Whitmore W. F. Jr., et al. (1989). Analysis of a Mouse Monoclonal Antibody That

Reacts with a Specific Region of the Human Proximal Tubule and Subsets Renal Cell Carcinomas1. Cancer Research, *49*(23), 6774-6780.

106. Sánchez-Romero N., Martínez-Gimeno L., Caetano-Pinto P., Saez B., Sánchez-Zalabardo J. M., Masereeuw R., et al. (2020). A simple method for the isolation and detailed characterization of primary human proximal tubule cells for renal replacement therapy. The International Journal of Artificial Organs, *43*(1), 45-57. https://doi.org/10.1177/0391398819866458

107. Burdeyron P., Giraud S., Hauet T., & Steichen C. (2020). Urine-derived stem/progenitor cells: A focus on their characterization and potential. World Journal of Stem Cells, *12*(10), 1080. https://doi.org/10.4252/wjsc.v12.i10.1080

108. Wing C., Komatsu M., Delaney S. M., Krause M., Wheeler H. E., & Dolan M. E. (2017). Application of stem cell derived neuronal cells to evaluate neurotoxic chemotherapy. Stem Cell Research, *22*, 79-88. https://doi.org/10.1016/j.scr.2017.06.006

109. Wang M., Wang J., Tsui A. Y. P., Li Z., Zhang Y., Zhao Q., et al. (2021). Mechanisms of peripheral neurotoxicity associated with four chemotherapy drugs using human induced pluripotent stem cell-derived peripheral neurons. Toxicology in Vitro, *77*, 105233. https://doi.org/10.1016/j.tiv.2021.105233

110. Inui K.-I., Masuda S., & Saito H. (2000). Cellular and molecular aspects of drug transport in the kidney. Kidney International, *58*(3), 944-958. https://doi.org/10.1046/j.1523-1755.2000.00251.x

111. Gene Expression Levels and Immunolocalization of Organic Ion... : Journal of the American Society of Nephrology. https://journals.lww.com/jasn/Fulltext/2002/04000/Gene_Expression_Levels_and_Immunolocalization_of.5.aspx. Accessed 17.2.2024. https://journals.lww.com/jasn/Fulltext/2002/04000/Gene_Expression_Levels_and_Immunolocalization_of.5.aspx. Accessed February 17, 2024

112. Vanslambrouck J. M., Tan K. S., Mah S., & Little M. H. (2023). Generation of proximal tubule-enhanced kidney organoids from human pluripotent stem cells. Nature Protocols, *18*(11), 3229-3252. https://doi.org/10.1038/s41596-023-00880-1

113. Vanslambrouck J. M., Wilson S. B., Tan K. S., Groenewegen E., Rudraraju R., Neil J., et al. (2022). Enhanced metanephric specification to functional proximal tubule enables toxicity screening and infectious disease modelling in kidney organoids. Nature Communications, *13*(1), 5943. https://doi.org/10.1038/s41467-022-33623-z

114. Pisapia F., O'Brien D., Tasinato E., Garner K. L., & Brown C. D. A. (2023). Development of a Highly Differentiated Human Primary Proximal Tubule MPS Model (aProximate MPS Flow). Bioengineering (Basel, Switzerland), *11*(1), 7. https://doi.org/10.3390/bioengineering11010007

115. Jenkinson S. E., Chung G. W., van Loon E., Bakar N. S., Dalzell A. M., & Brown C. D. A. (2012). The limitations of renal epithelial cell line HK-2 as a model of drug transporter expression and function in the proximal tubule. Pflugers Archiv: European Journal of Physiology, *464*(6), 601-611. https://doi.org/10.1007/s00424-012-1163-2

116. Pešková L., Vinarský V., Bárta T., & Hampl A. (2019). Human Embryonic Stem Cells Acquire Responsiveness to TRAIL upon Exposure to Cisplatin. Stem Cells International, *2019*, 4279481. https://doi.org/10.1155/2019/4279481

117. Fukusumi H., Handa Y., Shofuda T., & Kanemura Y. (2019). Evaluation of the susceptibility of neurons and neural stem/progenitor cells derived from human induced pluripotent stem cells to anticancer drugs. Journal of Pharmacological Sciences, *140*(4), 331-336. https://doi.org/10.1016/j.jphs.2019.08.002

118. Freedman B. S., Brooks C. R., Lam A. Q., Fu H., Morizane R., Agrawal V., et al. (2015). Modelling kidney disease with CRISPR-mutant kidney organoids derived from human pluripotent epiblast spheroids. Nature Communications, *6*(1), 8715. https://doi.org/10.1038/ncomms9715

119. Morizane R., Lam A. Q., Freedman B. S., Kishi S., Valerius M. T., & Bonventre J. V. (2015). Nephron organoids derived from human pluripotent stem cells model kidney development and injury. Nature Biotechnology, *33*(11), 1193-1200. https://doi.org/10.1038/nbt.3392

120. Koziolek M. J., Riess R., Geiger H., Thévenod F., & Hauser I. A. (2001). Expression of multidrug resistance P-glycoprotein in kidney allografts from cyclosporine A-treated patients. Kidney International, *60*(1), 156-166. https://doi.org/10.1046/j.1523-1755.2001.00782.x

121. Veiga-Matos J., Morales A. I., Prieto M., Remião F., & Silva R. (2023). Study Models of Drug–Drug Interactions Involving P-Glycoprotein: The Potential Benefit of P-Glycoprotein Modulation at the Kidney and Intestinal Levels. Molecules, *28*(22), 7532. https://doi.org/10.3390/molecules28227532

122. Saretzki G., Armstrong L., Leake A., Lako M., & von Zglinicki T. (2004). Stress defense in murine embryonic stem cells is superior to that of various differentiated murine cells. Stem Cells (Dayton, Ohio), *22*(6), 962-971. https://doi.org/10.1634/stemcells.22-6-962

123. Ransy C., Vaz C., Lombès A., & Bouillaud F. (2020). Use of H2O2 to Cause Oxidative Stress, the Catalase Issue. International Journal of Molecular Sciences, *21*(23), 9149. https://doi.org/10.3390/ijms21239149

124. Pierzyńska-Mach A., Szczurek A., Cella Zanacchi F., Pennacchietti F., Drukała J., Diaspro A., et al. (2016). Subnuclear localization, rates and effectiveness of UVC-induced unscheduled DNA synthesis visualized by fluorescence widefield, confocal and super-resolution microscopy. Cell Cycle, *15*(8), 1156-1167. https://doi.org/10.1080/15384101.2016.1158377

125. Wang L., Zhang F., Peng W., Zhang J., Dong W., Yuan D., et al. (2020). Preincubation with a low-dose hydrogen peroxide enhances anti-oxidative stress ability of BMSCs. Journal of Orthopaedic Surgery and Research, *15*(1), 392. https://doi.org/10.1186/s13018-020-01916-y

126. Cilião H. L., Ribeiro D. L., Camargo-Godoy R. B. O., Specian A. F. L., Serpeloni J. M., & Cólus I. M. S. (2015). Cytotoxic and genotoxic effects of high concentrations of the immunosuppressive drugs cyclosporine and tacrolimus in MRC-5 cells. Experimental and Toxicologic Pathology, *67*(2), 179-187. https://doi.org/10.1016/j.etp.2014.11.008

127. Korolczuk A., Caban K., Amarowicz M., Czechowska G., & Irla-Miduch J. (2016). Oxidative Stress and Liver Morphology in Experimental Cyclosporine A-Induced Hepatotoxicity. BioMed Research International, *2016*. https://doi.org/10.1155/2016/5823271

128. Rocha C. R. R., Lerner L. K., Okamoto O. K., Marchetto M. C., & Menck C. F. M. (2013). The role of DNA repair in the pluripotency and differentiation of human stem cells. Mutation Research, *752*(1), 25-35. https://doi.org/10.1016/j.mrrev.2012.09.001

129. Boulikas T., & Vougiouka M. (2003). Cisplatin and platinum drugs at the molecular level (Review). Oncology Reports, *10*(6), 1663-1682. https://doi.org/10.3892/or.10.6.1663

130. Ren F., Wang K., Zhang T., Jiang J., Nice E. C., & Huang C. (2015). New insights into redox regulation of stem cell self-renewal and differentiation. Biochimica Et Biophysica Acta, *1850*(8), 1518-1526. https://doi.org/10.1016/j.bbagen.2015.02.017

131. Gurusamy N., Mukherjee S., Lekli I., Bearzi C., Bardelli S., & Das D. K. (2009). Inhibition of Ref-1 Stimulates the Production of Reactive Oxygen Species and Induces Differentiation in Adult Cardiac Stem Cells. Antioxidants & Redox Signaling, *11*(3), 589-599. https://doi.org/10.1089/ars.2008.2195

132. Brinks R., Wruck C. J., Schmitz J., & Schupp N. (2023). Nrf2 Activation Does Not Protect from Aldosterone-Induced Kidney Damage in Mice. Antioxidants, *12*(3), 777. https://doi.org/10.3390/antiox12030777

133. Tang C., Livingston M. J., Safirstein R., & Dong Z. (2023). Cisplatin nephrotoxicity: new insights and therapeutic implications. Nature Reviews Nephrology, *19*(1), 53-72. https://doi.org/10.1038/s41581-022-00631-7

134. Deshmukh P., Unni S., Krishnappa G., & Padmanabhan B. (2017). The Keap1–Nrf2 pathway: promising therapeutic target to counteract ROS-mediated damage in cancers and neurodegenerative diseases. Biophysical Reviews, *9*(1), 41-56. https://doi.org/10.1007/s12551-016-0244-4

135. Michel H. E., & Menze E. T. (2019). Tetramethylpyrazine guards against cisplatin-induced nephrotoxicity in rats through inhibiting HMGB1/TLR4/NF-κB and activating Nrf2 and PPAR-γ signaling pathways. European Journal of Pharmacology, *857*, 172422. https://doi.org/10.1016/j.ejphar.2019.172422

136. Suliman F. A., Khodeer D. M., Ibrahiem A., Mehanna E. T., El-Kherbetawy M. K., Mohammad H. M. F., et al. (2018). Renoprotective effect of the isoflavonoid biochanin A against cisplatin induced acute kidney injury in mice: Effect on inflammatory burden and p53 apoptosis. International Immunopharmacology, *61*, 8-19. https://doi.org/10.1016/j.intimp.2018.05.010

137. Adeoye B., Asenuga E., Oyagbemi A., Omobowale T., & Adedapo A. (2018). The Protective Effect of the Ethanol Leaf Extract of Andrographis Paniculata on Cisplatin-Induced Acute Kidney Injury in Rats Through nrf2/KIM-1 Signalling Pathway. Drug Research, *68*(01), 23-32. https://doi.org/10.1055/s-0043-118179

138. Saretzki G., Walter T., Atkinson S., Passos J. F., Bareth B., Keith W. N., et al. (2008). Downregulation of Multiple Stress Defense Mechanisms During Differentiation of Human Embryonic Stem Cells. Stem Cells, *26*(2), 455-464. https://doi.org/10.1634/stemcells.2007-0628

139. Jennings P., Weiland C., Limonciel A., Bloch K. M., Radford R., Aschauer L., et al. (2012). Transcriptomic alterations induced by Ochratoxin A in rat and human renal proximal tubular in vitro models and comparison to a rat in vivo model. Archives of Toxicology, *86*(4), 571-589. https://doi.org/10.1007/s00204-011-0780-4

140. Kanai Y., Lee W. S., You G., Brown D., & Hediger M. A. (1994). The human kidney low affinity Na+/glucose cotransporter SGLT2. Delineation of the major renal reabsorptive mechanism for D-glucose. Journal of Clinical Investigation, *93*(1), 397-404. https://doi.org/10.1172/JCI116972

Publications

Isaac Musong Mboni-Johnston, **Nazih Mohamed Zakari Kouidrat**, Cornelia Hirsch, Andreas Georg Weber, Alexander Meißner, James Adjaye, Nicole Schupp – „*Sensitivity of Human Induced Pluripotent Stem Cells and Thereof Differentiated Kidney Proximal Tubular Cells towards Selected Nephrotoxins*“.

Paper published in „The International Journal of Molecular Science“ on December 20, 2023.

Conferences and presentations

Nazih Mohamed Zakari Kouidrat, Andreas Weber, James Adjaye and Nicole Schupp – „*Influence of Nephrotoxins on the Differentiation Process of Human Induced Pluripotent Stem Cells to Kidney Cells*“.

Poster Presentations:

02/2025	Evaluation of the German Research Foundation (DFG) of the RTG 2578 – Düsseldorf
03/2023	8. German Pharm-Tox Summit, Deutsche Gesellschaft für Experimentelle & Klinische Pharmakologie & Toxikologie – Ulm
09/2022	10. German Stem Cell Network Congress – Münster.

Oral Presentation:

11/2022	RTG 2578 annual retreat – Radevormwald.

Afir Y., **Kouidrat NMZ.,** Benaziza M., Sahnoun S., Bouasria K., Tir Y., Kassoul O., Benkouar R., Ait Messaoudene M.S., Bouhouita Y. – „*Resynchronisation Cardiaque Chez un Patient Atteint de Cardiomyopathie Dilatée Induite par une Acromégalie: À Propos d'un Cas*“. [Cardiac Resynchronization in a Patient with Acromegaly-Induced Dilated Cardiomyopathy: A Case Report].

Poster Presentation:

06/2021	Algerian Heart Rhythm Society Annual Congress, Algiers, Algeria.

Publications at the university and in the student magazine

Medicine:

Y. AFIR. , KOUIDRAT NMZ. - ***« Introduction à la Littérature Scientifique »*** *(Introduction to scientific literature)* - MedPress. 2021; 7.

A retrospective study of the activities of the Rhythmology Center of A1 Mustapha Bacha University Hospital (unpublished data).

KOUIDRAT NMZ. , SARI T. - ***« To Vaccinate or Not To Vaccinate? »***. MedPress. 2019; 2.

« Système Nerveux Central, Nerfs Crâniens & Organes des sens ». *(Central nervous system, brain nerves & sensory organs) - Editing of a neuroanatomy textbook for the medical faculty of Algiers as part of a student project - 2016.*

Literature:

Kouidrat NMZ. ***« Les Prolégomènes - Ibn Khaldoun part 2 »*** - (*The Prolegomena - 2*) MedPress Journal. 2021; 7.

Kouidrat NMZ. ***« Les Prolégomènes - Ibn Khaldoun part 1 »*** - (*The Prolegomena - 1*) MedPress Journal. 2021; 6.

Kouidrat NMZ. ***« Le Savant & le Politique - Max Weber »*** - *(The Scholar & the Politician*) MedPress Journal. 2020; 5.

Kouidrat NMZ. ***« La Barbarie Douce - Jean Pierre Le Goff »*** - (*The Soft Barbary*) MedPress Journal. 2020; 4.

Kouidrat NMZ. « ***Esquisse d'un Tableau Historique des Progrès Humains - Nicolas de Condorcet »*** - (*Sketch of a Historical Table of Human Progress*) MedPress Journal. 2020; 3.

Kouidrat NMZ. , Afir Y. ***« Économie de Santé : Interview avec le Professeur Omar AKTOUF »*** - (*Health economics: Interview with Professor Omar AKTOUF*) MedPress Magazine. 2020; 3.

Kouidrat NMZ. ***« De la Liberté - John Stuart Mill »*** - (*On Liberty*) MedPress Journal. 2019; 1.

Kouidrat NMZ. ***« Le Travail Intellectuel - Jean Guitton »*** - (The Intellectual work) MedPress Journal. 2019; 0.

Kouidrat NMZ. ***« La Société du Spectacle - Guy Debord »*** - (*The Entertainment Society*) ReMed Magazine. 2018; 6.

Kouidrat NMZ. ***« Tacfarinas, l'Appel de la Patrie - A. Akkache »*** - (*Call of the Fatherland*) ReMed Magazine. 2018; 5.

Kouidrat NMZ. ***« La Fabrique du Crétin - J-P. Brighelli »*** - (*The Dumb Factory*) ReMed Magazine. 2018; 4.

Kouidrat NMZ. ***« L'occidentalisation du Monde - Serge Latouche »*** - (Westernization of the world) ReMed Magazine. 2017; 3.

Kouidrat NMZ. , Afir Y. - ***« Les Auteurs à la Source : Interview avec Djawed Rostom Touati »*** - (*Interview with the novelist D.R. Touati*), ReMed Magazine. 2017; 2.

Expression of gratitude

First of all, I want to express my gratitude to Mrs. Prof. Dr. Nicole Schupp and Mr. Prof. Dr. Fritz for giving me the great opportunity to pursue my doctoral thesis at the institute of toxicology and be part of the GRK 2578. Nicole, your belief in me from the very beginning, despite my lack of experience and lab skills, was an incredible source of motivation. Your continuous support and your open-door attitude made communication uncomplicated and flexible throughout this journey.

I extend my thanks to Prof. Dr. James Adjaye from the Institute of Stem Cell Research and Regenerative Medicine for his kind willingness to supervise my doctoral thesis as second supervisor.

A big thank you goes to Isaac Mboni-Johnston for all the valuable lessons I learned while we navigated the challenges together in the lab. I am also grateful to Kerstin for guiding me through my first steps under the hood with such kindness.

I would like to highlight the wonderful atmosphere that made my time at the institute truly enjoyable, particularly with Lena, Julia and Frauke. A special thanks to Frauke for your support inside and outside the institute.

I also want to acknowledge some professors from the medical faculty of Algiers who significantly shaped my academic path, as well as my friends and colleagues from our student's magazine and literature groups. I am thankful to everyone who took the time to teach me something valuable.

Last but not least, I owe a tremendous debt of gratitude to my family. Your support and sacrifices have made this journey possible, and I am forever grateful for everything you have done to ensure that my siblings and I have opportunities that you never had.